UCLouvain

AGRO LOUVAIN

Faculté des bioingénieurs

Preventing infections of hip joint prostheses: activity of an antimicrobial coating based on the LL-37 peptide

Authors: Bastien Croës, Juliette Dewez

Supervisors: Prof. Christine Dupont, Ir. Cédric Vranckx

Readers: Prof. Sophie Demoustier, Prof. Annika Gillis

Academic Year: 2023-2024

Thesis presented in partial fulfillment of the requirements for the degree of Master in bioengineering: chemistry and bioindustries

Acknowledgments

First of all, we would like to express our deepest gratitude to Prof. Christine Dupont, Dean of the AGRO faculty at the UCLouvain, for her ongoing support and wise advice throughout this year. In spite of her professional and academic duties, Prof. Dupont made herself available to guide us in our experiments and follow us as promoter of this Master's thesis. Through precious exchanges, she shared her expertise and greatly helped the progress of this research.

To Cédric Vranckx, who proved that patience truly is a virtue, thank you for your constant help and availability. Your thesis project was the mainstay of our work and your mastery of the subject greatly contributed to the quality of our research, and simply, made all of this possible.

We are also profoundly grateful to the members of the jury, Prof. Sophie Demoustier and Prof. Annika Gillis, for the precious time they gave at reading and evaluating our Master's thesis. Their critical participation is essential to the validation of our work, and their expertise is much appreciated in defending this project.

We also owe a great deal of appreciation to Clément Guibert, researcher at the Laboratoire de Réactivité de Surface in Paris for taking the time to analyze our samples along with feeding interesting exchange on the project.

We would also like to extend our warmest thanks to everyone at the Lavoisier C2 (BMSA) and Van Helmont (Ecole de Pharmacie UCLouvain) laboratories. Their technical assistance was crucial; they were able to guide us on certain handling doubts during our experiments, offering a superior quality to this project.

Our thanks also go to our parents, whose moral support and advice were a constant help throughout the year, and all our academic years before that. Their presence and attentiveness have been key to our success, and extremely supportive in our daily lives during this intense period.

And last but not least, a special mention to the Lavoisier lab coffee machine, our companion for many hours, who offered constant fueling in times of doubt and intense work.

To all of you, we are infinitely grateful for your support, your guidance and presence throughout this journey.

Abstract

This Master's thesis studies the activity of an antimicrobial coating designed for the battle against *S. epidermidis* biofilms, which are the leading cause for nosocomial infections related to implants and medical devices, including prosthetic joint infection, an important worldwide consideration nowadays. New strategies based on the design of antimicrobial coatings are under current research to prevent and treat such infections.

The antimicrobial property of the investigated coating is conferred by LL-37, an antimicrobial peptide. The coating is constructed using the Layer-by-Layer self-assembly technique, allowing easy immobilization of proteins and other charged compounds on a surface. These multilayered films constitute a powerful tool for nanoscale surface functionalization. Here, LL-37 was immobilized together with chitosan and heparin, two bioactive PEs.

Two different LL-37-based coatings were constructed. A first coating was made of bare, positively-charged, LL-37, alternately adsorbed with negatively-charged heparin ((bare LL-37-HEP)$_n$). The second coating was made of LL-37 whose charges had been standardized by complexation with heparin to form Protein-Polyelectrolyte Complexes or PPCs, displaying a negatively-charged corona, and alternately adsorbed with positively-charged chitosan ((PPCs-CHI)$_n$).

Coatings activity was assessed through two approaches. The first objective was to study the secondary structure of LL-37 released from the coatings. The bactericidal activity of the peptide is conferred by its α-helical conformation, which could be revealed by circular dichroism (CD). To enable such analysis, the release protocol had to be optimized to maximize the concentration of the released peptide. Despite the use of different strategies to maximize this concentration, results showed that the concentration of LL-37 released by the coatings was not high enough for CD analysis.

Secondly, activity of the coating with bare LL-37 was assessed by studying its potential synergistic effect with four routinely-used antibiotics. Results showed a potential synergistic activity with all four antibiotics regarding the reduction of the biofilm biomass. In contrast, no significant effect of the coating compared to antibiotics alone was revealed for the reduction of metabolic activity of the biofilm.

This work brings a contribution to the understanding of the activity of LL-37-based antimicrobial coatings, that offer new ways to prevent prosthetic joint infections.

Table of contents

List of abbreviations

aa = Amino acids

AL = Anchoring layer

AMC = Antimicrobial coating

AMP = Antimicrobial peptide

AMR = Antimicrobial resistance

Atl = Major autolysin

AtlE = Autolysin *S. epidermidis*

BCA = Bicinchoninic acid

BL = Bilayer

C^+ = Positive control

CD = Circular dichroism

CFU = Colony-Forming-Unit

CHI = Chitosan

D-Ala-D-Ala = D-alanyl-D-alanine

DLS = Dynamic light scattering

EPS = Extracellular polymeric substances

EU = European Union

FITC = Fluorescein isothiocyanate

GAG = Glycosaminoglycan

GlcNAc = N-acetylglucosamine

HEP = Heparin

HGT = Horizontal gene transfer

HNP-1 = Human Neutrophil Peptide 1

IU = International Unit

LbL = Layer-by-layer self-assembly

LOQ = Limit of quantification

LPS = Lipopolysaccharide

MDK = Minimal duration for killing

MIC = Minimal inhibitory concentration

MOA = Mode-of-action

mRNA = Messenger RNA

MurNAc = N-acetylmuramic acid

M_W = Molecular weight

NMR = Nuclear magnetic resonance

np = Nanoparticle

ns = Non-significant

PBS = Phosphate-buffered saline

PE = Polyelectrolyte

pI = Isoelectric point

PJI = Prosthetic joint infection

PPCs = Protein-Polyelectrolyte complexes

PSS= Poly(styrenesulfonate)

QS = Quorum sensing

ROS = Reactive oxygen species

RPG = RPMI medium + glucose

RPMI = Roswell Park Memorial Institute Medium

SDS = Sodium dodecyl sulfate

SEM = Standard error of the mean

Ti = Titanium

TSA = Tryptic soy agar

UV = Ultraviolet

PART I – Introduction and context of the research

1. Prosthetic joint infection

Today, the ageing and enhanced sedentary lifestyle of our population leads to important underlying issues. One of them is the increasing number of people suffering from **osteoarthritis**, a degenerative joint disease characterized by the breakdown of joint cartilage and subchondral bone. [1] The most common joint disorder is hip osteoarthritis. To cure this particular disease, **hip replacement surgery**, also called hip arthroplasty, is performed to restore mobility and reduce pain for the patient. This intervention involves surgically removing the damaged or diseased parts of the hip joint and replacing them with a prosthetic one. [2]

Unfortunately, **prosthetic joint infection** (PJI) affects a significant number of patients worldwide. According to statistical data, PJI occurs in approximately 1 to 2% of patients who have undergone hip replacement surgery, making the prevention of such infections an important consideration in the medical field, highlighting the importance of further research to reduce these figures and increase patient's well-being and functional post-arthroplasty capacity. [2]

PJIs arise from various factors but primarily from contamination of the equipment used during surgical interventions. In addition to poor surgical techniques and underlying medical conditions, factors contributing to the development of such infections include compromised immune systems due to various diseases, such as obesity and diabetes, or the use of immunosuppressive drugs. The microorganisms settle on the surface of the prosthetic joint, which causes infection. In nosocomial infections, these microorganisms often are **biofilm-forming bacteria**, a very resistant organization that makes the fight against the infection even more fastidious. [2], [3]

When a PJI takes hold, it initiates a cascade of significant medical complications and challenges. Beyond the **physical health repercussions**, patients may experience substantial psychological and financial burdens. Treatment typically involves prolonged courses of antibiotics, repeated surgeries to address the infection, and in severe cases, removal of the infected prosthesis. These interventions not only disrupt the patient's daily life but can also result in loss of joint functionality, reduced mobility, and **heightened healthcare costs for both the patient and the healthcare system**.

2. The issue of antibiotic resistance

The rise of **antibiotic-resistant bacteria** is currently an undeniable issue. Every year, antimicrobial resistance (AMR) is responsible for 700,000 patients' death worldwide, a number expected to increase even more to reach 10 million by 2050 if no **viable alternative therapy** to antibiotics is found. Drug-resistant bacteria have made scientists wondering if the time of antibiotics was up, a question that led them to focus on finding new alternatives. [4]

Biofilms, surface-attached groups of bacteria embedded in an extracellular matrix, are significantly less susceptible to antimicrobial agents than free-floating, or planktonic, bacteria. [5] As **biofilm-associated bacteria are highly resistant to antibiotics** [6], it brings an important issue, in the case of hip joint prosthesis especially: in the long term, antibiotics alone cannot be the unique solution to cure biofilm-based infections.

Fortunately, other attractive antimicrobial compounds than antibiotics exist. Some of them are synthetically-designed strategies while others are naturally-occurring alternatives such as phage therapy, bacteriocins, and **antimicrobial peptides** (AMPs). Our research focuses on the latter and on one AMP in particular, **LL-37**. AMPs are promising alternative to traditional antibiotics thanks to their **distinct mode-of-action** (MOA) and underlying activity toward a broad spectrum of bacteria, both Gram-positive and Gram-negative. [7], [8] MOAs of antibiotics, AMP in general, and LL-37 in particular, are developed in the *State of the art*.

In this work, LL-37 has been chosen to be used as a constituent of an **antimicrobial coating (AMC)** designed to cover the hip prosthetic joint, conferring it the ability to prevent and fight biofilm-based infections. The coating is built using the **Layer-by-Layer self-assembly (LbL)** technique, a straightforward method enabling **protein immobilization** at interfaces. [9]

Hoping to completely replace traditional antibiotics by AMPs to limit bacteria resistance and expect to reach the same bactericidal result might be an idealist vision. Indeed, resistance to AMP could also be developed by bacteria overtime as it has already been observed. [10] Additionally, nowadays, antimicrobial results of antibiotics are still undeniably more attractive that the one offered by AMPs. [11] Following this idea, a part of the short-term solution would be to find treatments offering satisfying results and avoiding the rise of AMP- and/or antibiotics-resistant bacteria.

To do so, an eventual **synergy** between the **AMC** and routinely-used **antibiotics** could allow to use less of both treatments. Therefore, we focused on studying the activity of LL-37 and traditional antibiotics working in concert.

These experiments are conducted on *Staphylococcus epidermidis*, a human skin colonizer responsible for most of nosocomial infections. Even though this pathogen may have been regarded as having a benign relationship with its host, it is now widely studied for being an important opportunistic pathogen.

All in all, this work stands as a contribution to medical science, with a primary focus on enhancing the prevention and management of PJIs. Through leveraging the unique antimicrobial properties of LL-37 as well as its synergistic effect with antibiotics, and employing advanced techniques such as the LbL technique, we endeavor to develop novel and efficacious strategies aimed at reducing these infections.

PART II – State of the art

The following part lays the foundations of our work by developing important constituting aspects and elements aiming to help the understanding of the subsequent objectives and chosen strategies.

1. Hip joint replacement and underlying challenges

1.1 Arthroplasty and hip joint replacement

Arthroplasty, also known as joint replacement surgery, is a major surgical intervention aimed at restoring joint functionality and mobility in patients suffering from severe joint pain or decreased joint function due to injuries, degenerative, and chronic diseases such as osteoarthritis and rheumatoid arthritis, or other conditions. Yearly, joint replacement surgery is performed on millions of individuals worldwide.

The obvious primary goal of arthroplasty is to relieve pain for the patient and restore joint function by replacing the damaged joint surface with artificial components. This procedure can be performed on various joints in the body, including hips, knees, shoulders, elbows, and ankles, depending on the patient's specific needs. Since these various types of joint replacement are becoming increasingly available, the total number of patients experiencing arthroplasties continues to grow. While most joint replacements offer pain-free function, a minority of patients may experience device failure, requiring additional surgery at some point during the device's lifespan. Among the different types of arthroplasties, hip replacement is one of the most performed interventions. [1], [2]

The OECD[1] 2022 report confirms that hip replacements are among the most common non-urgent surgical procedures in the European Union (EU). In 2019, Germany, Austria, Finland, and Belgium had the highest rates of hip replacement surgeries in the EU. The report also notes that Belgium is in the top five for inpatient hospitalizations, with day surgery hip replacements rising from 0.1% in 2019 to 0.2% in 2021. The incidence of these surgeries is influenced by demographic factors such as age and gender, as well as the healthcare system, economic strength, availability of medical services, and patient expectations for quality of life. These factors are the reason why the number of hip replacement surgeries are expected to continue to rise. [2], [12], [13]

[1] Organization for Economic Co-operation and Development. The OECD is an international organization that works to promote policies that improve the economic and social well-being of people around the world. It provides a platform for governments to work together and share experiences to seek solutions to common problems.

The hip is a complex joint that connects the femur to the pelvic bone and plays a crucial role in body mobility and stability. [1] Hip replacement procedure typically involves removing the damaged hip joint, including the femoral head, followed by its substitution with a hip prosthesis. Such prostheses are usually made of materials such as metal, plastic, and ceramic, designed to mimic natural joint surfaces and ensure optimal joint function. [14] The main process of hip joint replacement is visualized in *Figure 1,* showing the femoral stem, femoral head and acetabular cup, which are composing parts of the hip prosthesis.

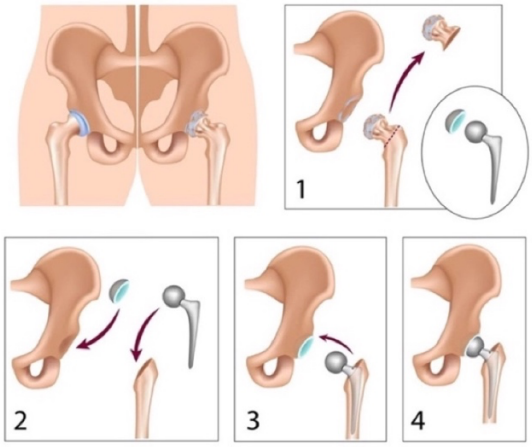

Figure 1: **Hip joint replacement surgery process**. During total hip replacement surgery, the damaged bone and cartilage are removed from the hip joint and replaced with synthetic parts. A zoom of the femoral head removing for further substitution is visualized in square 1. [14]

Different types of hip prostheses exist, including total hip prostheses, which replace the entire hip joint, and partial hip prostheses, to replace only part of the joint. The choice of prosthesis type will depend on various factors, such as the extent of joint damage, the patient's age and activity level, and other medical considerations. [14]

After a hip arthroplasty, patients may experience significant decrease of pain and improvement in mobility, making this procedure one of the major advancements in the field of orthopedic surgery. Although being considered as a high success rate intervention, 7% to 27% of the patients complain of persistent postsurgical pain 1 to 4 years post-arthroplasty. In fact, like any surgical intervention, hip replacement surgery involves potential risks, including post-operative complications such as aseptic failure or PJIs. [15], [16]

1.2 Arthroplasty failure and aseptic post-operative complications

Arthroplasty failure can either be aseptic, or infection-related. PJIs are the central part of this Master's thesis and will be described in more details in the following section: *2. Prosthetic joint infection*. However, aseptic failure and especially aseptic loosening is an important consideration in the case of hip joint replacement and is worth further development.

The most common failure in the implantation of joint prostheses is the aseptic loosening of said prostheses at the interface with the bone. This complication is characterized by the loss of fixation of the implant in the bone, at the femoral stem or acetabular cup levels and leads to technically demanding and expensive revision surgeries. Aseptic loosening can be heavily avoided by optimal osseointegration and prevention of wear and corrosion of the implant's material. [1], [17]

Osseointegration is the process by which the implant and the surrounding bone establish direct contact at the microscopic level and is essential for the prothesis durability. This process is crucial for the long-term stabilization and success of the implant, preventing inflammatory reaction or bone resorption. [1], [17] During hip replacement surgery, achieving stability is crucial for promoting osseointegration. Cemented surface replacement arthroplasty is one way to increase the desired initial stability through immediate fixation. This cementing is performed on the parts of the prosthesis in contact with the bones. A study conducted by B. Johnstone et al., revealed that aseptic loosening occurred more often in the uncemented surface replacement arthroplasties. [18]

However, their study was conducted in the short-term (5 years) and it is not excluded that in the long-term cemented surface replacement increases the risk of aseptic cement loosening. Additionally, in the event of an infection in a cemented prosthesis, it becomes more challenging to remove and replace the prosthesis, especially if osseointegration has already begun. This is why advancements in implant technology and surgical techniques have made uncemented implants more popular, particularly in younger, more active patients, as they may provide better long-term outcomes and reduce the risk of complications associated with cemented implants. [19]

The experiments in this Master's thesis were carried out on polystyrene plates. It is interesting to note that other materials are also of interest, such as titanium (Ti).

Ti is the preferred material for implant manufacture due to its unique properties that enhance the longevity and effectiveness of prostheses. Compared to other metal alloys, like cobalt-chromium, Ti has lower rigidity, which ensures better load distribution with the host bone and minimizes stress shielding, a phenomenon that can cause bone atrophy and implant loosening. Its biocompatibility is excellent, as Ti integrates well with the body's physiological environment, is resistant to corrosion, and does not trigger immune responses or inflammation, thus reducing the risk of allergic reactions or local toxicity. [20]

Ti also excels in promoting osseointegration, encouraging bone cells to adhere to its surface, which is crucial for the long-term stability of cementless prostheses. Clinical studies have shown that Ti provides superior cell adhesion compared to other alloys, enhancing the bond between bone and implant. Additionally, Ti is compatible with hydroxyapatite coatings, which further improves bone adhesion and implant fixation. [20], [21]

2. Prosthetic joint infection

2.1 Occurrence and challenge

As previously mentioned, another important case of post-operative complication is PJI. Although only a small percentage of joint arthroplasties develop infections (approximately 1 to 2% of patients who have undergone hip replacement surgery), it is essential to recognize and manage them effectively to maintain or restore proper joint biomechanics and prevent unwanted complications, especially considering the number of cases expected to keep increasing in the years to come. All of this together makes PJIs a real burden for both individual patients and the global healthcare industry. [2]

A PJI occurs when the joint prosthesis and adjacent tissue become infected. Progress in understanding the epidemiology, diagnosis, treatment, and prevention of PJI over the past 25 years has resulted in improved outcomes for this complex infection and allowed to identify the main causes for such infection.

Firstly, the majority of PJIs occurring within the first year following the surgery are typically initiated by the introduction of microorganisms during the surgical procedure. This introduction can occur either through direct contact, or through aerosolized contamination of the prosthesis or surrounding tissue. Once these microorganisms encounter the implant surface, colonization takes hold. [2]

Another mechanism through which infection can start is the contiguous spread from an adjacent site in the body. In the early post-operative period, superficial surgical site infections may progress to involve the prosthesis, especially if there are incompletely healed superficial and deep fascial planes. However, contiguous spread can also occur later if the normal tissue is disrupted again due to trauma or surgery at a nearby location. Additionally, erosion of the implant through an impaired soft tissue envelope can predispose patients to a delayed onset of contiguous infection. [22]

Lastly, the prosthesis remains at risk of hematogenous seeding throughout the lifespan of the arthroplasty. This means that microorganisms can enter the bloodstream from other sites in the body and potentially seed the prosthetic joint, leading to infection. [22]

2.2 Economic impact

The economic impact of hip replacement failure cannot be overlooked. The costs associated with the management of PJIs are significant. The annual hospital cost associated with hip and knee PJIs in the USA was estimated: it could reach $1.85 billion by 2030, including $753.4

million for hip prothesis PJIs alone. These costs are mainly due to an increase in the number of cases, even though the incidence of PJI and the cost per case remained relatively constant from 2002 to 2017. [12]

A study conducted by S. Klouche et al. has shown that hip replacement revisions due to infection cost 3.6 times more than primary operations. These additional costs are mainly due to a longer hospital stay and rehabilitation, which requires significant human and material resources. [23]

These mentioned studies highlight the importance of developing effective preventive strategies and treatments to reduce PJI rates, and underlying economic burden after total hip and knee arthroplasties. As a last information to insist on the importance of the research on PJI, the economic burden of osteoarthritis accounts for up to 1-2.5% of the gross national product of Western nations. [24]

2.3 Infection-causing pathogens

2.3.1 Resistance, tolerance, and persistence

Before developing which microorganisms are at the forefront of PJIs, and therefore why is *S. epidermidis* the microorganism studied in this Master's thesis, a closer look will be taken on the term "resistance" and the other strategies (tolerance and persistence) used by bacterial cells to survive during exposure to antibiotics. These three strategies adopted by bacteria, and especially biofilm-forming bacteria, will be for now on referred as "recalcitrance", a term to group resistance, tolerance and persistence mechanisms together.

Resistance to antibiotics is typically caused by inherited mutations within the bacterial strain[2]. This defense behavior is associated with numerous molecular mechanisms that have been comprehensively studied through isolation and genetic characterization of antibiotic-resistant bacterial strains. The genes that are involved in these mechanisms are now commonly called the "resistome". Some of the most studied resistance mechanisms are described in a following section, including biofilm formation, the central mechanism studied in this Master's thesis. [25]

In practice, microorganisms that have acquired resistance for a specific antibiotic are able to grow at high concentrations of the said antibiotic. Mechanisms of bacterial resistance therefore decrease the effectiveness of the antibiotic. Indeed, a higher concentration of the antibiotic is required to produce the same effect in a resistant strain as for a susceptible strain. Resistance is quantified by the minimum inhibitory concentration (MIC) of the antibiotic, the minimum amount of antibiotic required to inhibit visual bacterial growth, irrespective of the duration of

[2] A bacterial strain is a genetic variant or subtype of a bacterial species. Strains can arise from small genetic variations within a species, often due to mutation, horizontal gene transfer, or adaptation to different environments. For example, *ATCC 35984* is a specific strain of *S. epidermidis* species.

treatment. The MIC, therefore specific for each strain and antibiotic, is experimentally determined. A bacterial strain with a higher MIC for one antibiotic will be considered more resistant to this particular antibiotic that to another one with a lower MIC. [26]

Unlike resistance, persistence and tolerance do not lead to an increase in the MIC compared with susceptible bacteria, as shown on *Figure 2(a)*. This lack of a quantitative indicator, such as MIC for resistance, results in tolerance to be poorly characterized, and often leads to the misclassification of tolerant strains as resistant, or vice versa, resulting in ineffective treatments. There is therefore a serious need for accurate definition and metric for tolerance and persistence in order to identify the different strategies used by bacterial cells to survive during exposure to antibiotics. Following this idea, a newly defined quantitative indicator of tolerance is the minimum duration for killing (MDK). [27]

Tolerance can be acquired through a genetic mutation or by environmental conditions and may be inherited, or not. The genes that are associated with increased tolerance are called the "tolerome". [25]

This survival strategy of bacteria is generally described as the ability of the microorganism to survive transient exposure to high concentrations (that far exceed the MIC) of an antibiotic without a change in the MIC. Tolerance is often achieved by slowing down an essential bacterial process (slow growth) resulting in a slower killing (*Figure 2(b)*). An example would be the slowing down of the cell wall assembly processes, being the target of several antibiotics. "Dormancy" is considered as an extreme case of slow growth. [25]

Resistance and tolerance, described above, are strategies adopted by a whole bacteria population while persistence only applies to a subpopulation. The surviving bacterial cells, the subpopulation persisting for a much longer period of time, are commonly called "persisters". [27]

In fact, some antibiotic treatments effectively kill the majority of the bacterial population but subpopulations, typically less than 1% of the bacterial population as shown on *Figure 2(c)*, survive exposure to high concentrations of an antibiotic, leading to an heterogenous response compared to susceptible strains, and a biphasic killing. The presence of a bimodal (or multimodal) time–kill curve that deviates from the simple decay expected from a uniform, non-persistent, bacterial population, allows the detection of persisters[3]. [25]

The slower rate of killing observed in the persistent subpopulation is not inherited. When isolated, regrown, and re-exposed to the same antibiotic treatment, persistent bacterial cells exhibit the same heterogeneous response to the drug as the original population, maintaining the division between the two phenotypes inside the population: susceptible and persistent. [25]

[3] Pure exponential killing of the susceptible strain is rarely observed because most bacterial cultures have some level of persistence. [24]

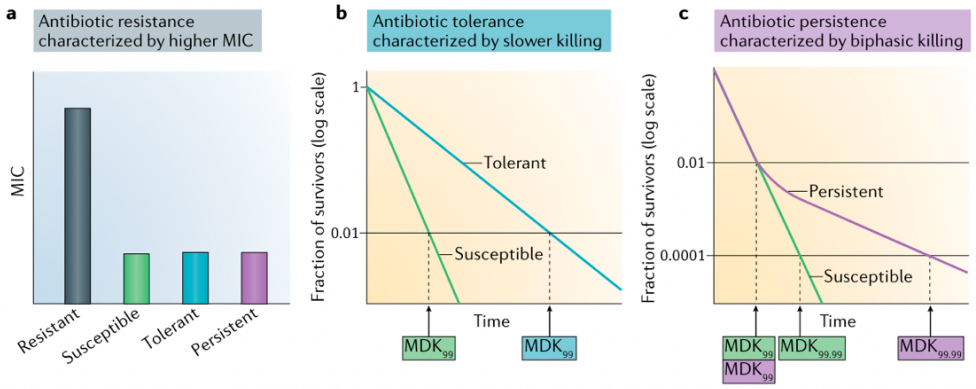

Figure 2: **Resistance, tolerance and persistence** are distinct responses to antibiotic treatment that lead to increased survival compared with susceptible cells. **(a)** To inhibit the growth of **resistant** bacteria, a substantially higher MIC of the antibiotic is needed than for susceptible bacteria. Notably, persistence and tolerance do not lead to an increase in the MIC compared with susceptible bacteria. **(b)** By contrast, **tolerance** increases the MDK (MDK; for example, for 99% of bacterial cells in the population (MDK99)) compared with susceptible bacteria. **(c) Persistence** leads to a similar MIC and a similar initial killing of the bacterial population compared with susceptible bacteria. However, the MDK for 99.99% of bacterial cells in the population (MDK99.99) can be substantially higher owing to the survival of the persistent cells. [24]

2.3.2 Identification of the common pathogens in prosthetic joint infection

A clinical study was carried out by Z. Li et al. to identify the most common PJI-causing microorganisms and to test the resistance spectrum against different antibiotics for each microorganism. Through the experiment, scientists have identified the pathogens at the origin of PJIs as being essentially Gram-positive bacteria and more precisely, *Staphylococci*. [28]

The experiment's microbiological cultures yielded positive results, and a total of 69 pathogen strains were isolated: 60 Gram-positive bacteria strains (86.96%), eight Gram-negative bacteria strains (11.59%) and one fungus (1.45%). Among Gram-positive bacteria, *Staphylococcus epidermidis* was the most common pathogen (27.54%), followed by *Corynebacterium* (10.14%), and *Staphylococcus aureus* (7.25%). [28]

S. epidermidis and *S. aureus* are bacteria known for their ability to form robust biofilms on implanted structures. This represents a major challenge in the treatment of PJIs, as already mentioned. *S. aureus* is notorious for its resistance to antibiotics. It is also the main cause of blood-borne infections in total knee arthroplasties, making them less receptive to treatment. [29]

2.3.3 *Staphylococcus epidermidis*

As the previously mentioned study has demonstrated, *S. epidermidis* is the most common PJI-causing pathogen. [28] *Staphylococci* are Gram-positive bacteria and traditionally present on human and other mammalian's skin and mucous membranes. Among them, *S. epidermidis* stands out as the most frequently encountered species on human epithelial surfaces, especially in areas like the axillae, head, and nares. [30]

While typically non-pathogenic, *S. epidermidis* can opportunistically cause nosocomial infections, especially on implanted medical devices, owing to its ability to form biofilms. These biofilms, multicellular surface-adherent agglomerates, pose significant challenges in treatment due to their high resistance and tolerance to antibiotics and host defenses. Such infections stem primarily from *S. epidermidis*' widespread presence on the skin, facilitating contamination of medical equipment. Despite their typically benign and non-fatal nature, the frequency and treatment-resistant nature of these infections pose significant challenges for healthcare systems. [30]

The virulence of *S. epidermidis* is primarily attributed to its biofilm formation and is kept relatively low compared to its cousin, *S. aureus*. Despite this, it significantly contributes to the persistence of the bacteria on medical devices and their resistance to therapeutic interventions. It is then vital to prevent and eliminate the biofilm to avoid recurrence of the infection, and allow joint replacement durability. [29], [31]

2.4 Biofilms

2.4.1 Biofilm formation

It is commonly known that a symbiotic, mutually beneficial, relationship exists between the human body and microorganisms. Nevertheless, under certain circumstances, infections can appear due to the formation of biofilms, a consequence of the incontrollable growth of these symbiotic microorganisms. [32]

Bacterial species such as *Staphylococci* form a biofilm that can attach to foreign surfaces, like implants, in a living organism. Biofilms are microorganisms communities, living biomass, possessing sophisticated social structure and able to live and reproduce themselves as a collective entity. [32]

Biofilm-forming bacteria or surface-adherent bacteria, oppose themselves to planktonic or free-floating bacteria. When bacteria attach to a surface, it triggers quick change in the expression of genes associated with maturation and production of extracellular polymeric substances (EPS). EPS are primarily composed of polysaccharides (glycocalyx), proteins, and extracellular DNA, serving to shield the cells from harmful environmental factors, including antibiotics and the host immune system. This transition between the non-adherent and biofilm-forming states initiates the immediate formation of this protective barrier, part of which is the glycocalyx, upon bacterial colonization of both living and non-living surfaces. [32]

The growth stages of biofilms encompass attachment of microbial cells to a surface, initial surface growth, biofilm maturation, and eventual detachment and dispersal. Mature biofilms exhibit a multicellular, non-homogeneous structure wherein microbial cells can communicate with one another, often through quorum sensing (QS). In this community, different subpopulations may serve different functions, collectively supporting the entire biofilm. [10]

Biofilm formation begins with the attachment of individual planktonic bacteria to the surface. The repulsion forces of the surface are countered by forces from the bacteria that allow it to irreversibly attach to the surface. This sticking ability from the bacteria is the result of the cumulative effect of hydrophobic, electrostatic, van der Waals, and protein adhesion forces. The formation of an external matrix of complex, multilayered biomolecules, and the formation of microcolonies, accompany the secretion of the EPS constituting this external matrix. Polysaccharide secretion in biofilm-forming strains facilitates aggregation, adhesion, and surface tolerance, enabling improved surface colonization. As biofilms mature, they acquire a three-dimensional structure based on the components of a self-produced extracellular matrix. Once fully matured, biofilms detach, allowing bacterial cells to return to a planktonic state and establish themselves in other locations. A schematized biofilm life cycle is illustrated below, on *Figure 3*. [32]

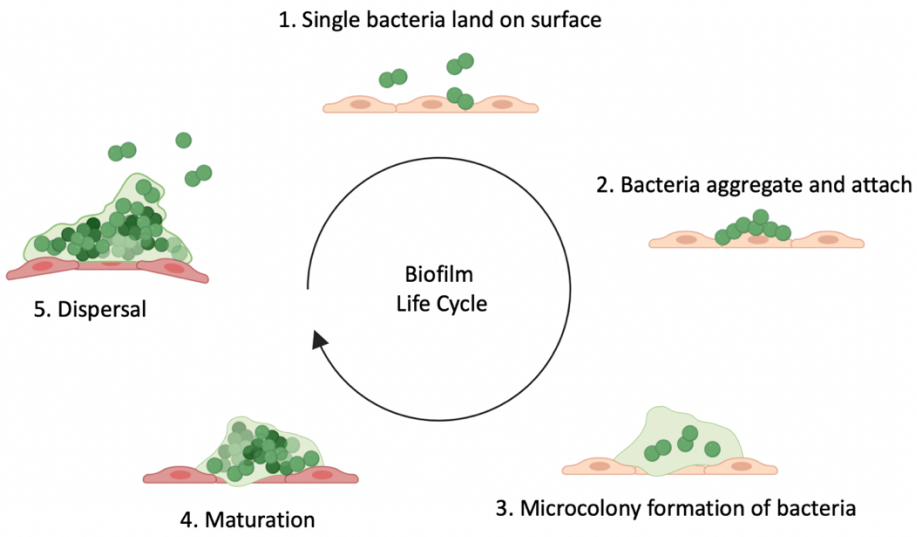

Figure 3: Schematic representation of **growth cycle of a biofilm** by a single bacterium species on a solid (living) surface.

Again, the extracellular matrix of biofilms is made of EPS, including exopolysaccharides forming the glycocalyx, but also proteins, lipids and extracellular DNA, with its composition varying among different organism types, and even within the same organism. [33]

Although the study of biofilms has historically focused on classic surface-attached structures, new research is demonstrating more nuanced and diverse patterns. It is essential to treat generalizations about biofilms with caution. The variations observed in their structures, the involved biochemical processes, and their interactions with the environment prove that each case of biofilm formation is unique, influenced by a multitude of both external and internal factors. So, while the traditional five-step approach *(Figure 3)* is useful from a pedagogical point of view, it may not fully reflect the complexity and diversity of biofilms, particularly under dynamic and heterogeneous environmental conditions. [34]

2.4.2 Mechanisms of recalcitrance in a biofilm

The resistance mechanisms in biofilms differ from the well-known plasmids, transposons, and mutations that provide inherent resistance to individual bacterial cells, essentially relying on genetic modifications, as explained above. In biofilms, resistance appears to rely on multicellular strategies such as the formation of a mechanically-hard to penetrate extracellular matrix, horizontal gene transfer (HGT), or QS. [10], [35]

As for tolerance, it has been suggested that cells within a biofilm exhibit a tolerance to antibiotics and AMPs that is 10 to 1,000 times greater than the tolerance of planktonic cells. While some antibiotics and AMPs exhibit a reduced ability to penetrate the biofilm matrix, the primary reason for the high tolerance of biofilms to therapeutic agents is the slowed down cell metabolism within the biofilm. Additionally, Staphylococcal biofilms in particular display a significant degree of cell heterogeneity, with distinct specialized subpopulations contributing to their high tolerance and the development of persistent cells subpopulations. [10]

This section is dedicated to review some of the most common recalcitrance mechanisms in biofilms. These multifaceted defenses highlight why biofilms are notoriously difficult to eradicate and why antibiotics often fail to clear infections involving biofilm-embedded bacteria.

2.4.2.a Hard-to-penetrate extracellular matrix

The production of the EPS matrix is one of the distinguishing characteristics of biofilms. It has been suggested that this matrix, among other functions, prevents the access of antibiotics to the bacterial cells embedded in the community. It consists of a physical barrier which allows shielding of the bacterial cells. EPS matrix is considered as a mechanism of resistance since it has been shown to decrease AMPs and antibiotics ability to penetrate the biofilm and display their bactericidal effect. [10], [36]

2.4.2.b Horizontal gene transfer

HGT occurs through three main pathways: transformation, transduction, and conjugation, and is a critical mechanism that contributes also significantly to the development of antibiotic resistance in biofilms. In these densely packed communities, the proximity and stable nature of the bacteria facilitate the efficient transfer of genetic material, including resistance genes. This transfer is notably more effective within biofilms than in planktonic bacterial cultures, making biofilms potent breeding grounds for the spread of antibiotic resistance. [5], [26], [37]

2.4.2.c Slow growth as a stress response

Nutrient scarcity more often occurs in biofilms than in planktonic bacteria, due to several factors intrinsic to the biofilm structure and environment, such as gradients within the biofilm, competition, or diffusion limitations inside the matrix. When they are starved of specific nutrients, phenomenon of slow growth in bacterial cultures takes hold, which is closely related to increased recalcitrance to antibiotics. [38]

This reduced growth rate is a common observation in mature biofilms. The link between nutrient scarcity and slow growth activates several mechanisms that collectively enhance bacterial tolerance and resistance to antibiotic treatments. Hereunder are two examples:

- Reduced metabolic activities: Direct consequence of nutrient limitation within biofilms. As bacteria downregulate their metabolic processes to conserve energy and resources, they also decrease the activity of cell systems that are typically targeted by antibiotics. These systems include cell wall synthesis, protein production, and DNA replication. [38]
- Gene expression changes: The stress of nutrient starvation triggers a sophisticated response in bacteria, characterized by altered gene expression. This adaptive response often involves the upregulation of specific genes associated with antibiotic resistance, such as those coding for efflux pumps and antibiotic-degrading enzymes. Efflux pumps expel antibiotic molecules from the cell, while degradative enzymes break down the antibiotic before it can exert its harmful effect. These changes ensure that the bacteria can not only survive in a hostile environment, but also resist the actions of antimicrobial agents. [38]

2.4.2.d Quorum sensing

Cell density and QS mechanisms are important in biofilm communities. High cell density enhances bacterial communication through QS, a process that regulates gene expression based on the local concentration of signaling molecules. This coordinated communication can lead to the increased production of molecules that fortify the biofilm's defense against antibiotics, such as the collective expression of resistance genes. [5], [38]

3. Infection prevention and antibacterial strategies

3.1 Asepsis measures

Several measures can be taken to avoid contamination of prostheses during surgery. These include controlling air quality in operating rooms, using laminar airflow to prevent bacteria from depositing on the prosthesis, and using ultraviolet (UV) light[4]. Of course, disinfection of skin, surgical instruments and orthopedic equipment is essential to avoid all kinds of potential

[4] UV light can help reduce contamination essentially through several mechanisms: direct microbial killing through DNA and RNA damage, sterilization of surgical instruments and air, and surface decontamination helping to maintain a sterile environment by continuously killing airborne pathogens, and those on surfaces that might be missed by conventional cleaning. Some studies suggest that UV light can inhibit the formation of biofilms.
Implementing UV light in surgical settings requires careful planning to ensure the safety of patients and medical staff, as direct exposure to UV light can be harmful for human tissues. [39], [40]

contamination. Human factor as the operating personnel also play an important role in prosthesis contamination and subsequent post-operative infections. [24]

These measures are designed to minimize the risk of contamination and are essential to prevent the formation of biofilms on implanted prostheses. Nevertheless, despite these precautions, contamination and underlying infection can still occur in 1 to 2% of the cases, an important percentage considering the millions of patients undergoing hip joint replacement every year. [2] Finding additional efficient methods like antibiotics or AMPs to prevent biofilm formation and treat formed biofilms is therefore crucial.

3.2 Antimicrobial treatment

3.2.1 Antibiotics and antimicrobial resistance

Antibiotics, described as "magic bullets" against bacteria, mark one of the most important medical breakthroughs of the 20th century. Their introduction revolutionized medical treatment, saving millions of lives from bacterial infections. Beyond their medicinal applications, antibiotics have become indispensable in fields such as animal breeding and agricultural production, acting as preventive measures in many countries for decades. However, the widespread and too frequent inappropriate use of antibiotics has led to the emergence of AMR. Antibiotics are compounds that inhibit bacterial growth or act as bactericides, playing a crucial role in the treatment of bacterial infections. Their MOAs include inhibition of cell wall synthesis, disruption of cell membrane, interference with protein synthesis, and inhibition of nucleic acid synthesis. With AMR on the rise, prudent use of these drugs and research into new classes of treatments are imperative to counter resistant bacterial strains. [41]

AMR allows microorganisms, such as bacteria, viruses, fungi, and parasites, to proliferate despite exposure to drugs designed to eradicate them. Infections caused by antimicrobial-resistant organisms pose significant challenges for treatment, increasing the risk of severe illness and mortality. Various types of antimicrobial agents, such as antibiotics, antifungals, antivirals, disinfectants, and food preservatives, are designed to either inhibit microbial growth (bacteriostatic) or completely eradicate microbes (bactericides). Among these, antibiotics are prominently used to combat bacterial infections, but their overuse contributes to the development of resistance.

AMR, an inevitable evolutionary process driven by genetic mutations, renders antibacterial drugs ineffective as bacteria adapt to survive to environmental conditions. The escalating use of antibiotics, particularly in developing countries, exacerbates the risk of AMR, leading to higher morbidity and mortality rates. The alarming rise in antimicrobial-resistant bacterial infections poses a silent pandemic, necessitating urgent interventions to safeguard global public health. AMR transcends borders, affecting individuals worldwide regardless of age or gender,

posing a significant threat not only to global health but also to food safety. The evolution and spread of AMR are influenced by a multitude of interconnected factors encompassing healthcare, agriculture, pharmaceuticals, waste management, trade, and finance, making it one of the most complex public health concerns. The rapid dissemination of "superbugs", microorganisms resistant to most known antimicrobials, amplifies the urgency of addressing drug-resistant pathogens. Recognizing its severity, the World Health Organization identifies AMR as one of the top three major public health threats, underscoring the critical need for collective action to minimize its impact. [42]

It is now obvious that relying heavily on antibiotics for treatment is not without drawbacks. Currently, it is imperative to explore alternatives that reduce antibiotic consumption. One such approach involves harnessing the synergistic effects between AMPs, like LL-37 in AMC, and traditional antibiotics to allow reduced use of antibiotics but reaching a comparable overall antibacterial result. LL-37 is known for its ability to disrupt cell membranes through pores formation, which can enhance the efficiency of intracellular-acting antibiotics by facilitating their entry into cells. This combined action may offer a more effective strategy for combating infections while minimizing antibiotic usage. [11]

3.2.2 Antimicrobial peptides

AMPs are key components of the innate immune system, playing an essential role in defense against pathogens. These peptides are produced by almost all living organisms, from microorganisms to plants, animals, and humans. AMPs are particularly interesting because of their broad spectrum of activity, their speed of action against microbes, and their ability to prevent the rapid development of resistance, which distinguishes them from traditional antibiotics. Structurally speaking, they can easily be part of an AMC. [43], [44]

The fact that microbial and multicellular organisms' membranes differ in their lipid composition allow AMP to be highly specific and weakly cytotoxic. In fact, bacterial membranes are rich in negatively-charged phospholipids, whereas multicellular organisms are zwitterionic. The overall negative charge of the membrane is largely due to the presence of lipopolysaccharides (LPS) and teichoic acids in the outer leaflet of Gram-negative and Gram-positive bacteria, respectively. Consequently, the cationic nature of AMPs accounts for their specificity against bacterial membranes. [45], [46]

The structure of AMPs varies considerably, but most share certain structural and physicochemical features that contribute to their antimicrobial activity. Typically, AMPs are composed of 10 to 50 amino acids (aa) and possess a structure that may include α-helices, β-sheets, loops, or a combination of these. These structures favor interactions with the lipid membranes of target cells. In addition, AMPs tend to be cationic (positively-charged) and amphipathic, enabling them to bind to the anionic (negatively-charged) cell membranes of microbes.

AMPs are characterized by their versatility of action against a wide range of pathogens, including antibiotic-resistant bacteria, viruses, fungi, and parasites. Their unique MOA and ability to target a broad spectrum of microbes make AMPs particularly promising potential therapeutic agents in the fight against drug-resistant infections. The ability of AMPs to prevent biofilm formation and to act against biofilm-forming microorganisms offers another major advantage over traditional antibiotics, which are often less effective against biofilms. [47]

These peptides primarily function by targeting the cell membranes of microorganisms through contact with lipids, causing disruption or lysis. AMPs can form pores within membranes, disturbing the cell's osmotic balance and ultimately cause cell lysis. The interaction between cationic AMPs and the negatively-charged microbial membranes enhances membrane permeability, which leads to the release of intracellular contents and cell lysis. This MOA provides a significant advantage over traditional antibiotics, particularly in the face of rising antibiotic resistance. [48]

Beyond their effect on the membrane, some AMPs are able to cross this barrier without damaging it, acting directly inside the cell. These other AMPs act by interfering with internal cellular processes, such as protein synthesis or DNA replication (i.e. Proline-Arginine-rich peptide with 39 aa - PR-39 and Human Neutrophil Peptide 1 - HNP-1), specifically targeting ribosomes or other components, like DNA or RNA (Buforin II), essential to cell processes. [48], [49],

In addition, some AMPs interact with cell wall precursors such as lipid II, inhibiting cell wall synthesis and causing cell death (i.e. Nisin). It is to note that enzymatic mechanisms are not usually targeted by the antimicrobial activities of AMPs. [48], [50]

AMPs therefore represent a promising avenue for the development of new antimicrobial therapies. Their unique MOA, their ability to modulate the immune response, their efficacy against biofilms and a variety of pathogens, and broad spectrum of activity offer significant advantages over traditional antibiotics, underlining their potential importance in the development of new antimicrobial strategies. [47], [51]

However, some resistance mechanisms to AMPs have already been observed in bacteria, including *Staphylococci* strains. The latter mechanisms include proteolytic degradation, cell wall alteration, and active secretion. *Staphylococci* also employ regulatory systems to enhance their resistance to AMPs. This consideration led scientific community to primarily focus on finding synergy between AMPs and other antimicrobial strategies, such as antibiotics, to fight bacteria and avoid development of further resistance in the susceptible strains. [10]

3.2.3 LL-37

LL-37 is the only peptide member of the cathelicidin AMP family in humans. LL-37 stands for the mature peptide, starting with two leucine residues (LL), containing 37 aa for a total of 4.5 kDa, and having a isoelectric point (pI) of 11. [52] Like the other AMPs, LL-37 plays a crucial

role in human innate immunity as being released from precursor proteins in tissues that first make contact with intruders. This peptide, naturally produced by many human cells, is known for its ability to combat a wide range of resistant and susceptible pathogens. These include Gram-positive and Gram-negative bacteria, along with other bacterial pathogens with undetectable or weak Gram staining results (i.e. *Mycobacterium tuberculosis*, *Mycoplasma pneumoniae*, etc.), or even yeasts. [46], [53], [54]

3.2.3.a Structure and activity

LL-37 is amphipathic with a strong net positive charge at physiological pH (pI = 11), enabling it to interact effectively with negatively-charged microbial membranes, as explained in the previous section. Numerous factors, including pathogen-associated molecular patterns and pro-inflammatory cytokines, can trigger the expression of LL-37 from its precursor, the human cathelicidin called hCAP-18, leading to the accumulation of a high concentration at the infection site. [55]

LL-37 has a secondary α-helical structure. In fact, in phosphate-buffered saline (PBS) solution, LL-37 exhibits an α-helical content of approximately 34%. The adoption of this α-helical conformation plays a crucial role in antimicrobial activities by enabling deep penetration into the bacterial cell membrane. The C-terminal LL-37 helix is not involved in antimicrobial activity of the peptide. In fact, the linear terminal tail residues 32–37 do not play a role in the peptide's interactions with bacterial membranes, as multiple studies have indicated through the truncation of residues 31–37 which did not impact the bactericidal activities of LL-37. In contrast, further truncation in the central helix, specifically in residues 17–31, does reduce the killing abilities of the peptide. [45]

The LL-37 α-helical structure is shown on *Figure 4(a)*. *Figure 4(b)* shows the organization of the aa in the amphipathic peptide structure. A quite obvious separation takes hold between hydrophobic aa, mainly non-polar hydrophobic (shown in yellow), and hydrophilic aa, mainly positively-charged (shown in blue) and negatively-charged (shown in red).

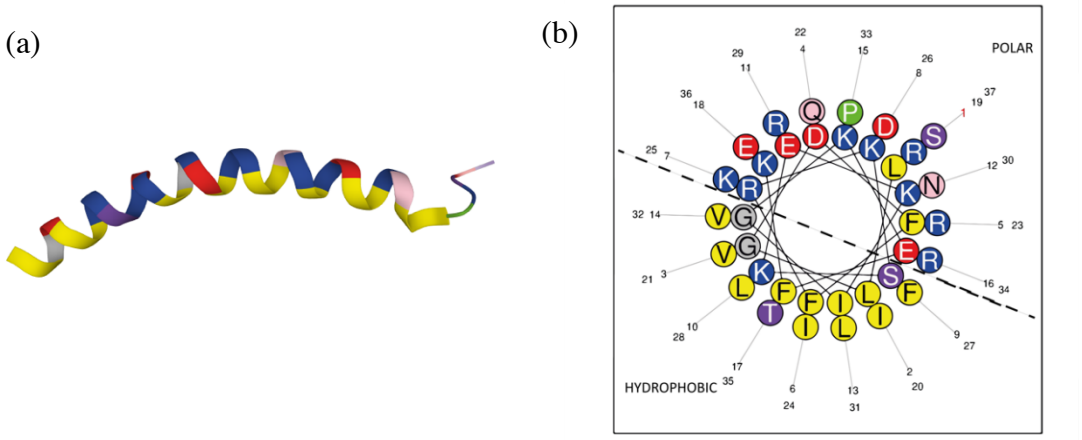

Figure 4: (a) **LL-37 α-helical structure**. (b) **LL-37 composition in aa** and subsequent separation between hydrophobic and hydrophilic parts of the peptide. The colors of the aa indicate: red = negatively charged (acidic), blue = positively-charged (basic), pink & magenta = polar uncharged, green, yellow & grey = non-polar. [56]

As mentioned before, this α-helical structure also helps promoting selectivity for the anionic membranes of bacteria over the zwitterionic membranes of mammalian cells, in addition to the net positive charge of the peptide at physiological pH (*Figure 5*). When binding to the bacterial membrane, LL-37's helicity increases, a commonly observed trait in lipid-binding AMP. [57], [58]

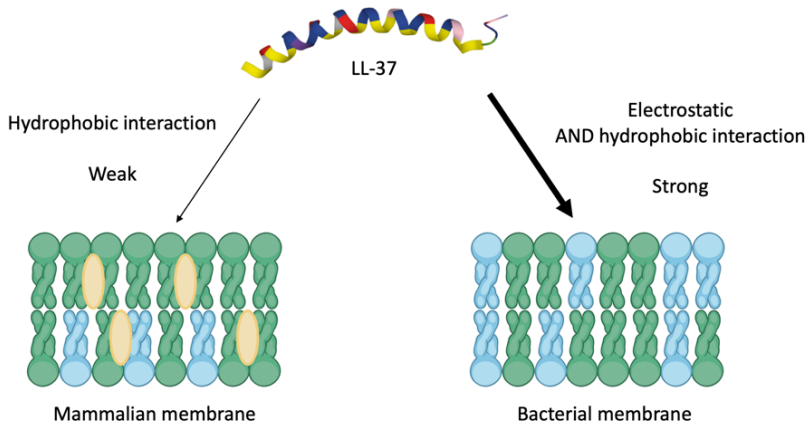

Figure 5: Mechanism of **selectivity of LL-37 AMP for bacterial cytoplasmic membrane** rather than for mammalian cells'. Negatively-charged phospholipids are shown in blue. Cholesterol is shown in light brown. [46]

LL-37 acts by disrupting microbial membranes, resulting in the formation of aqueous channels or pores that lead to hypoosmotic lysis and bacterial death. Circular dichroism (CD) and nuclear magnetic resonance (NMR) studies have provided valuable information on the α-helical conformation of LL-37 in solution and in interaction with membranes. These studies have shown that LL-37 adopts an α-helical structure in environments mimicking the presence of membranes, and aligns itself with the surface of model membranes, suggesting surface interaction with membrane lipids rather than transmembrane insertion. [53]

3.2.3.b LL-37 actions on biofilms

It was mentioned above that AMPs could be used as treatment as well as prevention for biofilms. In the case of LL-37, treatment of biofilm is made possible by its bactericidal effect explained above.

Additionally, in 2008, a study performed by J. Overhage et al. has demonstrated that LL-37 had also prevention role on biofilms of *Pseudomonas aeruginosa*, a previously unrecognized role. Their research has showed that subinhibitory concentration of LL-37, meaning concentration below the MIC, could already have a significant inhibitory effect on biofilms formation. They estimated the effect of 1/128 MIC to reduce 40% of biofilms biomass compared to biofilms formed in absence of LL-37 treatment. [59]

Lastly, LL-37 possesses other beneficial effects, including immunomodulatory activities, promoting wound healing, angiogenesis, chemotaxis and high-affinity binding to bacterial LPS, thereby neutralizing the inflammatory effects of LPS. [54]

3.2.3.c LL-37's MIC

LL-37 MIC was determined by Cédric Vranckx in the framework of its thesis[5]. Experiment was performed multiple times across a concentration range of 1 to 512 µg/mL. The MIC was finally determined as >512 µg/mL.

3.2.4 Antimicrobial coatings

New strategies focused on designing AMCs are under research to answer the problem of the rising number of nosocomial infections associated with implants and medical devices.

AMCs technologies are based on different principles to kill microorganisms on the top of the coated surface (i.e. prosthesis surface). According to a review in microbiology from W. Bäumler et al., AMCs can be classified in five main MOAs: anti-adhesive, contact-active, release of substances based, photocatalytic, and photodynamic (*Figure 6*). [60]

[5] MIC of LL-37 was determined for *S. epidermidis ATCC 35984* in RPMI medium as experiments of this Master's thesis were performed under these particular conditions (see *Materials and Methods* section).

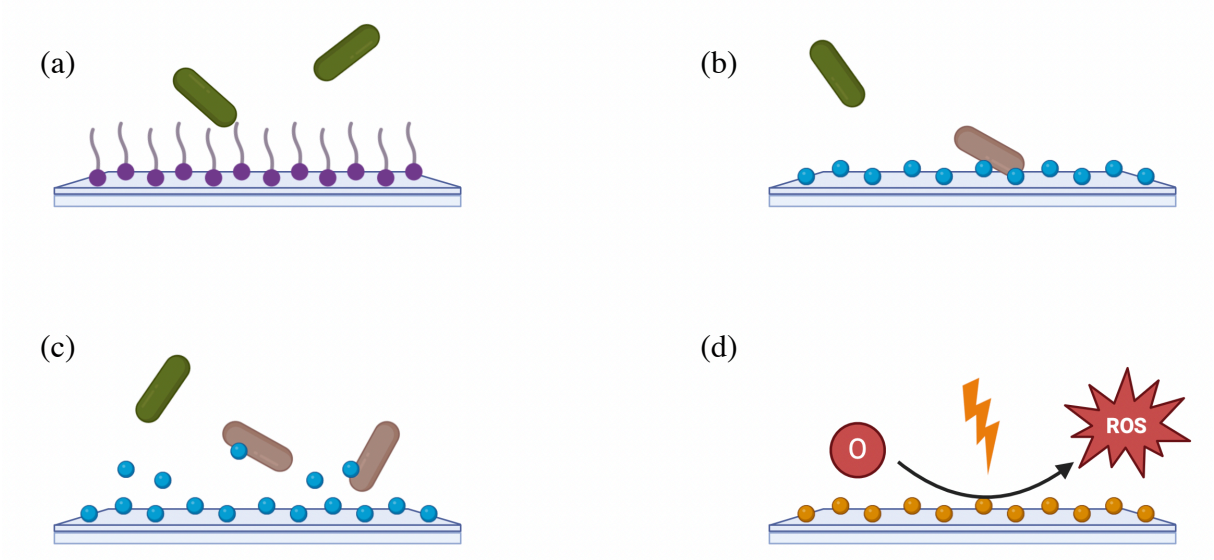

Figure 6: **Types of AMCs**. Alive bacteria are shown in green and dead bacteria are shown in brown. (a) **Anti-adhesive** coating. This coating repels bacteria attachment and avoid biofilm formation but has no biocidal activity. Example of repelling with polymer brushes. (b) **Contact-active** coating. Biocidal substances (blue) are chemically bound to the surface. (c) **Release-active coating**. Biocidal substances (blue) are released from the coating. (d) **Photo-active** coating. Biocidal substances are ROS derived from molecular O_2. [60]

As mentioned above, AMC can have anti-adhesive action. Super-hydrophobic surfaces and zwitterionic polymer brushes are some examples among others to delay or prevent attachment of the microorganism on the surface. AMC can also display a contact-active action through contact-killing of bacteria, which involves the antimicrobial agents being covalently bound to the surface without being released from the coating, most of the time quaternary ammonium compounds or copper as ions or nanoparticles. [60]

Photo-active AMCs use photo-activated molecules, most of the time ROS generated from molecular oxygen, for microorganism counteraction on environmental surfaces. Photocatalytic action is mainly obtained through TiO_2 absorbing UV radiation from (400 to 250 nm) and reacting with water and oxygen on its surface to generate mainly hydroxyl and superoxide radicals. Photodynamic action takes place when using photosensitizer absorbing visible light. Excited photosensitizer transfers the absorbed energy via its triplet state to adjacent molecules, including molecular oxygen leading to ROS generation. [60]

Other technologies rely on the release of the active biocidal agent from the coating such as antibiotics to provide local antibiotic prophylaxis directly at the implant-tissue interface to prevent initial infection[6]. In this research, we will be looking at the development of a LL-37-releasing coating, as a way to prevent and treat biofilm formation. The said peptide would be immobilized on the surface using two types of coatings, both built thanks to the LbL method. [58]

[6] Hydrogel coatings can be used to provide a physical barrier and controlled release of antibiotics at the implant. [57]

Note that even if this Master's thesis reviews widely AMPs and antibiotics as bactericidal agents, metals with antimicrobial properties are also widely used in AMCs. The antimicrobial properties of materials such as silver and copper (ions, nanoparticles) makes metal toxicity the most frequently published technology for AMC. [58]

Also, topographical and chemical modification of implant surfaces exist to create surfaces that minimize bacterial adhesion while promoting osseointegration. This is achieved by adjusting surface roughness, applying nanostructured coatings, and altering surface chemistry to influence interactions between the implant and bacteria or host cells. [58]

3.3 Coatings components and Layer-by-Layer self-assembly technique

In the development of antibacterial surfaces for prosthetic applications, the LbL technique proves indispensable due to its versatility in controlling the deposition of AMP such as LL-37. This method facilitates the assembly of polyelectrolytes (PEs) in layers through electrostatic interactions, along with hydrogen bonds and hydrophobic interactions, enhancing the chemical stability and robustness of the resulting films. These multilayered structures are not static; they continuously undergo molecular and chemical reorganization influenced by environmental conditions.

Hereunder is developed the LbL technique, and further, the PEs used in the two studied coating types ((bare -37-HEP)$_n$ and (PPCs-CHI)$_n$) are presented. A section on coating thickness presents the evolution of LbL coatings' growth evolution.

3.3.1 Layer-by-Layer self-assembly technique

The LbL technique is a versatile and powerful method to build a multilayered coating. This technique exploits electrostatic interactions to successively assemble oppositely-charged molecules on a surface (whether planar or colloidal). Among these charged molecules stand proteins, nanoparticles, PEs and DNA. The process starts by immersing a support material in a solution of positively-charged PE (polycation), which readily adsorbs to the surface. After a wash step to remove weakly attached PEs, a negatively-charged PE (polyanion) is adsorbed onto the now positive surface, followed by a similar wash (*Figure 7*). This repeatable sequence produces a PE multilayered film whose thickness and chemical composition can be controlled by the number of adsorption cycles. This self-assembled multilayered structure is formed only by alternating adsorption of PEs, and relies heavily on charge overcompensation with each new layer of adsorbed material, resulting in a surface charge inversion that allows adsorption of an additional layer of oppositely-charged material. [6], [25]

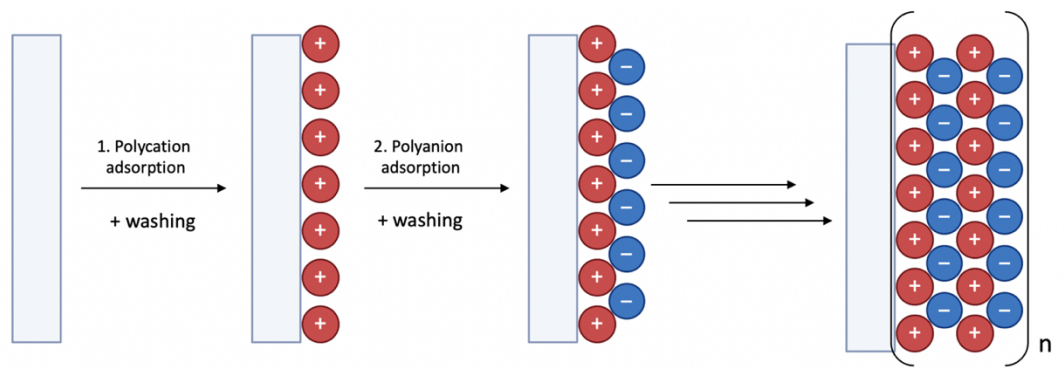

Figure 7**: LbL method**: step-by-step overview. The initial surface is modified with a charged layer. The surface is immersed in a polycation and a polyanion aqueous solution, respectively (i.e. protein, nanoparticles, PEs, DNA). [61]

In reality, electrostatic forces are not the only forces acting between PEs in a LbL coating. Forces in action include hydrogen bonds, and hydrophobic and hydrophilic interactions that contribute to layer stability. In addition, the formation of bridging bonds between layers enhances the chemical stability and robustness of the resulting films. [62]

Even if oppositely-charged layers assemble spontaneously, this LbL arrangement is not thermodynamically stable. Alternatively put, the film would not spontaneously arrange itself like a succession of layers if the solutions were put together all in once. The thermodynamically unstable construction then depends on the order of the operations, such as altering the charged solutions, including a washing step between each step, and preparing PPCs solutions in advance. Indeed, PPCs are not thermodynamically stable structures either (see section *3.3.3. Protein-Polyelectrolyte Complexes* for better understanding). There is therefore a need for preparing complexes by mixing the components before adsorption and adsorbing the building blocks sequentially. For this reason, the PPCs solution is prepared prior to adsorption.

Moreover, the obtained LbL film is not "perfectly stratified". These multilayers are not just the result of successive stacking of layers; as said before, they are also shaped by factors such as pH, ionic strength and temperature, which influence the interactions between the PEs and can induce predominantly exponential or linear growth of the films (see section *3.3.4 Coating thickness, exponential versus linear growth*). [63]

3.3.2 Polyelectrolytes

Polymers known as PEs are indispensable in LbL coatings due to their unique ability to dissociate into highly-charged polymeric molecules when exposed to an ionizing solvent, like water. This dissociation creates polymers that are either positively-charged (polycations), negatively-charged (polyanions), or both (polyampholytes). The intrinsic charges on the repeating units of these polymers are counterbalanced by smaller ions of the opposite charge, ensuring the maintenance of overall electro-neutrality within the system.

Natural polymers, such as proteins, chitosan (CHI), and heparin (HEP), are examples of PEs that exhibit variable properties influenced by environmental conditions such as pH and ionic

strength. For instance, proteins are polyampholytes, featuring both positively- and negatively-charged groups among their polypeptide chains. Variations in pH can cause these groups to protonate or deprotonate, significantly altering the proteins' electrostatic interactions, solubility, conformation, and overall functional activity. Similarly, CHI and HEP, also categorized as natural PEs, display properties that are depending on the nature and charge of their functional groups and how these groups interact with surrounding ions. Recognizing these dynamics is crucial for tailoring the LbL construction process, particularly by carefully monitoring the pH and ionic strength to optimize the functionality and stability of the resulting AMC. [64]

3.3.2.a Heparin

HEP, approved in 1935, is the world's oldest and most widely used anticoagulant. This PE is a highly sulfated linear glycosaminoglycan[7] (GAG) with a wide range of molecular weight (M_W) as HEP is a polydisperse mixture of GAG chains of varying lengths. Distributions of charge density of HEP also varies since the degree of sulfation is not uniform and different chains can have different charge densities.

These structural properties enable HEP to interact selectively with multiple proteins, leading to diverse pharmacological functions such as anticoagulant, antiviral[8], and anti-inflammatory[9] activities. Its anticoagulant activity is the result of the selective binding of HEP with the serine protease inhibitor antithrombin-III whose role is to inhibit thrombin (factor IIa) and other proteases involved in the coagulation cascade, such as factors IXa, Xa, XIa, and XIIa. The binding of HEP to antithrombin-III significantly enhances its anticoagulant activity. [65]

Such biocharacteristics make of HEP an interesting choice for being part of an AMC. Along with these medical advantages, HEP has the highest negative charge of all biological polyanions because of its high content in sulfonate (pKa 0.5 - 1.5) and carboxyl groups (pKa 2 - 4)[10], making it a very promising candidate for LbL technique. [65], [67]

This natural PE's backbone is composed of a repeating sulfated disaccharide unit linking α-L-iduronic acid (IdoA) or β-D-glucuronic acid (GlcA) to D-glucosamine (GlcN), with a trisulfated disaccharide unit GlcNS6S (1→4) IdoA2S as the major repeating unit. [65]

Figure 8 shows how HEP displays a negative net charge. This molecule will be used as polyanion to immobilize the net positively-charged bare LL-37 peptide in the LbL built coating

[7] HEP is obtained from animal tissues (i.e. pig intestinal mucosa and bovine lung). [65]
[8] HEP is undergoing research for its potential antiviral activity, as being a structurally competitive inhibitor for pathogens' binding on heparan sulfate, target for pathogens adhesion and invasion on host cell surface. [65]
[9] It is thought that HEP shows anti-inflammatory activities by binding to IFNγ cytokine. [66]
[10] As a reminder, pKa value gives information about the ionization state of individual acidic and basic groups on the molecule. The net charge of the PE is obtained by summing the charges of all ionizable groups. When pH is above pKa value, the groups are deprotonated. In this case, the small pKa values of the ionizable groups of HEP means they are mostly deprotonated, in this case negatively-charged, for the pH used for this research.

(bare LL-37-HEP)$_n$ as well as for protein-polyelectrolyte complexes (PPCs) formation, as explained in the section *3.3.3 Protein-Polyelectrolyte Complexes*.

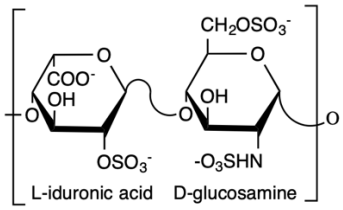

Figure 8: **Structure of HEP** major repeating unit (disaccharide). [65]

3.3.2.b Chitosan

CHI is a derivate from a partial deacetylation of chitin, and is the next most abundant natural polysaccharide after cellulose. This biopolymer is a linear polysaccharide composed of glucosamine (GlcN) and N-acetylglucosamine (GlcNAc) residues linked by β(1→4) bonds. *Figure 9* shows the deacetylation of chitin into CHI. Functional groups of CHI such as hydroxyl and amide groups allow interactions, making it a promising component for CHI -based architectures such as LbL. [67], [68]

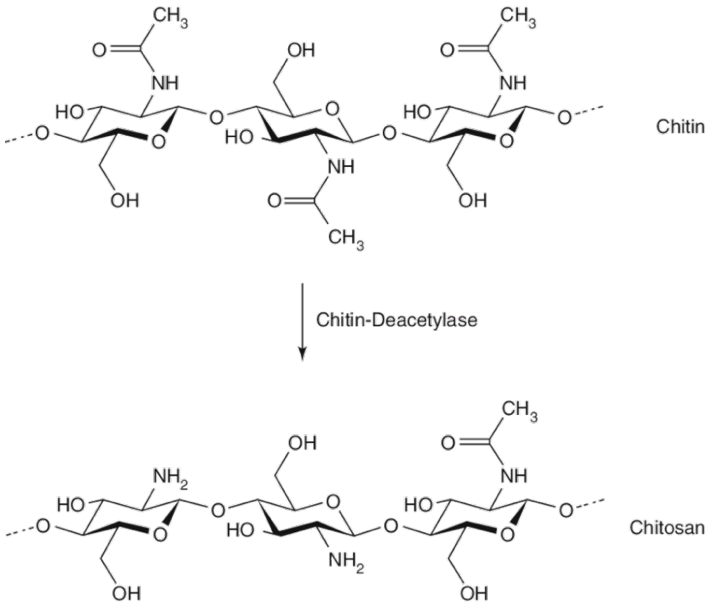

Figure 9: **Deacetylation of chitin** to form CHI. [69]

Soluble in acidic media thanks to the protonation of its primary amine groups (pKa 6.5), CHI stands out for its unique biological and technological properties, which depend on two factors: its M_W and its degree of deacetylation. CHI has, among others, anti-inflammatory, antioxidant, antimicrobial and antifungal properties. This PE is the only natural polycation, with a charge density influenced by its degree of deacetylation and the pH of the medium. Its solubility is essential for its applications. [68]

The biological properties of CHI are crucial for a variety of therapeutic and industrial applications. CHI's antimicrobial activity is particularly notable against a wide range of

microorganisms, including bacteria, fungi, and yeasts. This activity is attributed to the interaction of CHI's amine groups with the cell membranes of microorganisms, affecting their permeability and function. Due to these properties, it is interesting to use CHI in an AMC. [70]

3.3.3 Protein-Polyelectrolyte Complexes

The immobilization of proteins is quite straightforward due to their ability to spontaneously adsorb on surfaces. However, controlling the peptide charge can be challenging due to their polyampholyte nature, and this spontaneous adsorption may affect the protein functionality through conformation and orientation changes.

As explained before, PEs macromolecules display a uniform charge and exhibit flexibility. Proteins, however, are polyampholytes with differing degrees of charge anisotropy[11], and low conformational entropy[12]. Consequently, the growth of the multilayered coating may be affected based on the protein, PE, pH, and ionic strength used for the assembly. This effect is primarily attributed to the absence of charge overcompensation by the protein layer, resulting in repulsion between the further adsorbed PE and the protein patches of similar charge, resulting in a lower quality adsorption of the next layer and lower adsorption of PEs in the coating overall.

Considering this, PPCs are good candidates to serve as versatile and robust building blocks for LbL coating. Indeed, the charge of the protein can be normalized by electrostatic complexation with a PE, and the architecture and charge of the resulting PPCs can be more closely controlled. PPCs with a given charge and PE crown can be obtained and further used in the LbL coating $(PPCs\text{-}CHI)_n$. They provide a way to "standardize" the charge of the peptide and are free to interact with the oppositely-charged PE of the AMC. These complexes, measuring a few hundred nanometers, are colloidal particles. Their apparent charge, which can be positive or negative, influences their behavior in solution, where forces of attraction or repulsion dictate the movement of these complexes. [9]

PPCs allow the crucial conservation of the protein bioactivity through protein structure conformation in a more hydrated and preserved environment. In this Master's thesis, the protein to be used is LL-37, displaying a net positive charge, and it is complexed with HEP to create a crown, leading to apparent negatively-charged PPCs (*Figure 10*).

[11] In the case of proteins, charge anisotropy refers to the uneven distribution of charged aa residues within the protein's three-dimensional structure.

[12] Conformational entropy refers to the degree of freedom or disorder associated with the possible conformations (shapes) a molecule can adopt while maintaining its overall, or primary, structure. A low conformational entropy indicates that the molecule has fewer possible conformations available to it, which usually occurs when the molecule is constrained or restricted in its movements. This restriction in conformational flexibility can have implications for various biological and chemical processes, such as protein folding. [71]

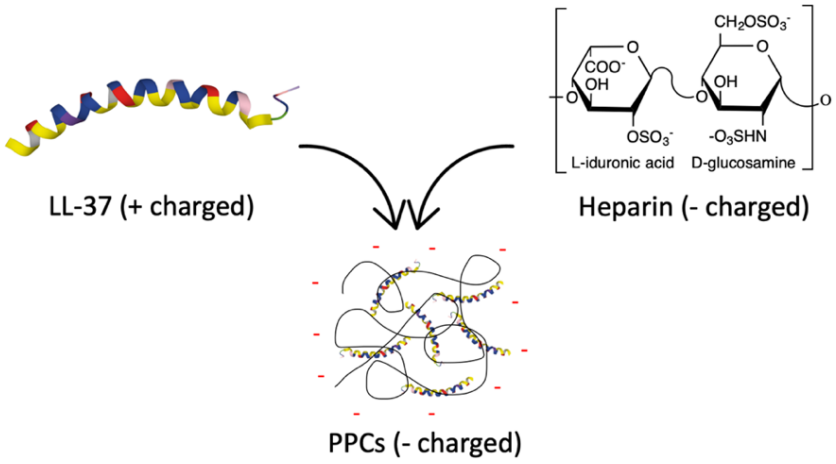

Figure 10: **PPCs formation** through LL-37 complexation with HEP.

For PPCs use in a coating, pH and ionic strength must be closely monitored since they significantly influence PPCs formation and assembly. Indeed, an experiment performed by A. vander Straeten et al., involving PPCs formed by lysozymes and poly(styrenesulfonate) (PSS), demonstrated that low pH and low ionic strength result in highly negatively-charged PPCs. [9]

The effect of pH on the formation of PPCs can be attributed to lysozyme molecules having a pI of 11. At lower pH values, lysozyme becomes more positively-charged, enhancing its interaction with the negatively-charged PSS. This strong net positive charge on the protein favors the formation of PPCs due to the increased electrostatic attraction between the protein and the oppositely-charged PE. [9] pI of LL-37 being around 11 too, a similar effect can be expected.

Conversely, higher ionic strength leads to significant charge screening, which reduces the electrostatic interactions between the protein and the PE, thereby hindering complex formation. [9]

PPCs formation, such as the size and number of complexes, will differ according to protein and PE concentration, ionization degree, charge distribution, hydrophobicity, ionizable group nature, and M_W.

Charge ratio of PPCs specifically denotes the proportion of negative charges (from either the protein or the polyanion component, here polyanion HEP) to positive charges (from either the protein or the polycation component, here LL-37 peptide), in the case of a -/+ charge ratio[13], within the complex.

However, PPCs charge distribution representations can be misleading. Indeed, -/+ charge ratio above 1 does not mean that negative charges, even in greater numbers, are on the outside of the complex, enveloping positively-charged peptide. As a matter of fact, PPCs are not in

[13] If the ratio is balanced (1:1): The complex is likely to be electrically neutral overall.
If there is an excess of negative charges (-/+) > 1: The complex may exhibit an overall negative charge.
If there is an excess of positive charges (-/+) < 1: The complex may exhibit an overall positive charge.

thermodynamic equilibrium and do not organize themselves spontaneously. Former ζ potential[14] measurements, performed by Cédric Vranckx, allowed to define charge distribution of PPCs and a negative outer corona is observed near 1.5 -/+ charge ratio. Charge ratio of PPCs will be studied and the confirmation of the previously determined optimal charge ratio for PPCs synthesis will be part of this Master's thesis experiments.

It is to note that, from now on, LL-37 complexed with HEP will be referred to as "PPCs" and non-complexed LL-37 will be referred to as "bare LL-37". If the wide term LL-37 is used, the latter will refer to the AMP in general, whether complexed or not.

3.3.4 Coating thickness, exponential versus linear growth

In the case of linear growth, the thickness of the films increases uniformly with each new added layer, thanks to robust interactions between the PEs that ensure complete coverage of the surface without the molecules significantly penetrating the lower layers. In contrast, exponential growth occurs when the PEs interpenetrate more intensely, allowing deeper and more extensive integration into existing layers. This rearrangement can expose more charged sites, increasing the number of available charges that can interact electrostatically with the subsequently added layer of oppositely-charged PE.

Figure 11 represents the evolution of film thickness according to the number of bilayers (BLs) for three different coatings studied by J. Borges and J. Mano on their research on the molecular interactions driving the LbL of multilayers. The evolution is linear for $(PEI/MTM)_n$ and exponential for $(PEI/PAA)_n$. Linear and exponential growth modes significantly affect the structural and functional properties of LbL films. Linearly grown films tend to have more defined and controlled layer structures. In contrast, exponentially grown films may exhibit improved mechanical properties due to layer entanglement, or enhanced functionality due to a larger active surface area. [63]

[14] ζ potential gives information about the charge of the ions surrounding the particle. Colloids in solution will then repel each other if they have a large negative or positive ζ potential. In the case of PPCs used in this research, such measurements give an indication about the apparent charge, or the charge of the outer region of the PPCs. [72]

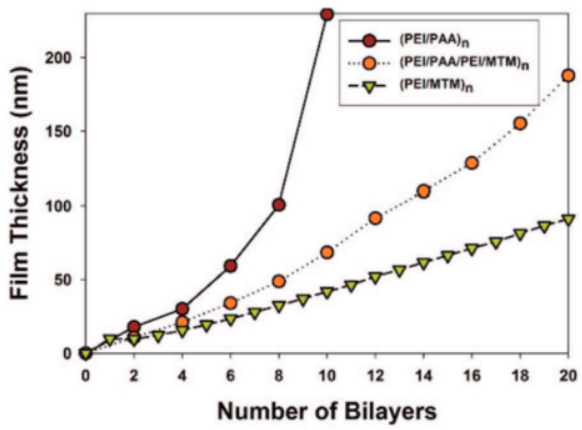

Figure 11: **Thickness evolution of linearly and exponentially growing LbL films** as a function of the number of layers, with and without MTM, measured by ellipsometry on a silicon substrate. PAA is poly(acrylic acid) / PEI is poly(ethylenimine) / MTM is Na+-montmorillonite. [63]

Increasing temperature tends to favor an exponential growth pattern by enhancing the mobility of PE chains, allowing more active and deeper intercalation into pre-existing layers. pH modifies the charge of PEs, affecting their interactions. Depending on the PE's pKa[10], pH can decrease its charge (by protonation of basic groups or deprotonation of acidic groups), reducing strong electrostatic interactions and encouraging less structured and more dynamic interactions. If pH significantly diverges from the pKa, the PE may lose its charges entirely, leading to a complete cessation of electrostatic-based interactions within the multilayered structure. [63]

On the other hand, an increase in ionic strength can shield electrostatic interactions between PEs, decreasing structured organization and encouraging more disordered, or even exponential, growth. Indeed, a high ionic strength allows greater freedom for PE chains to interpenetrate, leading to a significant increase in film thickness. [63]

The use of PEs in the LbL technique offers an exceptionally flexible method of modifying surfaces for a variety of applications, including the controlled release of drugs, the creation of antibacterial surfaces, or the enhancement of materials' compatibility with biological tissues, all of this having the major advantage of being achievable under soft conditions. [73]

However, in the case of the present research, immobilizing proteins on prosthetic surfaces presents several technical challenges, including protein stability, orientation, and bioactive activity after immobilization. Proteins, being complex macromolecules, can easily lose their native conformation when attached to a surface, which can lead to a decrease in their biological activity. Furthermore, the efficiency of binding between the protein and the surface can be affected by environmental conditions such as pH and salinity, which can limit the effectiveness of coatings under in vivo conditions. These concerns can apply to many proteins such as enzymes, antibodies, etc. [74]

3.4 Synergy between LL-37 and antibiotics

3.4.1 Expected effects

The synergistic effects of combining AMPs, such as LL-37, with traditional antibiotics offer a promising approach to improving infection control while mitigating the disadvantages generally associated with antibiotic therapy, as well as preventing development of resistance mechanisms regarding AMPs if used in too high quantity. This collaboration between AMPs and antibiotics could lead to a synergistic effect that significantly exceeds the additive contributions of each component independently. In particular, LL-37 enhances the efficiency of antibiotics by disrupting the integrity of microbial membranes, thereby increasing their permeability and making bacterial cells more sensitive to these agents.

This dual-action mechanism does not only facilitate the collapse of bacterial defenses more effectively than either agent alone, but also enables antibiotic doses to be reduced. Consequently, this reduces potential undesirable side effects, such as the development of antibiotic resistance. In our research, we will specifically explore the synergy of LL-37 with four antibiotics: vancomycin, tobramycin, doxycycline, and linezolid. By taking advantage of the unique properties of AMPs and antibiotics, this integrated approach aims to improve treatment efficacy and to reduce the risks associated with high doses of antibiotics, offering a more effective strategy in the fight against infections. [44]

3.4.2 Vancomycin, tobramycin, doxycycline, and linezolid

3.4.2.a Vancomycin

Vancomycin is a therapeutic agent used to treat serious infections caused by Gram-positive bacteria such as *Staphylococci*. This drug belongs to the class of tricyclic glycopeptide antibiotics, which act on cell wall synthesis. Glycopeptides then act outside the membrane, and are used to combat and prevent a spectrum of bacterial infections specific to Gram-positive strains, and as a prophylactic measure, against infections in joint prostheses. [75]

The MOA of vancomycin on bacteria takes hold through peptidoglycan biosynthesis inhibition. This antibiotic disrupts peptidoglycan polymerization, essential to bacterial cell wall synthesis, and structure. Since peptidoglycans are present on the vast majority of bacteria and nowhere else, this makes the inhibition of its synthesis a key mechanism for bacteria killing. [75]

The bacteria cell wall is composed of a robust network of peptidoglycan chains, featuring repeating units of N-acetylmuramic acid (MurNAc) and N-acetylglucosamine (GlcNAc). Vancomycin's mechanism is to bind to the D-alanyl-D-alanine (D-Ala-D-Ala) groups of the peptidoglycan molecule, thereby disrupting the action of enzymes such as glucosyltransferase, which is crucial for peptidoglycan synthesis, and lipid transporters, essential for the assembly and integration of MurNAc and GlcNAc into the cell wall. This blockage disrupts the integrity of

the cell wall, triggering the leakage of cell contents, leading to bacterial cell death. Under normal circumstances (without vancomycin), a bacterial enzyme catalyzes the formation of a cross-link between the pentapeptide of one disaccharide chain and the D-Ala of the neighboring chain to reinforce the cell wall. In the presence of vancomycin, the antibiotic prevents this reaction by binding strongly to the D-Ala-D-Ala ends of the pentapeptides. This binding disables the formation of pentaglycine cross-bridges. This weakens the cell wall and prevents bacterial growth. [76], [77]

The GlcNAc-MurNAc disaccharide chains are represented on *Figure 12* by the light purple and pink hexagons connected in a long chain. These chains form a mesh that is linked by pentaglycine cross-bridges. This structure lends a certain rigidity to the bacterial wall. [77]

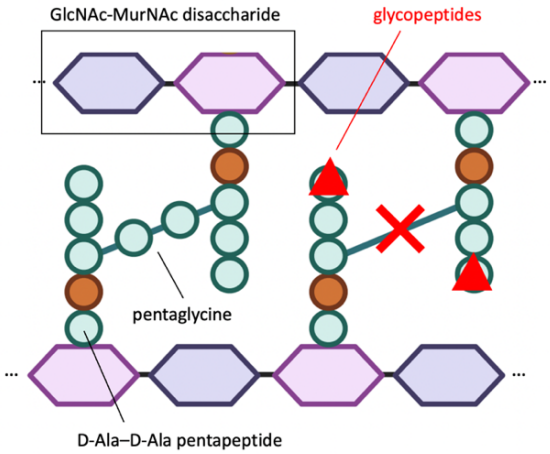

Figure 12: **MOA of vancomycin** (glycopeptide). By binding to the C-terminal D-Ala-D-Ala residues of the pentapeptide, glycopeptides inhibit the cross-bridge formation between pentapeptide and pentaglycine. GlcNAc = N-acetylglucosamine, MurNAc = N-acetylmuramic acid. [77]

Vancomycin is an antibiotic that has been used as a last resort medication in the treatment of infections caused by Gram-positive bacteria. Unfortunately, the number of vancomycin- resistant microorganisms has increased.

3.4.2.b Tobramycin

Tobramycin is an aminoglycoside antibiotic used to treat a variety of bacterial infections. This drug is effective against Gram-negative bacteria, and some Gram-positive bacteria. As all aminoglycosides, tobramycin inhibits protein synthesis. Antibiotics involved in protein synthesis are very different structurally but act similarly: they block ribosomes “pockets” intended for bacterial RNA synthesis by lodging themselves inside these pockets. [78]

In normal conditions, ribosomes move along the messenger RNA (mRNA) and add the appropriate aa one by one to form a polypeptide chain, then folding into a functional protein. Tobramycin induces misreading of the mRNA template, resulting in the incorporation of incorrect aa into the growing polypeptide chain. The result is a malformed and non-functional protein,

which causes the death of the bacteria, which can no longer supplement itself with working proteins. [78]

Figure 13 is an overview of the tobramycin mechanism, showing a ribosome and its two subunits: the 30S subunit and the 50S subunit. Ribosomes allow cells to read mRNAs to synthesize proteins useful for cell function. Tobramycin (represented by the red triangles in the image) binds irreversibly to the 16S rRNA of the bacterial 30S ribosomal subunit and this binding interferes with the formation of the initiation complex between mRNA and the 30S subunit. This impairing of proofreading results in the production of faulty proteins. [78]

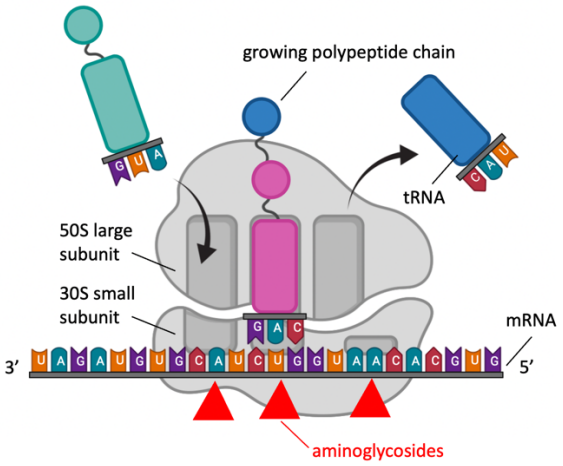

Figure 13: **MOA of tobramycin** (aminoglycoside). Site of inhibition on the prokaryotic ribosome by the drug aminoglycoside, which has a general effect of blocking the protein synthesis. [79]

Tobramycin is highly effective against aerobic Gram-negative bacteria, with a rapid bactericidal effect. It can act against multi-resistant bacteria. Thanks to its broad spectrum of action, tobramycin is a powerful agent for treating complicated infections and reinfections. [80]

3.4.2.c Doxycycline

Doxycycline is an antibiotic belonging to the tetracycline antibiotics family. It is synthesized from a compound naturally present in the *Streptomyces* bacterial species. As a member of tetracyclines, doxycycline is designed to combat a wide range of bacterial infections (both Gram-negative and Gram-positive) by inhibiting the production of proteins necessary for bacteria to grow and multiply. [81]

Doxycycline inhibits protein synthesis by binding to the 30S subunit of the ribosome, just as tobramycin does, but inhibits the attachment of tRNA to mRNA, as depicted in *Figure 14*. This mechanism prevents aa from being added to growing protein chains, and stops protein production, eventually preventing bacterial growth. This antibiotic is also being studied for its potential anti-cancer properties. Some evidence suggests that doxycycline may inhibit the growth of cancer cells and induce malignant cell death. [81]

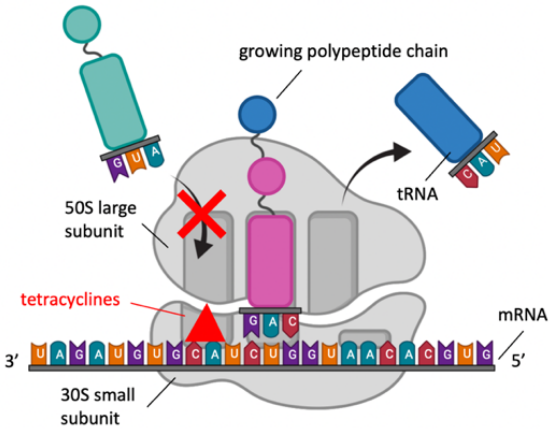

Figure 14: **MOA of doxycycline** (tetracycline). Tetracyclines reversibly bind to the 30S subunit of the bacterial ribosome, which prevents acyl-transfer RNA (tRNA) from binding to the ribosome. Thus, protein synthesis is ceased which stops growth and replication of the bacterial organism, producing a bacteriostatic effect. [82]

In conclusion, tobramycin and doxycycline are both antibiotics that inhibit the protein synthesis of bacteria but have a different mechanism of action. Tobramycin is found at the 30S subunit of the bacterial ribosome and causes misreading of the mRNA, leading to the creation of malformed proteins and therefore death of the bacteria. Doxycycline also binds to the 30S subunit but blocks access of the tRNA, which corresponds to stopping the addition of aa to the nascent protein. It is effective against a wider range of bacteria, both Gram-positive and Gram-negative.

3.4.2.d Linezolid

Linezolid is an oxazolidinone antibiotic, antibiotics that are a fully synthetic class of bacteriostatic agents. Oxazolidinones bind to the 50S ribosomal subunit, and therefore also inhibit the biosynthesis of bacterial proteins. [83]

Linezolid prevents the formation of the protein synthesis initiation complex by binding to rRNA and thereby reducing the length of developed peptide chains and lowering the rate of translation elongation reactions. It specifically targets protein synthesis in Gram-positive bacteria by binding to ribosomal RNA in the 50S subunit of the ribosome. This mechanism is not as effective against Gram-negative bacteria, as there are structural differences in their ribosomes, and their outer membrane limits the drug's access to ribosomal targets. [84]

Figure 15 shows the different parts of the ribosome and how the antibiotic linezolid interacts with them. On the left, we see the 50S subunit of the ribosome which, together with the 30S subunit, forms the complete 70S ribosome complex of bacteria. On the right is the 70S initiation complex, a combination of the 30S and 50S subunits attached to an mRNA strand. In the presence of linezolid, this structure cannot take shape, as the antibiotic binds to the 70S subunit and inhibits its formation. This binding inhibits a crucial step in bacterial protein synthesis, thus exerting its antibacterial effects.

Linezolid was previously used to treat bacteria resistant to antibiotics like vancomycin. However, at the start of the 21st century, reports emerged of a resistance mechanism against linezolid, involving changes to the antibiotic's binding site in the bacteria. This resistance mechanism, known as alterations in the binding target, has been identified in several bacterial strains. [85]

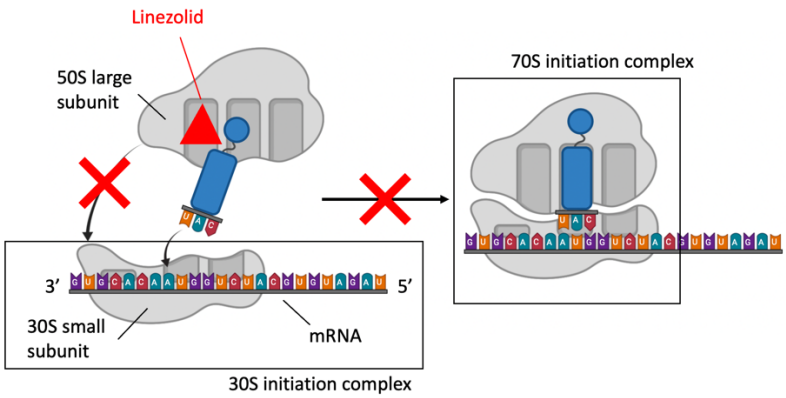

Figure 15: **MOA of linezolid** (oxazolidinone). By binding on the 50S large subunit of the ribosome, linezolid disables the binding of the 50S subunit with the 30S initiation complex, and therefore the 70S initiation complex formation.

PART III – Objectives and Strategies

1. Objectives

The objective of this Master's thesis is to study the activity of the LL-37-based AMC. This activity will be studied in two ways, and this section develops the two subsequent objectives followed.

The AMC is considered as being release-active, meaning its activity against bacteria is displayed through release of antimicrobial agent, here LL-37. Therefore, we firstly attempt to determine the conformation of LL-37 when released from two types of LL-37-based coatings: (bare LL-37-HEP)$_n$ and (PPCs-CHI)$_n$. As it is widely explained in the *State of the art*, the conformation (α-helical structure) plays a crucial role in this AMP's MOA. This first objective then pursues to assess AMC's activity through the determination of the secondary structure of LL-37 when released and, consequently, encountering bacterial membranes.

Activity of the AMC is then secondly assessed by studying the activity of LL-37 when put together with four traditional antibiotics: vancomycin, tobramycin, doxycycline, and linezolid, to determine whether there is or not an interaction between the AMP MOA and their respective MOAs. In fact, as LL-37's MOA mainly targets bacteria membrane, when it is under its α-helical structure, a possible interaction with the MOAs of the antibiotics suggests a possible synergistic effect. Since vancomycin is a glycopeptide targeting bacteria cell wall peptidoglycan, its effect is more comparable to the one of the LL-37. Therefore, its synergistic effect with the peptide is expected to be less important compared to the other three, taking action intracellularly, and potentially taking advantage of the LL-37's attack on the bacteria membrane to enter the cell more easily.

2. Former research on LL-37 conformation

CD experiments conducted by Cédric Vranckx have shown that in the conditions used to build the coatings ((bare LL-37-HEP)$_n$ and (PPCs-CHI)$_n$), namely in aqueous solution at pH 3.5 and 5, bare LL-37 does not adopt an α-helical conformation (*Figure 16*).

CD spectroscopy allows to determine whether a peptide displays an α-helical structure by analyzing its CD spectrum for the characteristic patterns associated with its secondary structure. This powerful technique works based on the differential absorption of left and right circularly polarized light by chiral molecules, and in this case, peptides. [86]

In an α-helical structure, the peptide backbone forms a right-handed spiral, with the carbonyl oxygen atoms and amine hydrogens oriented along the axis of the helix. This arrangement

results in a characteristic CD spectrum with two negative bands around 208 nm and 222 nm, and a positive band around 193 nm. [86]

The said experiments conducted by Cédric Vranckx allowed to obtain a CD spectrum of LL-37 in different conditions (*Figure 16*): aqueous solution at pH 3.5 and 5, physiological conditions (PBS) and a positive control in a solvent that promotes hydrophobic interactions and stabilize helical structures (EtOH).

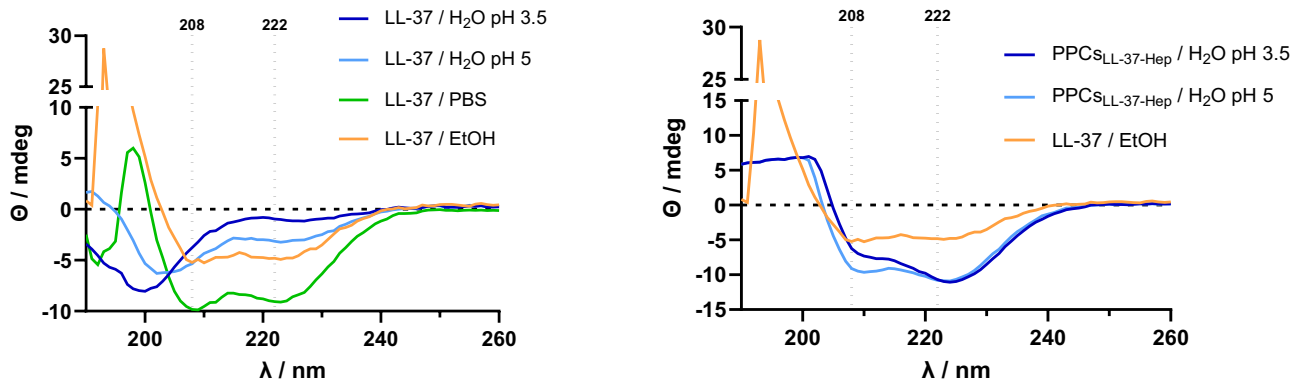

Figure 16: **CD spectra of (a) LL-37 and (b) PPCs in different solutions by Cédric Vranckx**. X axis represents the wavelength (λ) of light in nanometers (nm) and Y axis the ellipticity of polarized light passing through a sample (Θ) in millidegrees (mdeg).

When analyzing the CD spectrum of bare LL-37 (*Figure 16(a)*), the peptide exhibits these characteristic negative bands at 208 nm and 222 nm, and a positive band at 193 nm, suggesting the presence of an α-helical structure in EtOH, as expected, and in PBS solutions. Conversely, the absence of these bands for LL-37 in water indicate a different secondary structure, or a random coil conformation.

Figure 16(b) displays the CD spectrum of PPCs and shows quite clearly that PPCs allow LL-37 to keep its α-helical structure even in aqueous solution. The fact that PPCs allow the conservation of bioactivity of the complexed peptide make them a very interesting tool in the context of this research and will therefore be further studied.

3. Strategies

3.1 Conformation of released LL-37

To mimic the release of LL-37 from both coatings as it would be in physiological environment, the coatings are constructed under acidic conditions (water at pH 3.5 or 5 as a solvent) allowing them to release the immobilized LL-37 when put in physiological conditions (pH around 7.4). In fact, the difference between the acidic conditions at which the coating is built and the

physiological pH reduces the opposite charges between the PEs in the BLs and causes their release into the physiological environment.

Given the results obtained by former CD analysis described above, the first objective of our Master's thesis aims to determine whether the bare LL-37 released from the coating re-adopts a α-helical structure in PBS, after having been immobilized from an aqueous solution, where it is not in a α-helical conformation. Same experiment is performed for PPCs to determine whether the α-helical conformation of the LL-37 is kept after immobilization and release. Assessing this secondary structure could give information on LL-37 potential activity when released from the coating and when entering in contact with bacteria.

To perform a new CD analysis, there is a need for a certain concentration of released LL-37 to exceed the limit of quantification (LOQ). Experiments was conducted by building both types of coatings in a polystyrene microwells plates with the goal to release enough LL-37 for the new CD analysis.

Following these release experiments, a study on what quantity of LL-37 is left in the coatings in the microwells was also conducted to leverage some questions and hypothesis arisen from the release experiment, as well as to determine what was adsorbed best between bare LL-37 and PPCs and then select the alternative that constituted the best stock of AMP in the AMC.

3.2 Synergy between LL-37 and traditional antibiotics

To quantify the antimicrobial activity of the bare LL-37-based coating and antibiotics, resazurin and crystal violet analysis were performed to assess biofilm's metabolic activity and biomass, respectively.

Experiments on biofilms of *S. epidermidis* (here, *ATCC 35984* strain) were performed with and without coating, meaning under antibiotics treatment only, in order to determine what part of the observed effect are effectively related to a synergy between the coating and the antibiotics, and not due to the simple antibiotic treatment.

For each experiment, different multiples of the MIC have been tested on the *ATCC 35984* strain (MRSE). MIC is specific to each antimicrobial agent and each bacterial strain, and indicates the minimum amount of antibiotic required to inhibit bacterial growth. Testing to treat the biofilm with higher multiples of MIC (2x MIC, 5x MIC and 10x MIC) in addition to 1x MIC gives mainly two types of information.

Firstly, experiments at higher concentrations can reveal the presence of specific resistance mechanisms that may not be apparent at the MIC. This is particularly relevant in the context of biofilm-associated infections, where additional factors such as reduced antibiotic penetration

and altered bacterial physiology, increase their resistance to antibiotics compared to planktonic bacteria.

While a lower concentration of antibiotic may inhibit bacterial growth (MIC), higher concentrations may be required to achieve complete eradication of biofilms. This test allows us therefore to assess the appropriate dosages for effective treatment.

PART IV – Materials and Methods

1. Coatings construction

1.1 Layer-by-Layer self-assembly protocol

In order to pursue the main objectives of this Master's thesis, the LL-37-based AMC is always used as a starting point. To study the release and adsorption of LL-37 from and in the AMC, two different types of coating ((bare LL-37-HEP)$_n$ and (PPCs-CHI)$_n$) were built. But only the bare LL-37-based coating ((bare LL-37-HEP)$_n$) was used to determine how does the AMC interact with antibiotics through bacterial assays. Both coatings were assembled in polystyrene microwell plates through an equivalent protocol for every experiment, following the LbL method described in the *State of the art*. One BL is formed by the adsorption of two oppositely-charged PEs.

The successive adsorption of PEs to form a BL is performed as shown schematically on *Figure 17*. This image shows the construction of a BL made of a layer of positively-charged PE (in red) and a layer of negatively-charged PE (in blue).

This method requires an anchoring layer (AL) formed by two BLs, each composed of CHI and HEP ((CHI-HEP)$_2$). The positively-charged CHI binds to the negative charges of the polystyrene microwell plates, initiating the coating formation (see *Figure 17*).

As previously mentioned, in this Master's thesis, two different types of coating were built to study separately the effects of bare LL-37 and complexed LL-37 as PPCs. The first coating type ((bare LL-37-HEP)$_n$) is made of HEP (-) and bare LL-37 (+). The second coating ((PPCs-CHI)$_n$) contains CHI (+) and PPCs (-), the latter allowing LL-37's charge to be standardized by HEP, as described in the *State of the Art*. Combining these various components (AMP and other PEs) allows to exploit their biological properties.

Technically speaking, between each layer, a washing step with ultrapure water is performed before introducing the second component to form a BL, the latter being set for 20 minutes before the next washing step. The process is repeated to assemble as many BLs as required for the experiment.

In this experiment, 200 μL of solution is added for each step, and solutions' concentration and preparation are described in the next section.

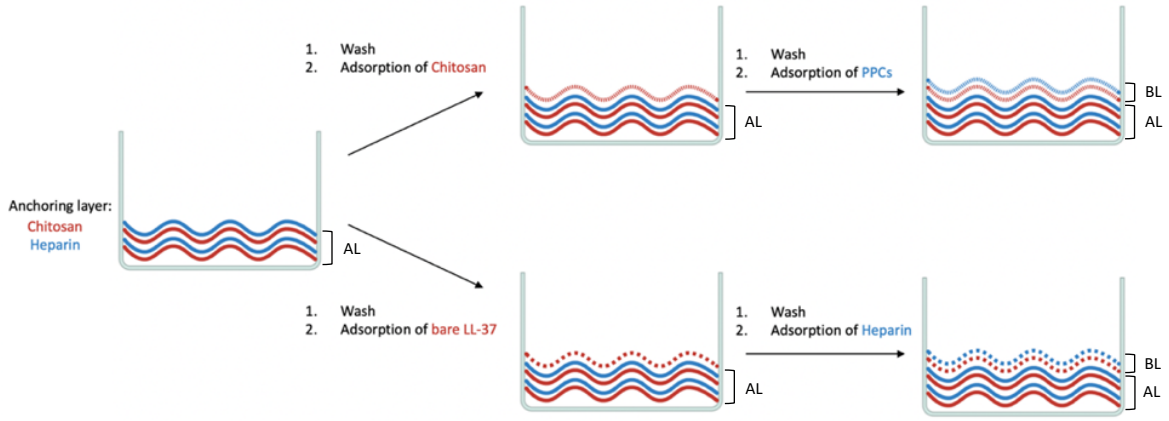

Figure 17: **Step-by-step schematic representation of the LL-37 immobilization technique for the construction of a multilayered coating** in a polystyrene microwell, starting with an AL. Positively- and negatively-charged PEs are represented in red and blue, respectively. One BL is formed by the adsorption of two oppositely-charged PEs, one red and one blue. This representation is not on scale.

1.2 Solutions preparation

The concentrations of the solutions used to build the coatings, being the starting point for each experiment of this Master's thesis, are mostly identical between the experiments, and their preparation is described hereunder.

It is to note that pH conditions for each solution do vary between experiments. In fact, tests were carried out for two different pH values: pH 3.5 and pH 5. The two values are determined to promote different levels of charge density for LL-37. Which pH was applied to which solution is explained in more details in the section *2.3 Experiment protocols*.

It is important to note that coating construction for bacterial assays is carried out under sterile conditions, in a laminar flow hood.

1.2.1 Ultrapure water

For washing steps as well as for coatings solutions preparation, ultrapure water (Elga Purelab Chorus 1, 18.2 MΩ cm, Veolia, United Kingdom), or milli-Q type water, is used to ensure an ionic strength as low as possible (meaning the closest to 0 mM). This enables the ionic strength of solution to be precisely controlled, minimizing the contribution of ions from the solvent. Significant charge screening due to higher ionic strength (I) is therefore avoided. The use of ultrapure water then allows to be more confident that the observed variations are primarily due to the species of interest rather than contaminants or undesirable ions present in the water.

Milli-Q water is pH-adjusted by adding either HCl 12 M or NaOH 10 M and is used as a solvent to set pH values for the following solutions. pH values were measured with a pH indicator strip (MQuant, Merck, Darmstadt, Germany). pH adjustment of the solutions of course brought ions into the ultrapure water, causing the ionic strength to slightly increase. According to a paper on LbL using PPCs written by Cédric Vranckx et al., the increase in ionic strength for the ultrapure water is equal to 1.8 and 0.25 mM at pH 3.5 and 5, respectively. [52]

1.2.2 Chitosan solution

CHI solutions were made at a concentration of 500 µg/mL, starting with 50 mg of CHI, M_W = 10 - 50 kDa, deacetylation degree of 95% (Heppe Medical Chitosan Gmbh, Halle, Germany). To dissolve the CHI, which does not dissolve in water, 60 μL of 12 M HCl is added, and the mixture is then heated to 60°C for 1h. Once cooled, 27.8 μL of 10 M NaOH is added to the solution to neutralize the acid, and the final volume is adjusted to 100 mL with milli-Q water. The solution is then filtered to remove impurities with 5 μm cellulose filter and 0.2 μm polyethersulfone filter. pH of the solution is then adjusted to 3.5 or 5. Due to the pKa[15] of its amine groups (pKa = 6.5), the charge level of CHI (+) is the same at these two pH values.

1.2.3 Heparin solution

HEP solutions are also prepared at a concentration of 500 µg/mL. A stock solution of HEP sodium (B. Braun, Melsungen, Germany) 5000 IU/mL and 200 IU/mg (equivalent to 25 mg/mL) is used. The term "IU" stands for International Unit and is a measurement in pharmacology to quantify the amount of a substance based on its biological activity or effect.

By diluting 1 mL of this stock solution into 49 mL of milli-Q water with adjusted pH, the desired concentration of 500 µg/mL is reached (dil 50x). Again, solutions at two different pH are prepared: one solution at pH 3.5 and another at pH 5. Due to the pKa of its sulfonate groups (pKa = 0.5 - 1.5) and carboxyl groups (pKa = 2 - 4), the charge of HEP (-) is the same at these two pH values.

1.2.4 Complexed LL-37 in PPCs

1.2.4.a Solution preparation

As it has been assessed by Cédric Vranckx, and will be shown once again in this Master's thesis, ideal PE-to-protein charge ratio, or -/+ charge ratio, for PPCs formation is 1.5.

[15] As a reminder, pKa value gives information about the ionization state of individual acidic and basic groups on the molecule. The net charge of the PE is obtained by summing the charges of all ionizable groups. When pH is above pKa value, the groups are deprotonated. In the case of CHI, the pKa values of its ionizable amine groups being above 3.5 and 5 means they are mostly protonated, in this case positively-charged, for the pH conditions used in this research.

Since the pI of LL-37 is 11, under the two pH conditions listed above, 3.5 and 5, the protein will carry a net positive charge[16]. However, at pH 3.5, which is more acidic than pH 5, the peptide would be more protonated. Therefore, the net positive charge of the peptide at pH 5 is lower than at pH 3.5, but would still be positively-charged overall. The number of charges of LL-37 is 10.39 and 7.02 at pH 3.5 and 5, respectively[17].

For PPCs formation, this particular (-/+) charge ratio of 1.5 will be used in this Master's thesis. In order to prepare PPCs respecting this ratio, 3 volumes of 0.5 mM(-) of HEP will be mixed with 10 volumes of 0.1 mM(+) LL-37 (FITC[18]-labeled or unlabeled).

Heparin dilution factor

To prepare the 0.5 mM(-) HEP solution, a dilution is performed from the 500 μg/mL stock solution, whose preparation was explained above. The dilution factor is obtained from the following calculations:

For this experiment, the sulfate groups of HEP were considered as fully negatively-charged. In this case, one trisulfated disaccharide unit of HEP carries 4 negative charges (3 from the sulfate groups and 1 from a carboxylate ion). Since this unit has a M_W of 665 g/mol, the stock solution of 0.5 g/mL then carries 3 mM(-) and has to be diluted 6x.

LL-37 dilution factor

For the 0.1 mM(+) LL-37 solution, dilution factor also has to be calculated as a stock solution of 500 μg/mL was also prepared. In this case, the dilution factor will vary according to pH and whether the LL-37 is FITC-labeled or not, as their M_W differ. FITC-labeled LL-37 was used for fluorimetry quantification, as explained further on the section *2.1.1 Calibration through fluorescence-based protein assay*.

pH 3.5 unlabeled LL-37

Unlabeled LL-37 solution has a M_W of 4493.26 g/mol. At pH 3.5, LL-37 carries 10.39 positive charges. The 0.5 g/mL stock solution then presents a concentration of 1.15 mM(+). The dilution factor to reach a 0.1 mM(+) solution is then 11.5.

[16] As a reminder, if the pH conditions are lower than the pI of a protein, the protein will carry a net positive charge since the acidic groups on the protein (like carboxyl groups) will tend to gain protons, becoming neutral, while the basic groups (like amine groups) will remain protonated and therefore positively-charged.

[17] Charges of LL-37 have been calculated by former students, Coralie Nerincx et Noémie de Suraÿ, thanks to the PDB2PQR server (an automated pipeline for the setup of Poisson–Boltzmann electrostatics calculations). This server allows to calculate charge as a function of pH from protein structure and aa sequence (file 2K6O for LL-37 from Protein Data Bank was used). [87]

[18] FITC stands for Fluorescein IsoThioCyanate and is used for protein quantification through fluorescence intensity measurement.

pH 5 unlabeled LL-37

Unlabeled LL-37 solution has a M_W of 4493.26 g/mol. At pH 5, LL-37 carries 7.02 positive charges. The 0.5 g/mL stock solution then presents a concentration of 0.78 mM(+). The dilution factor to reach a 0.1 mM(+) solution is then 7.8.

pH 3.5 FITC-labeled LL-37

Unlabeled LL-37 solution has a M_W of 4995.8 g/mol. At pH 3.5, LL-37 carries 10.39 positive charges. The 0.5 g/mL stock solution then presents a concentration of 1.04 mM(+). The dilution factor to reach a 0.1 mM(+) solution is then 10.4.

pH 5 FITC-labeled LL-37

Unlabeled LL-37 solution has a M_W of 4995.8 g/mol. At pH 5, LL-37 carries 7.02 positive charges. The 0.5 g/mL stock solution then presents a concentration of 0.7 mM(+). The dilution factor to reach a 0.1 mM(+) solution is then 7.

Volumes used for PPCs formation at a charge ratio (-/+) of 1.5 at pH 3.5 and 5

Table 1: Volumes used for PPCs (unlabeled LL-37 – HEP) formation at pH 3.5 and pH 5. pH of the solution was determined by adjusted pH of the ultrapure water.

	pH 3.5	**pH 5**
HEP 0.5 mM(-) (μL)	49.88	49.88
LL-37 0.1 mM(+) (μL)	86.45	128.01
Ultrapure water (μL)	1163.6	1122.1

Table 2: Volumes used for PPCs (FITC-labeled LL-37 – HEP) formation at pH 3.5 and pH 5. pH of the solution was determined by adjusted pH of the ultrapure water.

	pH 3.5	**pH 5**
HEP 0.5 mM(-) (μL)	49.88	49.88
LL-37 0.1 mM(+) (μL)	96.12	142.33
Ultrapure water (μL)	1154	1107.8

1.2.4.b PPCs optimal charge ratio determination

This part is a digression from this part on *Solutions preparation* for coatings construction, aimed at explaining the protocol of the confirmation of the optimal (-/+) charge ration for PPCs formation, which was taken as reference for the PPCs solution preparation explained in the section right above.

To determine charge ratio between the PE (HEP) and the protein (LL-37) that will allow the successful LbL of the PPCs with CHI is therefore an important predisposition prior to coating building. Former studies on the subject have been performed by Cédric Vranckx but we chose

to redo the experiment for further checking. To do so, PPCs are studied in suspension by turbidimetry.

The charge ratio describes the relationship between positive and negative electrical charges in a system. In our case, PPCs are built using HEP, which carries a negative charge, and LL-37, which is positively-charged, in the used pH conditions, at a chosen charge ratio of 1.5 (-/+). Following this logic, varying the amount of one of the two components subsequently changes the charge ratio. Working at an optimal charge ratio is crucial for producing PPCs in sufficient size and quantity. To investigate this effect, PPCs at different charge ratios were formed and examined using turbidity measurements, or turbidimetry.

Turbidimetry is the measurement of the degree of turbidity in a suspension. In other words, it is a method for dosing molecules/particles in suspension (in this case, PPCs), using optical means to measure the turbidity they produce in a liquid medium. Turbidimetry relies on measuring the decrease in intensity of light as it passes through the sample containing the suspended PPCs particles. This decrease is caused by scattering, where light is deflected by particles in different directions. The extent of this scattering provides information about the number and size of the particles, allowing for the quantification of turbidity.

To build these PPCs, 0.5 g/L stock solutions of HEP and LL-37 are used, both at pH 3.5. Volume of HEP were varied to make the (-/+) charge ratio vary. Exact volumes used are visualized in *Appendices, Table I*. Results are obtained by analyzing the plate by absorbance at $\lambda = 450$ nm.

1.2.5 Bare LL-37 solutions

As explained in the previous section on PPCs solution preparation, LL-37 will carry a net positive charge as the two pH conditions we are working at, 3.5 and 5, are below its pI (11). As a reminder, the number of charges of LL-37 is 10.39 for pH 3.5 and 7.02 at pH 5.

As 10 volumes of LL-37 solution have been mixed with 3 volumes of HEP for PPCs preparation, the bare LL-37 solution has been diluted 1.3 times. The experiment aims at introducing a similar quantity of LL-37 for both coatings: bare LL-37 and PPCs-based. Note that the engaged quantity is the same but does not reflect the quantity effectively adsorbed in the coating. Indeed, depending on the experimental conditions and the nature of LL-37 (PPCs or bare LL-37), the adsorbed quantity will differ. Considering this, the desired concentration of bare LL-37 is then 0.1 mM (+) solution diluted 1.3 times, being 0.08 mM (+).

To reach this concentration from a 500 μg/mL stock solution, similar calculations as the ones performed for PPCs solution preparation are done, taking into account the number of charges for LL-37 in both pH conditions and its M_W. As a reminder, M_W of unlabeled LL-37 is 4493.26 g/mol and M_W of FITC-labeled LL-37 is 4995.8 g/mol. *Tables 3* and *4* show volumes used for 0.08 mM (+) LL-37 solution.

Table 3: Volumes from a 500 μg/mL stock solution used for unlabeled bare LL-37 solution at pH 3.5 and pH 5. pH of the solution was determined by the adjusted pH of the ultrapure water.

	pH 3.5	**pH 5**
LL-37 (μL)	66.49	98.48
Ultrapure water (μL)	933.5	901.5

Table 4: Volumes from a 500 μg/mL stock solution used for FITC-labeled bare LL-37 solution at pH 3.5 and pH 5. pH of the solution was determined by the adjusted pH of the ultrapure water.

	pH 3.5	**pH 5**
LL-37 (μL)	73.93	109.48
Ultrapure water (μL)	926.1	890.5

2. Circular dichroism analysis of LL-37 released from the coating

This experiment will study the structure of the LL-37 peptide when released from the two types of coating. As explained in the *State of the art*, the AMC being studied is expected to display antimicrobial activity as follows. During prosthesis implantation, LL-37 previously immobilized in the surface coating, is released by conditions difference with physiological pH to prevent biofilm formation by targeting pathogens' membrane. As LL-37 manifests its antibacterial properties only in its α-helix form, as explained in the *State of the art*, CD would aim to confirm whether LL-37 is under its active form when released from the AMC, under its two forms studied: (bare LL-37-HEP)$_n$ and (PPCs-CHI)$_n$.

To study the structure of the released peptide, its release is triggered by a medium mimicking human physiological conditions, a PBS solution at 37°C. The samples obtained by the release of LL-37 from both coatings (bare LL-37-based and PPCs-based) are then analyzed by CD, a spectroscopic method that evaluates the difference in absorption of right- and left-handed circularly polarized light.

CD analysis requires a sufficient concentration of the compounds to enable detection and analysis, which was estimated to be close to 30 μg/mL. The first goal of this Master's thesis was therefore to improve the protocol of LL-37 release for both bare LL-37 and PPCs in order to obtain a concentration that exceeds CD analysis LOQ. Released peptide quantification in the following experiment will be carried out using fluorescence-based protein assay.

2.1 Analytical methods

2.1.1 Calibration through fluorescence-based protein assay

2.1.1.a Context and principle

Fluorescence-based protein assay, or fluorescence spectroscopy, is an analytical technique used to measure the concentration of molecules in solution by exploiting their fluorescence and was used in this Master's thesis for accurate quantification of FITC-labeled LL-37 released from the coatings.

FITC is a fluorophore widely used to label molecules such as proteins, antibodies and peptides. This molecule emits green light ($\lambda_{emission}$ = 520 nm) when excited by UV or blue light ($\lambda_{excitation}$ = 490 nm), making the labeled molecules visible by optical detection techniques. FITC contains an isothiocyanate group (-N=C=S) which reacts readily with amine groups. This reaction forms stable covalent bonds, enabling molecules such as LL-37 to be durably marked. [88]

Fluorescence is a luminescence phenomenon. When a fluorescent molecule (here, the FITC-label) receives energy in the form of UV light, it will re-emit light (photons) as long as the light source is applied. Some molecules, called fluorophores, are capable of fluorescence. When these molecules are excited by light energy (UV), their electron delocalizes to a higher energy layer. While other molecules would dissipate this absorbed energy by releasing heat for example, fluorophores will release a photon. This photon will be of lower energy than the absorbed energy, since some of this energy is dissipated through relaxation upstream, and will therefore emit light in the visible wavelength range. This phenomenon is described by the Jablonski diagram in the *Figure 18*. The blue arrow representing the absorbed energy (UV) is, as previously stated, larger than the green arrow, the emitted energy (visible). This difference is due to the different vibrational relaxations that dissipate the energy (orange) as heat before releasing the visible photon. [89]

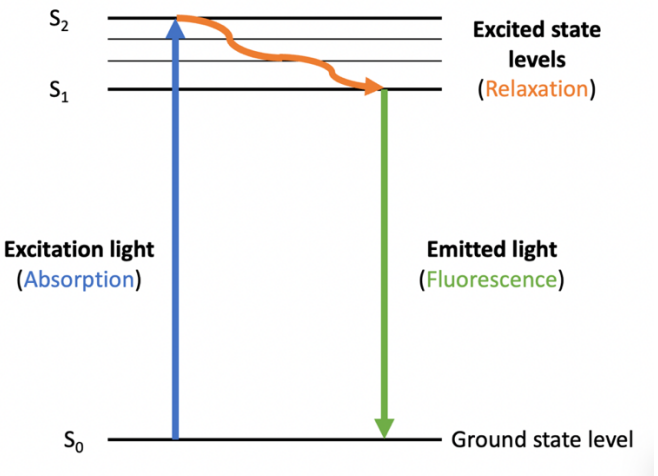

Figure 18: **Principle of fluorescence** illustrated by the Jablonski diagram (simplified).

The advantage of this technique over BCA assay, explained in the section *3. Study of LL-37 adsorption in the coatings*, is its greater selectivity. Indeed, the only molecule that emits a signal is the FITC-labeled LL-37. It is not affected by interference from CHI or HEP, as they are not fluorophores. The signal we obtain is therefore only due to the emission of light from the peptide, which is not the case of BCA assay (see section *3.1 Calibration through BCA assay*).

Additionally, fluorimetry stands out from many other techniques for its sensitivity, being able to detect very low concentrations of fluorescent substances. The notable disadvantage of this technique is the requirement for coating building in dark conditions to avoid early reactivity of LL-37 with daylight. Lack of visibility can be a considerable constraint when working with small volumes, giving rise to risk of experimental error.

2.1.1.b Calibration curve

Fluorescence of the molecule is then linked to LL-37 quantity present in the sample through the relationship depicted by an upstream elaborated calibration curve. To construct the calibration curve to quantify LL-37, dilutions were made from a stock solution of 0.02 g/L FITC-labeled LL-37 with PBS to give a final volume of 150 μL.

Then, the plate is measured in a spectrophotometer (SpectraMax iD3, Molecular Devices) with $\lambda_{excitation}$ at 490 nm and $\lambda_{emission}$ at 520 nm. The following polynomial calibration curve is obtained (*Figure 19*), which enables to determine the quantities of labeled LL-37 in the experimental samples.

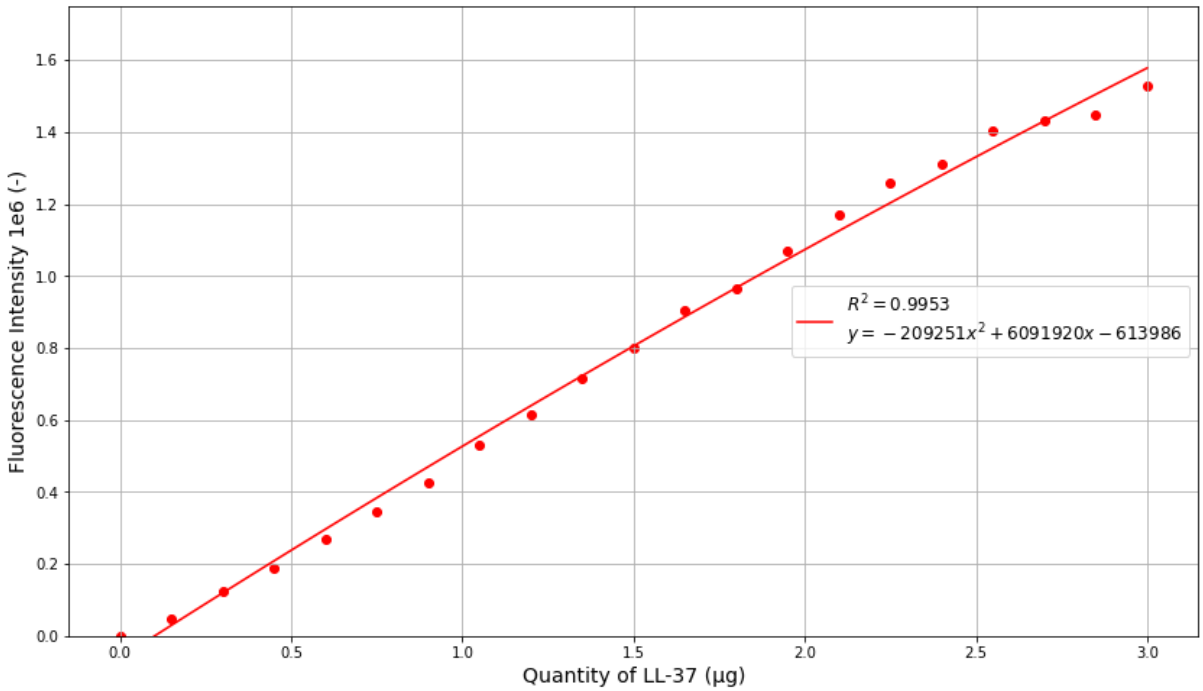

Figure 19: **Calibration curve** for a 0-3 μg range of **FITC-labeled LL-37** by fluorescence spectroscopy.

2.1.2 Circular dichroism

CD is a spectroscopic technique measuring the difference in absorption of left and right circularly polarized light by a substance.

Visible light is made up of photons traveling as electromagnetic waves. When light is circularly polarized, the electric field of the light describes a helix in space as the wave advances. There are two types of circular polarization: right and left. In right-hand polarization, the direction of the electric field turns clockwise as you look at it, and vice versa in left-hand polarization. A chiral molecule can absorb left- and right-hand circularly polarized light differently, depending on its structure. This difference in absorption results in a characteristic spectrum that can be measured. This is ellipticity, which is a measure of the difference in absorption of left- versus right-hand circularly polarized light by chiral molecules, that can be identified in a CD spectrum.

CD can be used to obtain information on the secondary structure of a protein, i.e. α-helix or β-sheet. This is of interest to us in determining the conformation of LL-37 when released from the coatings and whether it is in its active form when released or not.

Figure 20 displays an example of CD spectra. In this case the spectra show results for LL-37 peptide in different solutions: water at different pH values, PBS and ethanol (EtOH). In CD spectroscopy, Y axis often represents the measured signal in terms of the ellipticity of polarized light passing through a sample (Θ). The unit "mdeg" stands for millidegrees, meaning the measurements are in millidegrees of ellipticity.

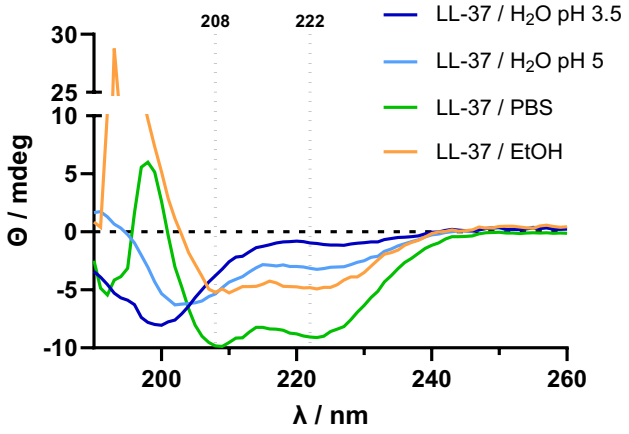

Figure 20: Example of **CD spectra by Cédric Vranckx**. LL-37 in different solutions. X axis represents the wavelength (λ) of light in nanometers (nm) and Y axis the ellipticity of polarized light passing through a sample (Θ) in millidegrees (mdeg).

In a CD spectrum, α-helices (right-handed coiled structure where the polypeptide chain is tightly wound around a central axis, like a spiral staircase) are distinguished by two absorption minima at 222 nm and 208 nm, and a maximum at 190 nm, as shown in *Figure 20*, while β-sheet structures show a minimum at 218 nm and a less pronounced maximum at 195 nm. If LL-37 is not in an α-helix conformation, it is likely in a random coil conformation. This structure

lacks a regular repeating pattern and does not form any specific secondary structure like an α-helix or β-sheet. However, the presence of coil conformation in a protein can contribute to the overall CD signal, particularly in the absence of well-defined secondary structure elements.

2.2 PBS solution preparation

For release experiments, a PBS solution is used. This buffer simulates the ionic environment and pH similar to the human body's (7.4), enabling the peptide's behavior to be tested under conditions that mimic those in which it will eventually act naturally. This allows to predict more accurately the peptide's efficiency and stability in a biological environment.

It is specifically the difference between conditions of pH 3.5 and 5 at which the coatings are built and the physiological pH 7.4 of PBS that makes it possible to reduce the opposite charges between the PEs in the BLs and causes their release into the PBS solution.

The 1x PBS solution is obtained by dilution of a 10x PBS solution containing 80.15 g/L NaCl, 2.0015 g/L KCl, 14.203 g/L $Na_2HPO_4.2H_2O$, 2.003 g/L KH_2PO_4 in milli-Q water.

2.3 Experiment protocols

2.3.1 Determination of optimal conditions for LL-37 release

LL-37 from the coatings is released into PBS by difference of pH conditions, as explained before. For both types of coating (bare LL-37-based and PPCs-based), the LL-37 used in this experiment is FITC-labeled. It is detectable and quantifiable by fluorescence spectroscopy to measure LL-37 concentration through accurate quantification and according to the fluorescence calibration curve on *Figure 19*. This concentration is influenced by several factors, such as the pH of the solutions used, the number of BLs for the coating building, and the volume of PBS used for the release of the peptide. The goal of this experiment was to determine which conditions would optimize the concentration of released LL-37 in PBS.

To determine the optimal pH for LL-37 peptide release from a coating PPCs- or bare LL-37-based, the process was tested at two different pH levels, 3.5 and 5. Coatings of both 16 and 20 BLs were built on 48 microwells plates (CELLSTAR®) from Greiner Bio-One. To assess whether a larger volume of PBS could influence the amount of LL-37 released, we carried out trials with 200 μL and 300 μL of PBS. Larger volume could avoid saturation of LL-37 in the PBS solution. Frequent renewal of PBS solution was performed to potentially accelerate the release process as well as to study the release kinetics of the peptide. The tested conditions are shown in the *Table 5*.

Table 5: Tested conditions for coating building to determine which condition(s) allowed optimized release of LL-37. All 6 conditions were performed once for PPCs- and bare LL-37-based coatings each.

Condition	**1**	**2**	**3**	**4**	**5**	**6**
PBS (μL)	300	300	200	300	300	200
BLs (number)	20	16	16	20	16	16
pH	3.5			5		

The release method involves to regularly replace volumes of PBS for analysis and quantifying the amount of LL-37 released at different intervals. 13 release measurements were carried out at specific times: every 30 min for six hours and one last time 24h after the beginning of the experiment. This monitoring gives information on LL-37 release kinetics and allows identification of potential "burst release" of the peptide.

2.3.2 Protocol for LL-37 release preceding CD

Based on the results obtained in the previous experiment, presented in the *Results and Discussions* section, the optimal conditions for coatings construction and release have been identified. These will allow the peptide to achieve a sufficient concentration that could be analyzed in CD.

Concerning the sampling times and the PBS volume used for LL-37 release from the coatings, the release was carried out in two stages. The first volume of PBS remains for 6 hours in the wells as an intense release of the peptide have been identified during first this time period, called the "burst release". After these 6 hours, a new PBS volume is added and removed 24 hours after the addition of the first PBS volume. This second sampling is carried out after 24 hours to allow LL-37 to be released and accumulate in the PBS because the release is no longer as intense as in the first hours (see *Figure 32* and *33* of the *Results and Discussions* section). These two volumes of PBS used for this release were of 100 μL each.

In the previous experiment (2.3.1), a plate of 48 microwells was used. 48 microwells plates (CELLSTAR®) from Greiner Bio-One offer a minimal working volume of 200μL. This second experiment, using a volume of 100μL of PBS for release then required to use 96 microwells plates (CELLSTAR®) from Greiner Bio-One, whose minimal working volume is 50 μL.

The coatings (50 BLs) were then applied to 10 wells for PPCs at pH 5 and to 10 wells for bare LL-37 at pH 3.5. As we have two samples of 100 μL for each well, the total volume of PBS for each type of coating is 2 mL.

2.3.3 Circular dichroism analysis

To prepare this experiment, the protocol developed above from the conclusions drawn from the section *2.3.1 Determination of optimal conditions for LL-37 release* is used to prepare the coated plates and carry out peptide release. The resulting samples, containing PPCs and bare LL-37 in PBS, are analyzed by CD. As the concentration in the samples is not quantified

upstream, the exact concentration is not known. Additional samples were prepared to complete the analysis and compare obtained CD results with standard solutions:

- LL-37 in PBS at 30 μg/mL
- PPCs[19] in PBS at 30 μg/mL
- HEP in PBS at 30 μg/mL
- CHI in PBS at 30 μg/mL
- PBS (as blank)

CHI and HEP samples are used to verify the presence of detectable CD signals. This method helps to refine the results for LL-37 and PPCs by eliminating potential interference caused by these two compounds, which are also released from the coatings, along with the peptide of interest. The same goal to eliminate potential interference of the solution applies to PBS.

In addition, analysis of bare LL-37 and PPCs samples at 30 μg/mL offers an overview of the response curve when LL-37 is in PBS solution. If a signal is detected with these prepared samples, this indicates that LL-37 is indeed detectable at this concentration. This observation is essential to determine whether the concentration of LL-37 is sufficient in samples with released LL-37. If no signal for the samples containing the bare LL-37 and LL-37 in PPCs released is obtained, it means, most likely, that the obtained concentrations after LL-37 release from the coatings did not reach 30 μg/mL.

3. Study of LL-37 adsorption in the coatings

Additional experiments were conducted on the plates after the release experiment to assess the adsorption capacity of bare LL-37 and LL-37 contained in PPCs. The LL-37 remaining in the coatings after the release experiment was quantified using a BCA assay. That way, the remaining and released amount of LL-37 together enable to deduce the adsorbed LL-37 quantity in the microwells during coating formation. Optimal conditions for the coatings construction to achieve a substantial LL-37 reservoir will be determined. This experiment also allows to answer some questions and hypothesis risen from the release experiment results.

[19] An experimental mistake was made while preparing PPCs in PBS. Volumes used for PPCs formation were the ones for a -/+ charge ratio of 1.5 in pH 3.5 in ultrapure water, and not pH 7.4. This error led to uninterpretable results regarding PPCs. More about this in the *Results and Discussion* section.

3.1 Calibration through BCA assay

3.1.1 Principle

The BCA assay is an effective method for determining the concentration of proteins in solution. In this research, BCA assay was used to measure the quantity remaining on the coated microwells plates after release of LL-37 in PBS.

This assay is based on the formation of a colored complex between copper(I) ions (Cu^{+}) and BCA under alkaline conditions. Initially, copper(II) ions (Cu^{2+}) are reduced to Cu^{+} by proteins present in the sample. Subsequently, Cu^{+} reacts with BCA, under the form of an "AB reagent", to form a purple complex whose color intensity, measured at $\lambda = 562$ nm, is proportional to the amount of protein present in the sample. [73] The reactions of the BCA assay principle are schematized on the *Figure 21*:

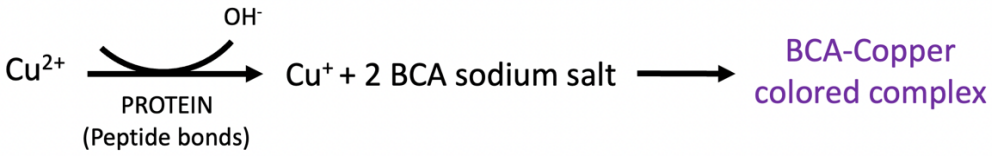

Figure 21: **BCA assay reaction.** AB reagent reaction quantifies peptide present in a sample. "BCA sodium salt" stands for the "AB reagent". [90]

3.1.2 Solutions preparation

In a BCA assay, AB reagent is prepared by mixing product A (Thermo Scientific™ Pierce™ BCA Protein Assay Reagent A) with product B (Thermo Scientific™ Pierce™ BCA Protein Assay Reagent B), at a 50:1 ratio. The reagent is then added in required quantities in the microwells, whether to establish the calibration curve, or to measure the amount of LL-37 remaining in the coatings after the release experiment. Incubation takes place at 60°C for 1h, allowing the AB reagent to react with the Cu^{+} ion reduced by the proteins present, producing a colored signal.

A 5% sodium dodecyl sulfate (SDS) solution is used to prepare the BCA calibration curves as it denatures proteins by breaking down their secondary, tertiary, and quaternary structures. This process exposes the peptide bonds and functional groups of aa, making them more reactive for interaction with the BCA reagent. It is prepared by dissolving 5 g of SDS in 100 mL of ultrapure water, as 5% is the compatible concentration for BCA assays according to ThermoFisher™ .

3.1.3 Calibration curve

A 0.5 g/L solution of LL-37 is used as a base to build a 0 - 8 μg range calibration curve. This stock solution is diluted to obtain a volume of 16 μL for each LL-37 quantity, with ultrapure water volumes varying to get a range of different LL-37 concentration. SDS solution always

accounts for 1/5 of the total volume, then 4μL is added to obtain a final volume of 20 μL. A well containing 0 μg of LL-37 is used as blank.

The alkalinity[20] of the AB product allows the calibration curve to be applicable to any pH condition of the ultrapure water used for the calibration curve or in which the coatings were constructed. Indeed, 200 μL of AB product is added to the total 20 μL developed above. This significant quantity thus allows the alkalinity to prevail, and the small difference of pH is considered non-significant.

It is essential to consider potential interferences with other components also present inside the coatings. To identify interferences of HEP and CHI, specific calibration curves were built by replacing the volumes of LL-37 with equivalent volumes from stock solutions of HEP and CHI at 0.5 g/L. The calibration curves are shown on *Figure 22*.

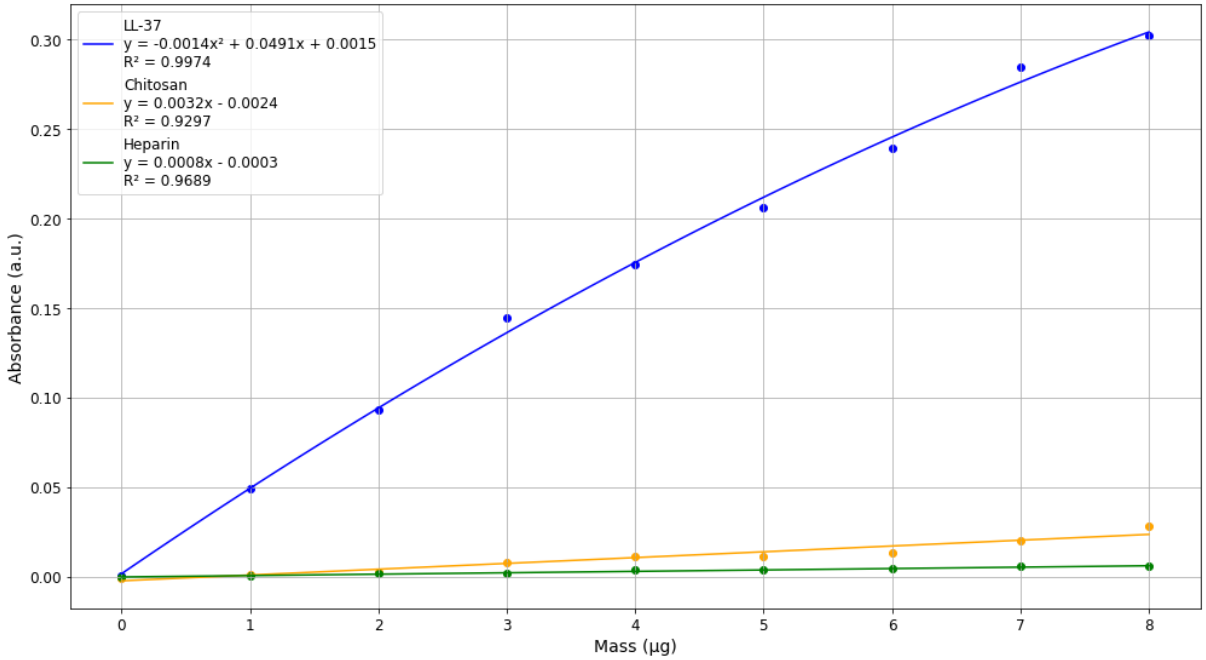

Figure 22: **Calibration curve** for pure **(unlabeled) LL-37**, pure **CHI** and pure **HEP** quantification through BCA assay

Results showed that CHI, which contains amine groups (-NH_2) on its glucosamine structure, can complex copper ions (Cu^{2+}). This interaction can interfere with the BCA assay, in which Cu^{2+} ions are normally reduced to Cu^{+} by proteins, then react with BCA reagent to form a colored complex. The presence of CHI can therefore lead to premature Cu^{2+} reduction or the formation of stable complexes with Cu^{2+}, altering the measured spectral absorption and affecting the test results accuracy. However, the exact contribution of CHI in the obtained results is unknown. Considering this, it will be assumed that the absorbance measurements used to quantify LL-37 are fully attributable to the presence of the latter, but CHI could have contributed to the

[20] The AB reagent used for BCA assays is alkaline primarily due to the presence of sodium hydroxide (NaOH)., Alkaline pH facilitates the reduction of Cu^{2+} ions to Cu^{+} (see previous section *3.1.1 (BCA assay) principle*).

BCA reaction, causing to overestimate in a certain extent the quantity of LL-37 still remaining in the microwells plate after LL-37 release.

Conversely, HEP, predominantly sulfated GAG, interacts differently with metal ions. Its negative sulfate groups can bind to cations such as sodium (Na^+) or calcium (Ca^{2+}), but this binding does not promote the reduction of copper ions in a way that significantly interferes with the BCA assay. Although HEP can bind to metal ions, this interaction does not substantially influence the necessary reduction of Cu^{2+} to Cu^+ in the BCA assay. In conclusion, the interference with HEP is virtually non-existent.

The LL-37 quantification equation used in BCA assay in this Master's thesis is shown in *Figure 22*.

3.1.4 Samples quantification

The LL-37 remaining in the microwells following the release experiments is quantified by simply adding 600 μL of AB reagent to perform the BCA assay in the 48 microwells plates. The samples are then placed in an oven at 60°C for 1h, before being analyzed in a spectrophotometer (λ = 562 nm).

The BCA assay is proving to be an essential and reliable tool for quantifying LL-37, being a simple, sensitive, and effective method for protein quantification.

3.2 Adsorption experiment

BCA assay was then performed on the plate containing the coatings after release experiment to determine the remaining quantities of LL-37 in the coatings[21]. As this experiment is considered as a closed system, the initially adsorbed quantity in the coatings can be obtained with the simple formula:

$$Adsorbed\ LL-37 = Released\ LL-37\ + Remaining\ LL-37$$

4. Study of the antibacterial synergy between LL-37 and antibiotics

In this research, *S. epidermidis ATCC 35984* strain is used to explore the synergistic effect of the LL-37 AMP with four routinely-used antibiotics in the fight against *S. epidermidis* biofilm. These antibiotics are vancomycin, tobramycin, doxycycline and linezolid, proposing different MOAs, as detailed in the *State of the art* section, able to show variable synergy with the LL-37 peptide, which acts on bacterial membranes. To assess this potential coupled effect, two types

[21] The coatings here are not compared to the initially engaged quantity of LL-37, as we consider the obtained coatings after all the steps for their construction, including losses due to washing steps and partial release into the water used for storage overnight (as the coatings were never built in one single day).

of tests were performed: quantification of the reduction of biomass through crystal violet staining, and of metabolic activity through resazurin testing.

4.1 Analysis methods

4.1.1 Crystal violet staining

The first analysis carried out allows to quantify the biomass of bacterial biofilm using crystal violet, whose structure is represented on *Figure 23*. This fluorescent compound is a basic dye with the ability to bind to negatively-charged cell components such as bacterial walls and plasma membranes, as well as EPS of the extracellular matrix, thanks to its cationic properties. In this experiment, crystal violet acts by binding to the bacterial biomass. Excess dye is washed away, resolubilized and analyzed by measuring the absorbance of the resulting solution at λ = 570nm. The greater are the absorbance values, the greater is the dye's quantity, and the greater is the biomass of the biofilm. [91]

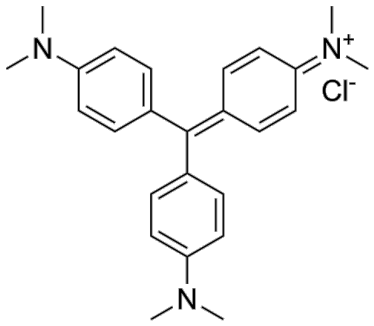

Figure 23: **Crystal violet** dye cationic structure.

4.1.2 Resazurin

The second method to quantify the effect of antibiotics combined with the AMC is resazurin. This technique is fluorescence-based and assesses bacteria's metabolism. Resazurin is a non-fluorescent blue substance reduced by metabolically active cells, converting the molecule into a pink-red fluorescent compound: resorufin. This reaction, showed on *Figure 24*, makes it possible to assess the metabolic activity of the cells: the more cells are alive and metabolically active, the greater the quantity of fluorescent resorufin. [92], [93] Analysis is performed by fluorescence at $\lambda_{emission}$ = 590 nm and $\lambda_{excitation}$ = 550 nm.

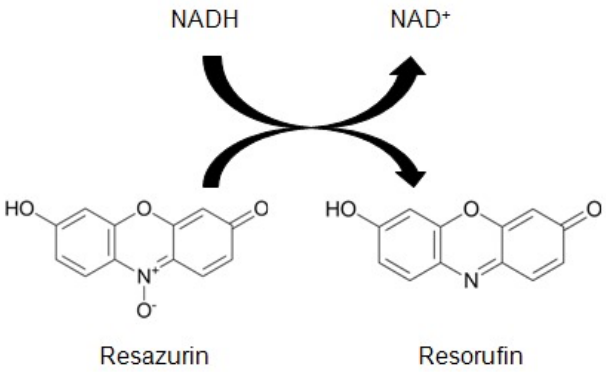

Figure 24: Structure of blue **resazurin substrate** reduced into the pink fluorescent resorufin product by viable cells metabolism (NADH is the electron donor, oxidized in NAD^+). [94]

4.2 Experiment protocol

To study the synergistic effects between the bare LL-37 immobilized in the coating and vancomycin, tobramycin, doxycycline, and linezolid in the fight against *S. epidermidis* biofilm, the experiments will be divided in two parts. These two parts use a similar protocol, with the only exception that the first experiment makes the biofilm grow on the AMC, where the second experiment does not use the AMC, in order to assess the activity of the antibiotics acting alone.

For the first experiment, microwell plates are coated with one AL ($(CHI\text{-}HEP)_2$) and 14 BLs of bare LL-37 and HEP, finishing with one layer of bare LL-37 (1 AL and 14.5 BLs in total). The obtained coating can then be referred as $(LL\text{-}37 – HEP)_{14.5}$.

Due to a lack of time, no experiment was performed to test the synergistic activity of antibiotics with PPCs-based coating. However, this test is an interesting perspective to determine whether PPCs, apparently allowing to preserve the conformation of LL-37 in the coating, also allow a subsequent increased activity of the peptide on bacteria compared to bare LL-37. More about this perspective is detailed in the *Future prospects* section.

To avoid any contamination that might distort the results, the whole experiment, from coating construction to bacterial assays, was performed under sterile conditions, in a laminar flow hood. Laminar flow hoods are designed to create a particle-free work surface by drawing air through a high-efficiency filtration system and exhausting it across the work surface in a unidirectional airflow. [95] All equipment used was sterilized with 70% ethanol to eliminate any contamination risk, and all solutions were prepared in sterile conditions (by filtration or autoclaving).

4.2.1 Solutions preparation

4.2.1.a PBS

A solution of sterile PBS is prepared at pH 7.4. This buffer solution is used to wash the microwells and remove any residual culture medium. Like said previously, PBS has the

particularity of providing an ionic environment similar to the human body's and has a pH mimicking the physiological one, in body fluids. The PBS solution is the same as the one used for the LL-37 release experiment, as for difference that it has then been prior sterilized by autoclaving.

4.2.1.b RPG Medium

The medium used for bacteria growth is RPG medium, made of RPMI 1640 cell culture medium at adjusted pH of 7.4 (ThermoFisher Gibco™ RPMI 1640 Medium , powder), to which a glucose solution of 100 g/L is added, to meet the energy needs of the cultured bacteria. For 50 mL of RPG, 5 mL of glucose solution is added to 45 mL of the RPMI medium.

RPMI medium contains aa, vitamins, mineral salts, glucose, and buffers such as sodium bicarbonate. This provides cultured bacteria with a favorable environment for growth proliferation. [61] To prepare it, 10400 mg RPMI/1640 powder, 6800 mg KH_2PO_4, 13200 mg $Na_2HPO_4.2H_2O$ and 950 mL of ultrapure water were used.

4.2.1.c Resazurin and crystal violet

The resazurin solution is at 10 μg/mL in PBS. To prepare the solution, 500 μL of a resazurin 1 mg/mL stock solution is put in 49500 μL of PBS for it to be diluted 100x.

The crystal violet dye solution is diluted at 1% with ultrapure water.

4.2.1.d TSA plates

Tryptic Soy Agar (TSA) plates are required for bacteria growth. TSA is a culture medium that allows bacteria to grow on petri dishes. TSA powder (Ph. Eur., USP, JP; Casein soya bean digest agar; 84602.0500) and milli-Q water were used for a 40 g/L TSA solution, further autoclaved for sterilization, and flowed on the plates.

4.2.1.e Heparin and bare LL-37

The HEP and bare LL-37 solutions used for coating construction are at pH 3.5 and in same concentrations as explained in the section *1. Coatings construction*, except that they are prepared and used under sterile conditions.

4.2.1.f Antibiotics solution preparation

To study the effect of antibiotics on biofilms, the MICs of the four antibiotics (*Table 6*) were prior determined by Cédric Vranckx for *ATCC 35984* strain in RPG. As a reminder, MIC represents the minimal concentration of an antimicrobial agent required to inhibit the growth of bacteria. [96]

The potency of an antibiotic (%) represents how much of the active ingredient in the antibiotic is present and active compared to the amount specified on the label[22].

Table 6: MIC and potency of vancomycin, tobramycin, doxycycline and linezolid

Antibiotic	MIC (μg/mL)	Potency (%)
Vancomycin	1	97.5
Tobramycin	256	99
Doxycycline	0.25	100
Linezolid	1	100

To obtain the desired MICs, stock solutions of 1 mg/mL for vancomycin, doxycycline and linezolid and 12.8 mg/mL for tobramycin are prepared.

Next, stock solutions of vancomycin, doxycycline and linezolid 1mg/mL are diluted 20x by diluting 250 μL of these solutions in 4750 μL of RPG. This new solution of 50 μg/mL is added to RPG to reach various final concentration, for the preparation of the different MIC solutions. Tobramycin is not diluted 20x, as strain *ATCC 35984* is resistant to this antibiotic. The MIC for tobramycin is therefore higher, as explained in the *State of the art* and as presented on *Table 6*.

These stock solutions were used to prepare the MICs 1x, 2x, 5x and 10x solutions. Exact volumes used to reach these different concentrations of antibiotic are presented in the *Appendices, Tables VIII, IX, X* and *XI*.

4.2.2 Inoculation and biofilm formation of *S. epidermidis*

Around 20h before the beginning of the experiment, *S. epidermidis ATCC 35984* strain is inoculated onto TSA plates and placed in a 37°C incubator. *S. epidermidis* is not let to grow on TSA plates for more than 24h to avoid the potential activity of autolytic enzymes. In fact, prolonged incubation of *S. epidermidis* on TSA plates can cause nutrient depletion as growing bacteria consume available nutrient. Nutrient limitation triggers the activity of major autolysin AtlE, responsible for cell wall turnover and separation of daughter cells during cell division. [97] 20h was then a good compromise between avoiding AtlE activity[23] and having colonies grown enough for uptake.

After the 20h incubation, the grown colonies are suspended in PBS to obtain a McFarland index of 1.8, measured with a densitometer. The McFarland index is a scale used to estimate the

[22] Potency should not me mistaken with purity as the latter is a measure of how chemically pure the antibiotic is. This measurement is useful to ensure the product is not contaminated during the manufacturing process, or to identify the presence of impurities. Potency, on the other hand, is a measure of how active the antibiotic is. This efficacy is measured using microbiological assays, chemical assays, or immunological assays. However, impurities may influence the potency of the antibiotic.

[23] This hypothesis of autolysin activity rose from unexpected and non-reproductible results from this very same experiment, performed on 72h incubated *S. epidermidis ATCC 35984 strain*. Said results are presented in *Appendices* in section *3.3 Results after potential autolysin AtlE activity on* S. epidermidis ATCC 35984 *strain*.

turbidity of a bacterial suspension, making it possible to standardize the concentration of bacteria prior to microbiological testing. [98]

This suspension is then diluted 40x in RPG. Each of the following wells is filled with 200 μL of our bacterial suspension as shown in the *Figures 25* and *26*:

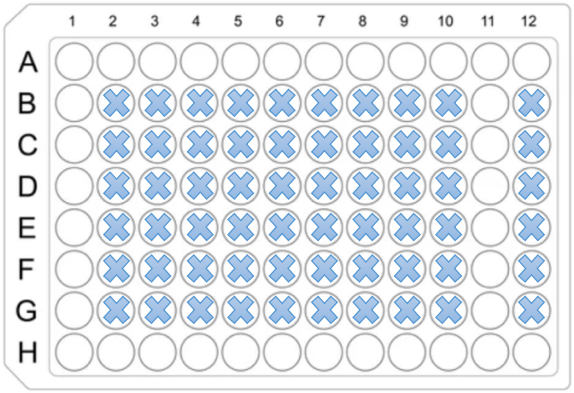

Figure 25: **Coated 96 microwells plate.** Wells on which biofilms of *S. epidermidis ATCC 35984* are grown are shown with blue crosses. Said wells were all coated upstream with a $(LL\text{-}37 - HEP)_{14.5}$ coating.

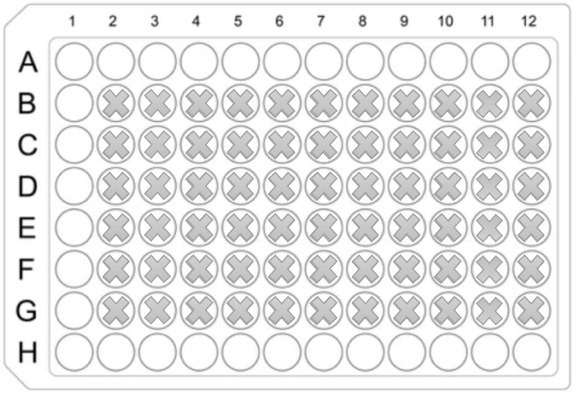

Figure 26: **Uncoated 96 microwells plate.** Wells on which biofilms of *S. epidermidis ATCC 35984* are grown are shown with grey crosses. Said wells were all not coated upstream.

The plates are then placed in an incubator at 37°C for 24h. Bacteria then grow and form a 24h pre-formed biofilms on the surface of the bottom of the microwells. The plates are then washed 2x with 200 μL of PBS to remove unattached bacteria and residual medium. After washing, 200 μL of antibiotic solutions with different MICs, as explained above, are added as shown in the following *Figures 27* and *28*.

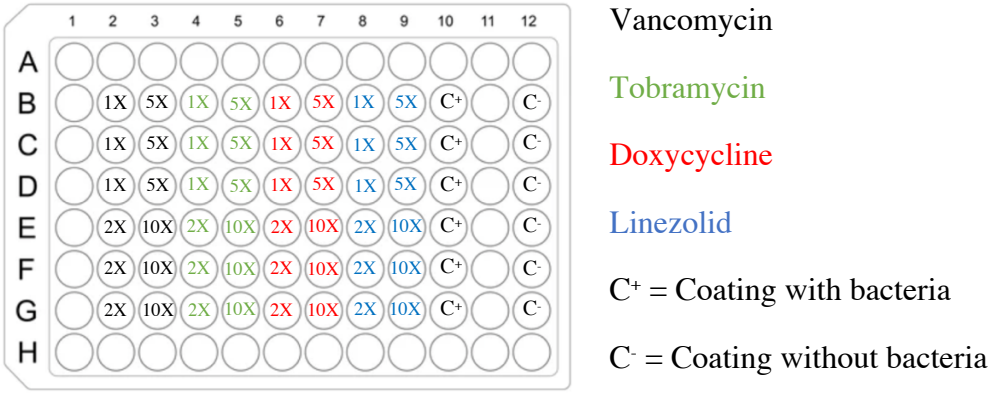

Figure 27: Introduction of **antibiotics at different concentrations**, corresponding to a multiple of their MIC (1x, 2x, 5x, or 10x) on 24h-preformed biofilms of *S. epidermidis ATCC 35984* on coated wells.

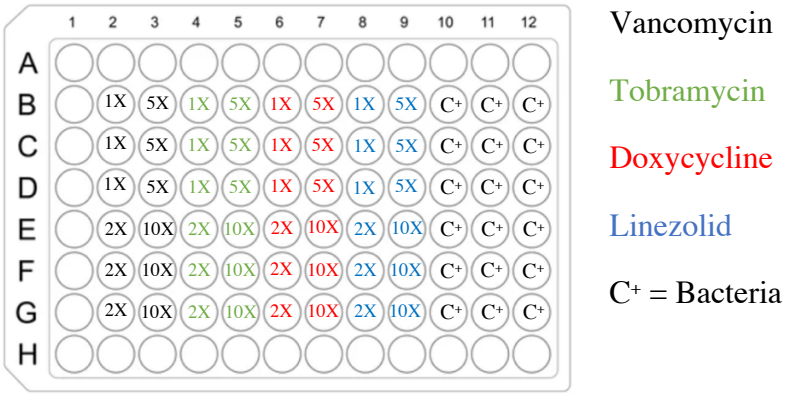

Figure 28: Introduction of **antibiotics at different concentrations**, corresponding to a multiple of their MIC (1x, 2x, 5x, or 10x) on 24h-preformed biofilms of *S. epidermidis ATCC 35984* on uncoated wells for the study of biomass and metabolism reduction.

Once the antibiotics have been added to the microwells, the plates are incubated for 24h at 37°C and then washed with PBS. Plates used for the crystal violet testing are placed in an oven at 60°C for 24h to remove residual PBS and stabilize the biofilm. The other plates used to study bacterial metabolism (resazurin) are processed after the 2 washes.

4.2.3 Crystal violet test

24h after the plate has been placed in the oven at 60°C, 200 μL of 1% crystal violet is added to the microwells and allowed to act for 10 min in the dark. Excess crystal violet is then removed by rinsing the wells with demineralized water to remove crystal violet not attached to the biomass. In order to resolubilize the crystal violet and analyze it by absorbance at $\lambda = 570$ nm, 200 μL of 66% acetic acid are set into the microwells for 1h.

4.2.4 Resazurin test

200 μL of resazurin 10 mg/L solution is obtained from the 100x dilution in PBS of a stock solution of 1mg/mL. After 4h incubation at room temperature and protected from daylight,

analysis under fluorescence in a Spectramax at $\lambda_{emission}$ = 590nm and $\lambda_{excitation}$ = 550nm is performed.

4.2.5 CFU counting

CFU, or Colony-Forming-Units, counting, was also performed to test antibiotics and coating treatment on bacteria. Unfortunately, experimental error based on misuse of the sonicator led the wells to mix with each other and distorting results. Protocol and results for CFU counting are available in *Appendices* in section *3.2 CFU counting*.

PART V – Results and Discussions

The results of the various experiments mentioned in the *Materials and Methods* section will be presented in this section, organized in four parts.

The first part will describe and analyze the results concerning the formation of PPCs. The charge ratio at which the formation of PPCs seems favored will be identified. The second part will focus on the optimization LL-37 release from the multilayered coatings to enable CD analysis. As a continuation of this second part, a third part is dedicated to the determination of the best conditions for LL-37 adsorption in both types coatings, from results of LL-37 remaining in the microwells after the release experiment. Finally, the last part will discuss the synergy between the bare LL-37-based AMC and the four studied, routinely-used, antibiotics.

1. PPCs optimal charge ratio determination

This experiment was conducted to assess what charge ratio would seem to optimize PPCs formation. In other words, what ratio of negatively-charged HEP and positively-charged bare LL-37 will be used to assemble the PPCs-based coating used in further experiments, as being the ratio at which PPCs are formed, and especially at which the most PPCs are formed.

As explained in the *Materials and Methods* section, turbidimetry measures the reduction in light intensity as it passes through the sample containing the PPCs. This reduction occurs due to light scattering, where particles deflect light in various directions. The degree of scattering is function of the number and/or size of the particles.

The experiment gave absorbance values as a function of charge ratio to quantify reduction of light intensity. The experiment was carried out with pH 3.5 solutions and in triplicate to obtain reliable statistical data (see *Appendices, Table II*).

The mean and standard deviation were calculated from the results of the triplicate values obtained for this experiment and plotted on *Figure 29*.

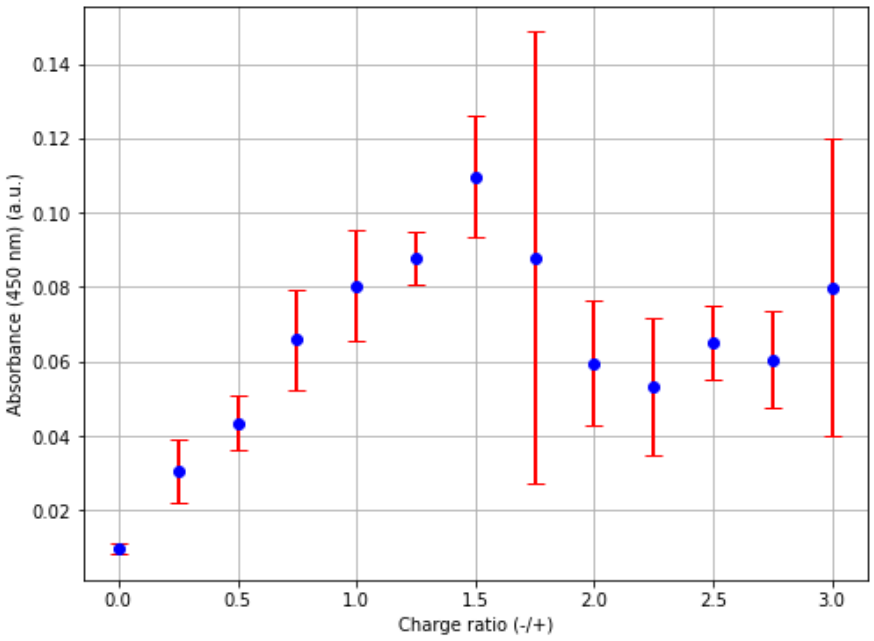

Figure 29: Absorbance as a function of charge ratio (-/+) used to form PPCs.

Data reveals that absorbance values increase progressively with charge ratio, reaching a maximum when the negative charges of HEP and the positive charges of LL-37 reach a total net ratio of 1.5 (-/+), before decreasing, and then stagnate. This maximum indicates the optimum charge ratio for PPCs formation, being the value for which the solution is the most turbid. Under these conditions, the light is the most scattered by PPCs meaning they are in the highest number or in the biggest size possible.

As explained in the *State of the art*, molecular charges play a crucial role in PPCs formation. At a charge ratio (-/+), the opposing charges are visibly balanced in a way that allows maximum interaction between HEP and LL-37 molecules, resulting in the formation of numerous, or large, complexes.

The obtained results for experiment in pH 3.5 conditions give information on the charge ratio for which the solution is the most turbid. For further experiments, the charge ratio (-/+) will be respected, varying quantities of LL-37 according to its charge level in the pH conditions of the said experiment (see *Materials and Methods*). Indeed, for experiments at pH 5, the quantities of LL-37 must be adjusted accordingly, taking into account the differences in charge of the molecules under these modified pH conditions, as shown in the *Materials and Methods* section.

As mentioned from the beginning of this section, a more turbid solution can either be a result of a higher number of complexes, as well as complexes of more important size. Either way, our hypothesis would be that adsorbing PPCs at charge ratio (-/+) in the AMC could allow to have an optimized reservoir of LL-37 in the coating, whether PPCs are bigger or more numerous. However, we also think that size of PPCs may affect coating's formation dynamics or further rearrangements within the coating, resulting in a more heterogenous charge compensation of

the layer and further repulsion of the next layer, all in all leading to a lower quantity of LL-37 adsorbed in the coating.

To determine whether the optimal charge ratio is due to the high number of PPCs or their large size, a dynamic light scattering (DLS) analysis could be considered. Although beyond the scope of this thesis, such a study is an interesting prospect.

2. Study of LL-37 release from the coating

2.1 Determination of optimal conditions for LL-37 release

Hereunder are presented the results and the discussion of the experiment aiming to determine the optimal conditions for coatings construction (pH and number of BLs) as well as the volume of PBS for LL-37 sampling when released from the coatings. As a reminder, this experiment aims at finding conditions to release as many LL-37 as possible from the AMC, to detect a signal in CD, and finally determine LL-37 conformation while released from the coatings. To detect LL-37 signal in the PBS solution by CD, it is necessary to reach a sufficient and detectable concentration (estimated around 30 μg/mL), to gather information on the peptide's secondary structure. The experiment was quantified through fluorescence spectroscopy as described in *Materials and Methods* section, using labeled LL-37 in the two types of coatings (bare LL-37-based and PPCs-based).

2.1.1 Results

Results were then obtained in duplicate, for 6 different conditions (varying the volume of PBS for release, the number of BLs of the coating, and the pH used for coating construction), for both types of coating, at 13 different times. Indeed, release of LL-37 was performed in 13 steps, at 13 different times for sampling the released peptide in the PBS volume present in the coated microwells. For each step, the PBS solution in the microwells was renewed and each solution of PBS containing the released LL-37 was quantified through fluorescence spectroscopy. The calibration curve showed in the *Materials and Methods* section allowed to determine the mass of released peptide at each sampling time, for each condition, from the obtained fluorescence data. Quantities in μg of released LL-37 (PPCs and bare) from the coating for 13 sampling depending on the condition at different times are available in *Appendices, Tables III* and *IV*.

PBS solution renewal was performed to study release kinetics, but also to prevent the solution from becoming saturated with the released peptide, and thus maintain continuous release.

As CD analysis will be performed on one single sample, optimal conditions for LL-37 release must be determined from one final concentration. Indeed, technically speaking, for CD analysis, all solutions sampled would be gathered in one final sample, in one final tube, giving one final

concentration that corresponds to the mean of the concentration of all the samples added. Using the quantities released for each condition obtained by fluorescence spectroscopy, the final concentrations are obtained by dividing the total mass of released peptide by the total volume of the solution (13 times 300 μL or 200 μL) and are presented in the following table (*Table 7*).

Table 7: Concentration of released LL-37 from a coated polystyrene microwell obtained by summing quantities released for 13 sampling times and divided by total PBS volume, meaning 13 x 300 μL or 200 μL, depending on the condition. (μg/mL)

Condition	**1**	**2**	**3**	**4**	**5**	**6**
PBS (μL)	300	300	200	300	300	200
BL	20	16	16	20	16	16
pH	3.5			5		
LL-37 in PPCs (μg/mL)	0.86	0.80	0.90	1.77	1.43	2.01
Bare LL-37 (μg/mL)	13.36	7.54	13.17	4.10	2.90	3.35

Note to reader: The authors made the choice to present data from *Table 7* in several graphs (*Figures 31* and *34* use concentration values from *Table 7, Figures 30* and *32* use mass values derived from *Table 7*) to illustrate the effect of different conditions on LL-37 release. The displayed data on the figures is then every time obtained from *Table 7*, but according to the section, a variable (BLs number or PBS volume) will be fixed to observe the influence of the other variable.

Results show that concentrations for PPCs and bare LL-37 released, at any condition, are not sufficient to enable CD analysis (all < 30 μg/mL). However, thanks to these results, it is possible to discuss and identify the best conditions to exploit for coating construction, to optimize peptide release for further experimentation.

As concentration of PPCs released is very low at both pH conditions, even if the latter will be discussed, this part will focus essentially on optimizing the conditions for bare LL-37 release. Nevertheless, the following part, discussing LL-37 adsorption, will attempt to identify what factor could have led to a small release of PPCs.

Attention must be paid to the fact that fluorescence spectroscopy calibration curve was performed for a 0-3 μg range (see *Materials and Methods* section) considering the small quantity of LL-37 expected to be released between each sampling (every 30 min for 6h and then once after 24h). However, samples for release after first 30 min and 24h for bare LL-37 at pH 3.5 gave results way above 3 μg (max = 24.51 μg). This must be taken into account as the values may have diverged from the calibration curve, and may have been underestimated or overestimated. Indeed, we do not know whether the calibration curve follows the same trend for larger quantities. With hindsight, we realized that we could have performed a 10X dilution of the samples presenting a released quantity above 3 μg, to quantify more accurately the LL-37 in this new sample. Although non as precise as desired, the obtained results already give a general

idea on LL-37's release behavior in different conditions. These conditions are discussed here-under.

2.1.2 Discussion of conditions studied for LL-37 release

This section will discuss the optimal conditions for LL-37 release. Highlighting these optimal conditions aims to remodel the protocol to obtain a sufficiently high, analyzable concentration of LL-37 by CD.

2.1.2.a Optimal PBS volume for LL-37 release

The release in PBS of the LL-37 contained in the coating was performed using two volumes: 200 μL and 300 μL. To enable consistent comparisons, data obtained at pH 3.5 and pH 5 with 16 BLs (conditions 2 and 3, and conditions 5 and 6) for PPCs and bare LL-37 are compared, giving results for a fixed number of BLs (16) and varying PBS volume, to study the effect of this variable.

Results are displayed for accurate comparison in terms of mass since a smaller volume (200 μL) of PBS would anyways lead to a higher concentration than a higher volume (300 μL).

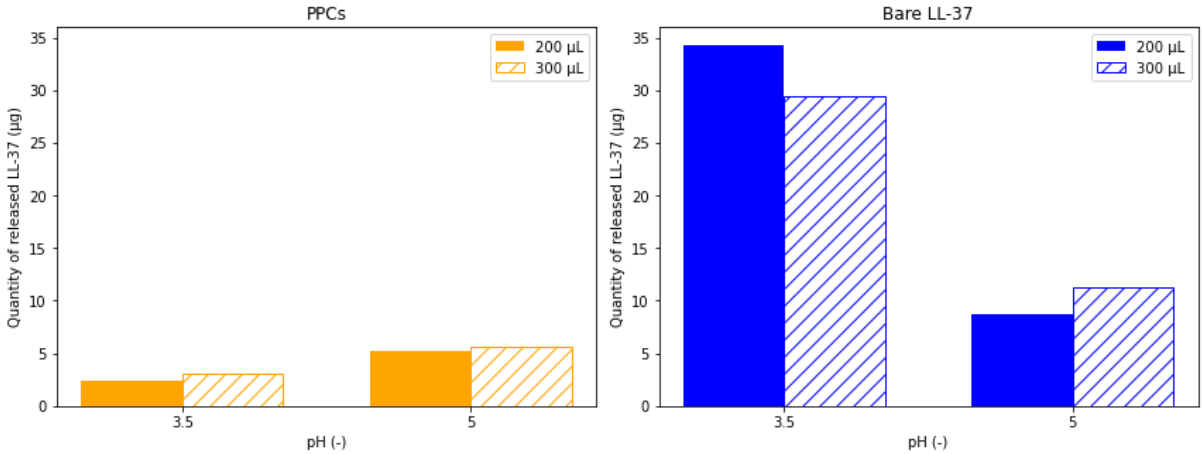

Figure 30: Quantity of released LL-37 as a function of PBS volume in μg (left = PPCs, right = bare LL-37) for a 16 BLs coating.

Graphs in *Figure 30* show that, for PPCs and bare LL-37, at the two pH values, the mass released is comparable for 200μL or 300μL. As a reminder, the purpose of using 300 μL was to determine whether the solution was saturated at 200 μL, and to assess the kinetics of the release. Results, especially for bare LL-37, led us think that PBS solution is not saturated in released peptide while working with a volume of 200 μL, since the quantity released in 200 μL and 300 μL are comparable.

In the interest of continuity between the results presented in this section, the quantities released are expressed in terms of concentration (see *Table 7*). *Figure 31* then presents the results of *Figure 30* in μg/mL.

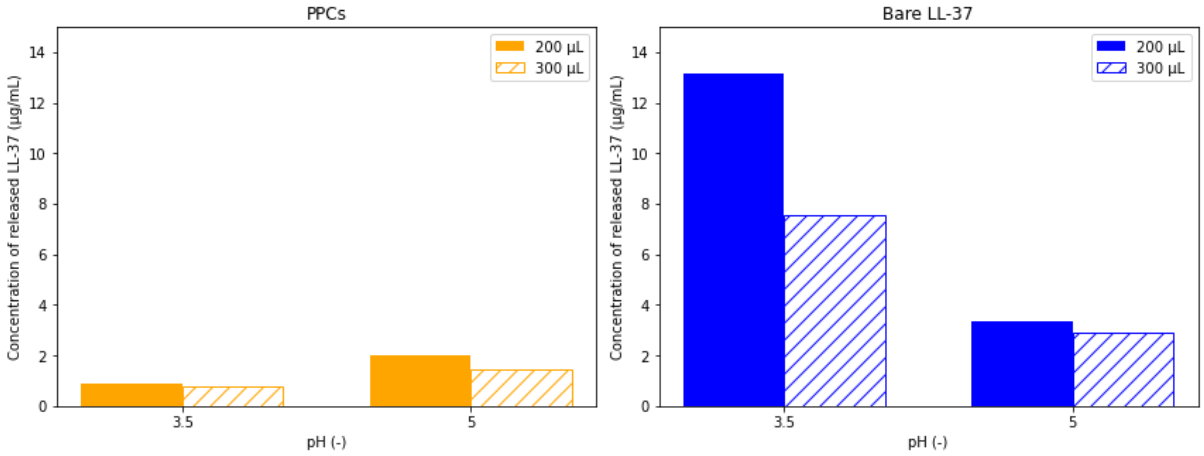

Figure 31: Concentration of released LL-37 as a function of PBS volume (μg/mL) (left = PPCs, right = bare LL-37) for a 16 BLs coating.

When taking into account the total PBS volume, the results expressed in concentration show, as expected, that for any condition, 200μL of PBS allows to reach a higher concentration than a volume of 300μL. The difference between the two PBS volume conditions is more obvious for bare LL-37 at pH 3.5. Anyways, given that a minimal concentration of 30 μg/mL must be achieved for CD analysis, results suggest that using a high volume of PBS for releasing the peptide is not relevant as it dilutes too much the LL-37 in the solution.

In conclusion, it is necessary to minimize the release steps and use small volumes of PBS to avoid diluting the peptide too much in solution. To do so, the used PBS volume to optimize released LL-37 concentration for CD analysis has then been chosen to be 100μL. As results showed no saturation of the solution for 200μL, we made the hypothesis that there would be no saturation of the released LL-37 in 100μL either.

Since the coating has been constructed with 200μL of each condition, 100μL of PBS do not cover the entire surface of the coating, leaving some non-submerged coating on the wells' walls. However, the submerged surface for 200 μL of PBS is 1.56 cm^2, versus 0.95 cm^2 of the coated well covered by 100 μL of PBS. For a volume reduced by a factor 0.5, the coating surface releasing in the volume is only 0.61 times lower. Ratio of these factors show that there is an advantage to reduce PBS volume even more as it will cover more coating in comparison, and potentially allow a better concentration of the LL-37 released from the submerged coating[24].

2.1.2.b Optimal sampling times for LL-37 release

Another factor increasing LL-37 dilution in the final solution is the too recurrent PBS solution renewal. Indeed, *Figure 32* shows the cumulative curve of the quantity of bare LL-37 released for bare LL-37 for condition 1, and shows that there is little interest in replacing the PBS solution often, as the gain in mass between each step is not very significant, which leads to a dilution

[24] Afterthought leads us to say that building the coating with 100 μL to avoid coatings losses on the wells' walls could have been of interest in this case. However, since release experiment has been undergone on a turntable, we allow ourselves to think that the 100 μL PBS solution could have partially covered the coating left on the walls (that would not be submerged in 100 μL of PBS without the turntable).

of this released quantity, resulting in a non-optimized final concentration of the sample to be analyzed by CD.

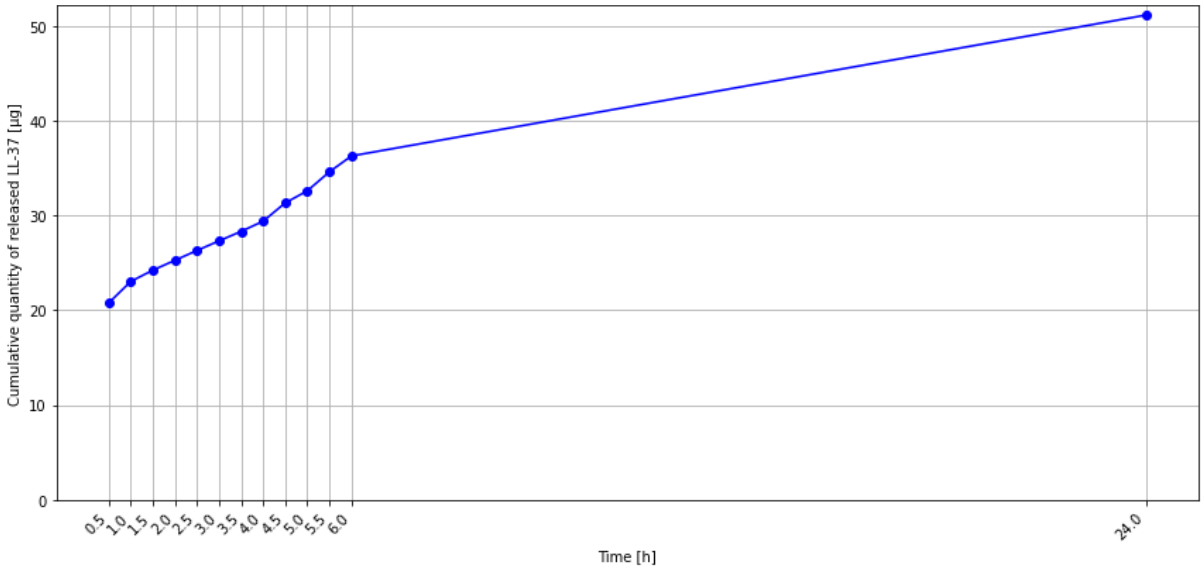

Figure 32: Cumulative curve of bare LL-37 release kinetics (μg) (PBS volume = 300, pH = 3.5, BLs number = 20)

Figure 32 also shows that the quantity contained in the volume of the first sampling (30 minutes) is greater than the sum of all the quantities released between 30 minutes and 6 hours (20.77 μg against 15.51 μg). In fact, a burst release is then observed during the first 30 minutes of release, which is very interesting. This trend can be observed for all other conditions, for bare LL-37 and PPCs. This observation can also be confirmed by *Figure 33*, thanks to the results of former students, Coralie Nerincx and Noémie de Suraÿ, in their Master's thesis[25].

This graph also shows that release of LL-37 is still important after 24h of release. However, it gave no information on whether the released stopped before 24h after the experiment. Yet, *Figure 33* shows that LL-37 release does continue after 24h.

[25] This discussion will refer several times to the work of Coralie Nerincx and Noémie de Suraÿ. All the experiments we will refer to are obtained from their work performed in the context of their Master's thesis on *Preventing bacterial infections of hip prostheses: study of interactions between antimicrobial agents and of LL-37 release from a coating*.

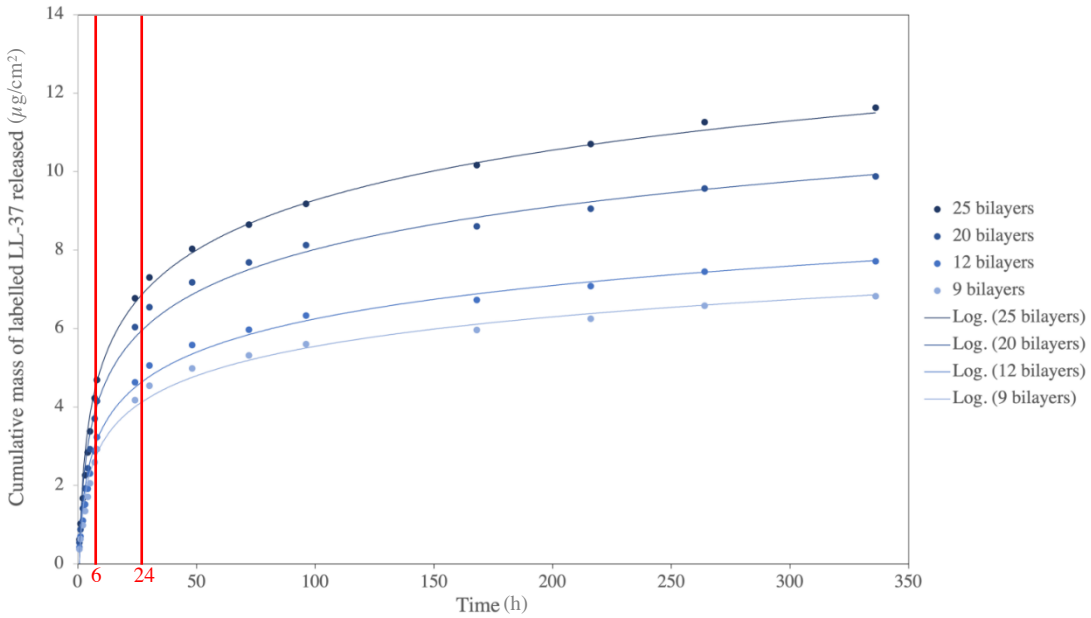

Figure 33: Cumulative curves of the mass of LL-37 released per square centimeter of coating from different bare LL-37 - based multilayers constructed at pH 3.5 ($\mu g/cm^2$)

After the kinetics analysis of the LL-37 release from the coating, samples were chosen to be taken out after 6h and 24h. These times were chosen because, as shown in *Figures 32* and *33*, the amount of LL-37 released is significant during the first 6 hours. The second sampling is carried out after 24 hours to allow LL-37 to be released and accumulate in the PBS, as we can see that the release is no longer as intense as in the first hours. This minimizes the number of steps and avoids diluting the amount of peptide.

To enable CD analysis, a volume greater than 200 μL (2 times 100 μL, sampled after 6h and 24h) is needed. To achieve this volume, 10 coatings (in 10 microwells) were constructed. All samples were mixed, giving a total final volume of 2 mL, sufficient for CD analysis. The experiment is performed for bare and complexed LL-37, resulting in two tubes of 2 mL, one containing the released bare LL-37 obtained from the two sampling times of 10 coatings, and the second one containing PPCs.

2.1.2.c Optimal bilayers number

To assess whether increasing the number of BLs during coating construction improves the release, *Figure 34* shows the concentration of released LL-37 from *Table 7*, for a fixed PBS volume (300 μL) for release, under conditions 1 and 2 at pH 3.5 (*Table 7*), and under conditions 4 and 5 at pH 5 (*Table 7*).

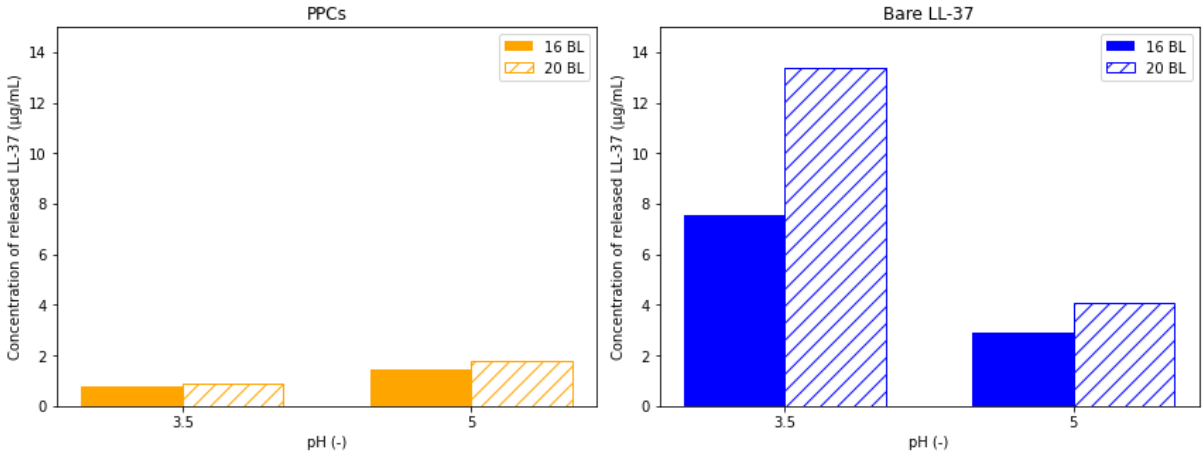

Figure 34: Concentration of released LL-37 as a function of BLs number (μg/mL) (left = PPCs, right = bare LL-37) for a fixed PBS volume for release (300μL)

In both cases, the concentration of LL-37 released increases when the coating is constructed with more BLs, even if this tendency is less pronounced for PPCs at pH 3.5. These results seem logical, as it would be expected from a coating with more BLs to adsorb more LL-37, and subsequently release more of the said peptide. This hypothesis will be discussed in the section *3. Study of LL-37 adsorption in the coatings*.

To determine the number of BLs needed to reach a concentration of 30 μg/mL of the released peptide, results shown in *Figure 33* were used. We chose to use these data for our predictions, as our values in *Table 7* are higher than those obtained by Coralie Nerincx and Noémie de Suraÿ, then certainly overestimated. The option to base our predictions on their smaller values allowed to minimize the risk of overestimation of the released quantity of the new experiment. Prediction based on their data, obtained from a 96 microwells plate, led us to build 50 BLs in 96 microwells plate. In these conditions, the expected concentration released of bare LL-37 would be 54.15 μg/mL (see *Appendices*, *Table VII*).

2.1.2.d Optimal pH for coating construction

Figure 31 and *Figure 34*, displaying our results for PBS volume and BLs number variables, respectively, show that the concentration of LL-37 released is higher for bare LL-37 when pH 3.5 is used for coating construction, and pH 5 for PPCs. To optimize LL-37 release, coatings were then built at pH 3.5 for LL-37 and pH 5 for PPCs.

2.1.2.e Specific area

As *Figure 34* showed an increased release potential for LL-37 in plates containing more BLs, this led us to think that a coating that have adsorbed a more important quantity of LL-37 up-stream would allow a more important release of its components. In order to increase the amount of LL-37 adsorbed in the coatings, increasing the specific surface area on which the coatings would be constructed may be an interesting option. Specific surface area is a measure of the total surface area of a material per unit mass, volume or quantity. [99]

As the experiment was carried out on a 48 microwells plate, calculations were performed to study a new method that would allow an increase in specific area. In fact, we implemented a whole different protocol involving the use of 20 nm diameter gold nanoparticles, in stabilized suspension in citrate buffer (Sigma-Aldrich®). After nanoparticles washing, LbL process is performed by immersing the suspended nanoparticles in PEs solutions, in 2 mL Eppendorf tubes. After being set for 20 minutes, the suspension was centrifuged, the supernatant collected and the pellet recovered, which was then resuspended with the new PE solution of opposite charge after washing.

With these nanoparticles, we planned to increase the specific surface area of the microwells by 25 times compared with the initial microwells surface. Once again, prediction calculation of the amount of LL-37 these nanoparticles could release was performed based on results obtained by Coralie Nerincx and Noémie de Suraÿ, as our results in *Table 7* seem to have been overestimated. According to their data, the amount of LL-37 released per unit of area ($\mu g/cm^2$) for 20 BLs, after 24h, is 6 $\mu g/cm^2$. After prediction calculation, the expected concentration of bare LL-37 released from a 20 BLs coating built on the gold nanoparticles was expected to reach 64.1 μg/mL after 24h (see *Appendices*, *Table V*). Unfortunately, during coating construction, two major problems arose.

Firstly, centrifugation to recover the pellet containing nanoparticles was not optimal. Some of the nanoparticles remained in suspension, resulting in a loss at each centrifugation when the supernatant was collected. To reach the concentration of 64.1 μg/mL with 20 BLs, 88 washes and 44 solution changes (20 BLs + 1 AL) would have had to be performed. After the 132 centrifugations to construct the 20 BLs, the nanoparticles loss was too important. The hypothesis made was that this low-quality centrifugation was due to the quite small size of nanoparticles, which are colloidal particles. At this scale, van der Waals and other intermolecular forces could prevent the eased separation of colloids and the supernatant after centrifugation.

Secondly, an aggregation problem has arisen. During AL formation, the positively-charged CHI adsorbs itself on nanoparticles, as required to initiate LBL. After removal of the CHI solution and two washes, the HEP solution resuspended the nanoparticles in order to continue AL construction. However, when this solution was added, a black aggregate formed. The positively-charged nanoparticles reacted with the negatively-charged HEP, forming a nanoparticle complex, making LbL impossible.

In conclusion, although theoretically promising for increasing the concentration of LL-37 adsorbed and then released, the nanoparticles presented separation and aggregation problems that prevented us from pursuing this approach.

2.2 Released LL-37's conformation determination by CD

The previous experiment allowed us to assess the parameters optimizing the release of bare LL-37 and complexed LL-37. *Table 8* summarizes the conditions used to build the coating and to release the LL-37, for further CD analysis.

Table 8: Conditions for coatings building to maximize release of LL-37 in PBS.

Coating	**PPCs**	**LL-37**
PBS (μL)	2 x 100	
BL	10 coatings of 50 BLs	
pH	5	3.5
Sampling time	6h and 24h	
Microwells plate	96	

Samples of LL-37 released from the 50 BLs coating formed with bare LL-37 and complexed LL-37 as PPCs were analyzed by CD. The following graphs show the obtained results. Firstly, the signals for standard solutions, being the PBS solution and LL-37, PPCs, HEP and CHI prepared at 30 μg/mL in PBS, are shown on *Figure 35*:

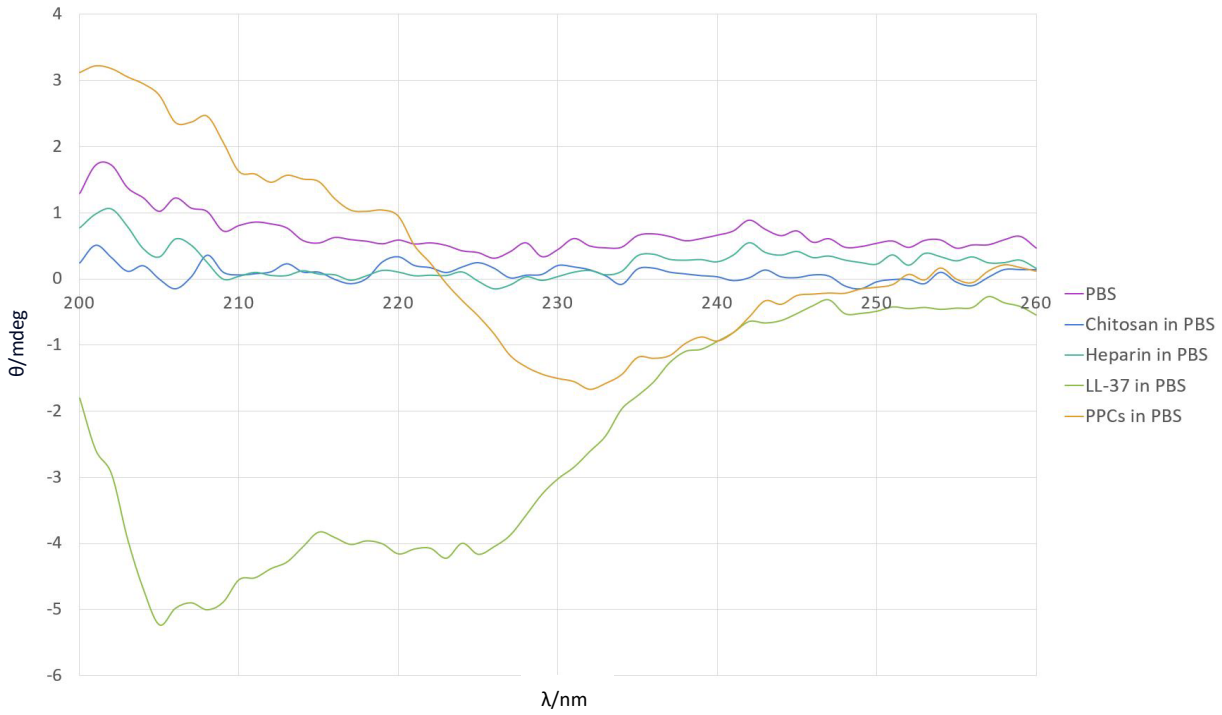

Figure 35: CD spectra of PBS and CHI, HEP, LL-37 and PPCs at 30 μg/mL.

CD analyses the secondary structure of proteins or other chiral molecules in solution (α-helices and β-sheets). HEP and CHI show stereogenics centers, but the CD signals oscillate around zero over the entire wavelength range. This observation suggests the absence of well-defined secondary structures, or that the structures are poorly organized. As explained in the *State of*

the art, CHI and HEP, being polysaccharides, show little conformational regularity, which explains their weak signal. Finally, PBS is a buffer that shows no CD signal, as it contains no chiral molecule.

LL-37 at a concentration of 30 μg/mL in PBS seems to adopt an α-helix conformation, as revealed by the minima observed at 208 and 222 nm, and the positive band around 193 nm (not shown on the graph[26]). However, the curves are not as defined as those shown in *Figure 16* (Cédric Vranckx's results), suggesting that the concentration of LL-37 in the PBS solution may not be sufficient to achieve comparable precision. These results then seem to confirm that 30 μg/mL is the minimal concentration allowing to identify the peptide conformation, and provide non-precise but acceptable signal.

The signal obtained by PPCs did not display the recognizable spectrum of an α-helical. In fact, this solution was wrongly prepared with the same volumes of HEP and LL-37 used for a charge ratio (-/+) of 1.5 at pH 3.5 (see *Table 1*). To maintain this charge ratio at 1.5, it would have been necessary to adjust the volume of LL-37, whose charge varies according to the pH, which corresponds to the physiological pH of 7.4 for PBS. The obtained (-/+) ratio has been calculated afterwards, in a similar way as the calculations in the *Materials and Methods* section, as being 2.58[27]. *Figure 29* shows that this ratio is not optimal for PPCs formation. It is then possible that the complexation did not take place, which could have led to the aggregation of the components used for PPCs formation instead, being the potential reason that the expected pattern of the signal showing an α-helical structure is not observable on the spectrum.

Additionally, the ionic strength of PBS, different from that of ion-free ultrapure water, could have influenced PPCs formation. Indeed, when PPCs are in ultrapure water, the ionic strength is very low, allowing the opposite charges to interact without interference. However, when the two oppositely-charged compounds are in PBS solution, the ions in the PBS screen the charges of the compounds, reducing their electrostatic interactions.

An experiment was conducted by Zhang et al. to study the influence of ionic strength on the stability of PPCs formed by positively-charged poly(diallyldimethylammonium chloride) and negatively-charged poly(sodium 4-styrenesulfonate). The study found that in low ionic strength environment, PPCs remain stable, with strong electrostatic interactions preventing aggregation. However, as ionic strength increases, added salt screens these interactions, leading to larger aggregates and instability. At very high ionic strengths (e.g., 3.0 M NaCl), PPCs may de-

[26] When CD analysis is performed, voltage values are used to compensate for sample absorbance. If the absorbance of the sample is too high, the compensation voltage can reach considerable values. When these voltage values reach around 600V or more, the data obtained by CD becomes unreliable and is therefore not taken into account. For this reason, values between 190 and 200 nm are not shown on the graph. As a result, the positive band at 193 nm is not visible.

[27] The (-/+) charge ratio is then more important since the LL-37 is less positively-charged at pH 7.4 (+6) than at pH 3.5 (+10.39). The charge ratio was calculated for PPCs formation in ultrapure water and did not take into account the ionic strength of PBS.

complex back into individual PE chains due to excessive screening of electrostatic interactions. [100]

To avoid the risk of aggregation, PPCs should be constructed at different charge ratios in PBS and the same turbidimetric analysis, as described in the section *1. PPCs optimal charge ratio determination*, should be performed to identify the charge ratio favorable to their formation in PBS.

Figure 36 shows the signals for LL-37 released from both types of coating, following the protocol showed in *Table 8*. These signals were obtained by subtracting the contributions of HEP and PBS in the case of the coating with bare LL-37, as it is found in PBS and HEP is also released with the peptide. For the coating constructed with PPCs, the contributions of HEP, PBS and CHI have been subtracted.

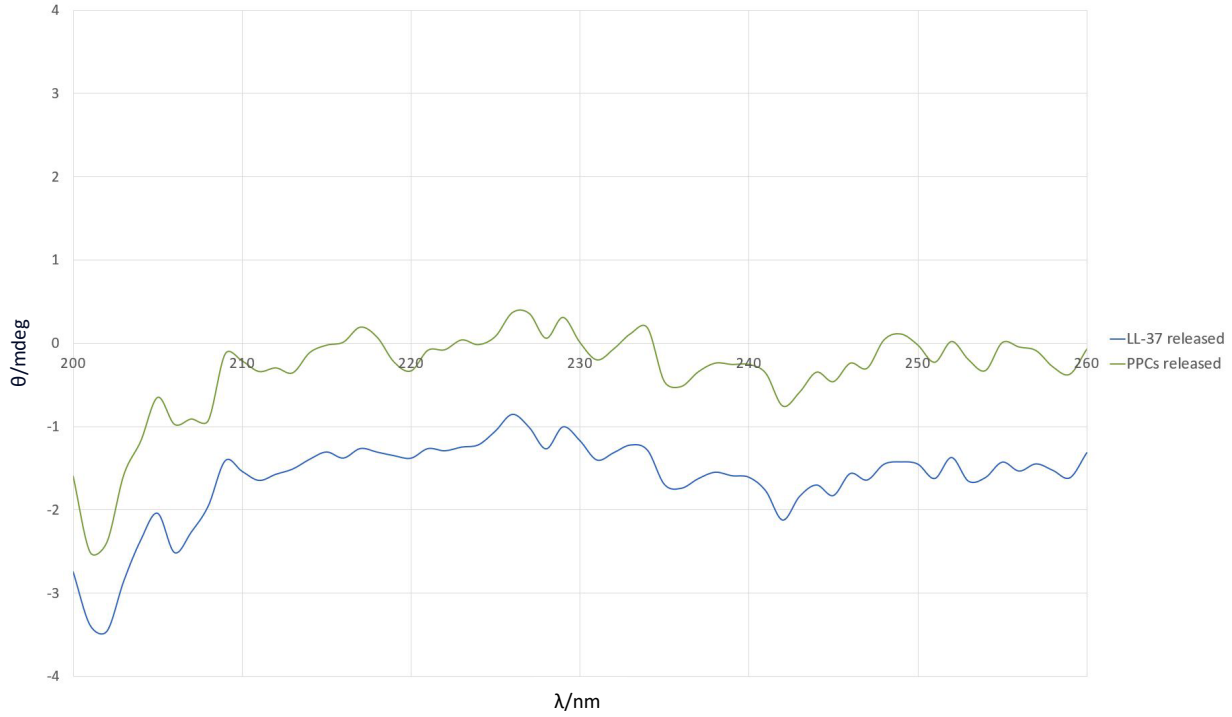

Figure 36: CD spectra of released LL-37 from PPCs-based and bare LL-37-based coatings at unknown concentration, estimated around 30 μg/mL.

The signals in *Figure 36* do not allow to determine the conformation of LL-37 when released. The curves obtained for bare LL-37 and PPCs are similar, and the signals obtained are quite low (same order of magnitude than signals obtained from PBS, CHI and HEP in *Figure 35*). This suggests that the LL-37 concentration in the samples is not sufficient. As explained after the presentation of the results of the released LL-37 (*Table 7*), PPCs-based coating does not have an important release capacity. It is then not surprising that the 30 μg/mL concentration was not reached for PPCs.

However, in the case of bare LL-37, we can also see that the concentration released did not reach 30 μg/mL, as we did not detect the minimal signal that would allow us to determine its conformation, which is surprising as our calculations predicted a concentration of 54.15 μg/mL.

The first hypothesis as to why this concentration was not achieved is that the amount before the release was not optimal. Given that a BL requires 50 minutes to construct, the formation of the 50 BLs took place over a period of 5 days. When the plate was kept refrigerated overnight, water at pH 3.5 or 5 was added to the microwells, depending on the coating. It is possible that some of the LL-37 was released into the water during these waiting periods, resulting in peptide losses. In addition, LL-37 may have degraded over time, leading to its denaturation and consequent loss of α-helix conformation.

A second hypothesis can be also considered. The fact that the 30 μg/mL concentration was not reached could mean that the LL-37 released only concerns the surface layers in contact with the PBS, meaning that increasing indefinitely the numbers of BLs for coating formation has no interest. By optimizing conditions such as the number of BLs, the stock of LL-37 may be greater, but the release would not be more intense. To verify this hypothesis, an experiment could be carried out to determine whether the increase of LL-37 release due to an increase of the BLs reaches a threshold before 50 BLs.

3. Study of LL-37 adsorption in the coatings

LL-37 remaining in the coatings after the release experiment was quantified through BCA assay (see *Materials and Methods* section) to determine what conditions were optimal for LL-37 adsorption, to pursue the following goals.

Firstly, the previous experiment showed that LL-37 release from the coating is not as straightforward as we thought. Indeed, after 24 hours, the coating did not even release a concentration of 30 μg/mL of the peptide. This following experiment will therefore determine whether this small release concentration is due to a small amount of LL-37 adsorbed in the coating upstream, when it was constructed, or a small release rate.

Also, in the previous section *2. Study of LL-37 release from the coating*, we made the hypothesis that a coating with more LL-37-containing BLs was destined to release more LL-37, following the observation that a coating of 20 BLs released more LL-37 than a 16 BLs coating. This section would then confirm whether this assumption was correct or if something else explained the difference in release of the two different coatings.

Lastly, the following section covering LL-37's synergy with antibiotics shows a significant activity of the peptide on biomass (through synergy with antibiotics). The AMC is thought to be release-active, but the release experiment showed that even after 24 hours, the latter did not release a concentration close to its MIC (>512 μg/mL), showing that the released LL-37 can either have an effect on bacteria below its MIC, or that the activity of the coating is partially due to the LL-37 immobilized. In this idea, the following experiment would be interesting to

assess the optimal conditions for LL-37 immobilization, and therefore, for coating's potential contact-activity on bacteria[28].

3.1 Remaining LL-37 in the coatings after release

The experiment enabled to determine the quantities (through BCA assay) of LL-37 remaining after release. Knowing the quantities released from and remaining in the coating will allow to deduce the mass of LL-37 adsorbed during coating construction for a certain polystyrene microwell area[29] (in $\mu g/cm^2$).

Table 9: Quantity of LL-37 remaining per cm^2 of coated polystyrene microwell after LL-37 release in PBS. ($\mu g/cm^2$)

Condition	**1**	**2**	**3**	**4**	**5**	**6**
PBS (μL)	300	300	200	300	300	200
BL	20	16	16	20	16	16
pH	3.5			5		
LL-37 in PPCs ($\mu g/cm^2$)	18.40	18.01	18.26	17.72	17.72	17.46
Bare LL-37 ($\mu g/cm^2$)	11.58	13.52	13.20	16.40	16.80	16.76

The values in *Table 9* show that the amount of the AMP remaining in the microwells seems to be more important in the case of PPCs. But, attention must be paid that, in the case of PPCs-based coating ($(PPCs\text{- }CHI)_n$), CHI is also quantified through BCA assay since its amine groups also reacts in the BCA reaction. As explained in the *Materials and Methods* section, the exact interference of CHI is unknown, but estimated quite low. Considering this, the BCA signal will be fully attributed to LL-37 in our discussions, but the potential of an overestimation of LL-37 quantity due to CHI quantification cannot be ignored.

While quantities remaining at pH 5 for PPCs and bare LL-37 at pH 5 are comparable, at pH 3.5 however, the difference between PPCs and LL-37 coatings is quite important. A higher quantity remaining in the PPCs-based coatings at pH 3.5 than for bare LL-37-based coating can either be due to a lower PPCs release, or to a higher adsorption of PPCs inside the coating during coating construction, or both. Next section will allow us to answer this question.

[28] The authors made the hypothesis that, if the coating reveals in the future to be contact-active, a higher quantity of LL-37 adsorbed in the coating would lease to an increased activity of the coating. However, nothing now allows us to say that all the LL-37 immobilized in the coating can enter in contact with bacteria cell membrane. This hypothesis is more developed in the *Future prospects* section.

[29] Area of the coating on a polystyrene microwell was determined by summing the bottom area of the microwell with the walls area coated by the 200 μL solution volume added for each step of the LbL construction.

3.2 LL-37 adsorbed in the coatings

The total quantity of LL-37 adsorbed during the coating's construction, corresponds to the released quantity of the peptide ($\mu g/cm^2$) shown in *Table 10*, adapted from *Table 7*, summed with the remaining quantity ($\mu g/cm^2$) in the microwells after release experiment, shown in *Table 9*. These values enable us to assess the adsorption capacity of the different coating conditions. They are shown in *Table 11* (sum of *Table 9* and *Table 10* values).

Before further discussion of the results, to conclude the previous section *2. Study of LL-37 release from the coating*, the values of *Table 11* allow us to think that the higher values of complexed LL-37 remaining in the PPCs-based coating after release experiment compared to the bare LL-37-based coating is well due to a lower PPCs release potential, and not to a higher adsorption of PPCs inside the coating during coating construction.

When the coating is constructed with PPCs, two parameters differ from a coating constructed with bare LL-37: the use of CHI as an oppositely-charged PE and the complexation of LL-37 with HEP. The lower release capacity can be explained either by the CHI, which could reduce release, or by the PPCs themselves. A study of the dynamism of PPCs could provide an answer to these hypotheses.

Table 10: Quantity of released LL-37 per cm^2 of coating polystyrene microwell obtained by summing quantities released for 13 sampling times and divided by the total coating area ($\mu g/cm^2$)

Condition	**1**	**2**	**3**	**4**	**5**	**6**
PBS (μL)	300	300	200	300	300	200
BL	20	16	16	20	16	16
pH	3.5			5		
LL-37 in PPCs ($\mu g/cm^2$)	1.96	1.82	1.37	4.05	3.26	3.05
Bare LL-37 ($\mu g/cm^2$)	30.48	17.20	20.04	9.35	6.61	5.09

Table 11: Quantity of adsorbed LL-37 per cm^2 of coating in polystyrene microwell obtained by summing quantities released and remaining in the microwells ($\mu g/cm^2$)

Condition	**1**	**2**	**3**	**4**	**5**	**6**
PBS (μL)	300	300	200	300	300	200
BL	20	16	16	20	16	16
pH	3.5			5		
LL-37 in PPCs coating ($\mu g/cm^2$)	20.36	19.83	19.62	21.76	20.98	20.51
LL-37 in bare LL-37 coating ($\mu g/cm^2$)	42.06	30.72	33.24	25.75	23.41	21.85

Results from *Table 11* show that LL-37 adsorption is favored when bare LL-37 is used rather than when it is complexed with HEP, even if this tendency is more pronounced at pH 3.5 than at pH 5. As HEP and CHI charges are stable at pH 3.5 and 5, the change in adsorption capacity according to the pH is most certainly due to a different charge density of the LL-37. This could explain the increased adsorption of bare LL-37 at pH 3.5 compared to its quantity adsorbed at pH 5. Indeed, at pH 3.5, LL-37 has a higher charge density than at pH 5, which may allow it to interact and bind more efficiently to HEP in the coating, as well as to diffuse more easily between the layers.

PPCs do not show a significant variation in adsorption capacity when comparing values at pH 3.5 and pH 5[30]. A hypothesis for this non-obvious difference would be that the negative corona of the complexes made of HEP maintains a certain homogenous charge density, not varying with pH. With CHI also displaying a homogenous charge density at both pH values, this could explain why no significant change is observed in the adsorption capacity of PPCs.

The first stated goal of this experiment was to test whether the relatively small released quantity of LL-37 was due to a small quantity of LL-37 immobilized in the coating upstream. This explanation will not be retained as the quantity of LL-37 released from the coating seems to be a relatively small part the quantities adsorbed during coating construction, for every condition. Indeed, quantities left in the wells after release of the LL-37 seem to still offer a reasonable stock of LL-37 (see *Table 9*).

Results obtained for LL-37 adsorption led us to discuss three parameters to assess optimal conditions to immobilize bare LL-37 and PPCs in the coating. This discussion will then firstly focus on the effect of the number of BLs, following with the effect of the pH, and lastly, we will discuss the intrinsic adsorption ability of both used forms of LL-37 used: bare and complexed.

[30] The fact that PPCs did not show in our results a significant difference in adsorption between pH 3.5 and 5 has led us to build a coating at pH 5 for PPCs coating to improve their release (see *Table 8*).

The results presented in *Table 11* enabled the construction of *Figure 37* (conditions 1, 2 and 3, 4). They show that the amount of LL-37 adsorbed in the coatings, per cm^2, does seem to increase with the number of BLs, especially for bare LL-37. This observation could confirm our hypothesis that a coating that have immobilized more LL-37 upstream would offer a better release of the components and responds to the second goal stated at the beginning of this section.

Note that the difference in adsorbed quantity per cm^2 is most marked between 16 and 20 BLs for bare LL-37 at pH 3.5. This significant variation can be seen in *Appendices, Table IV* which details the quantities released of bare LL-37. After 30 minutes, the difference between the 20 and 16 BLs is more than double the amount released at 16 BLs, which seems anomalous. We believe this is due to an experimental error in filling the microwells prior to analysis. In fact, the filling, carried out in the dark, may have been carried out with a larger volume, which would explain the large quantity released with 20 BLs. In our case, the main aim is to identify a general trend from these results, which minimizes the impact of this imprecision.

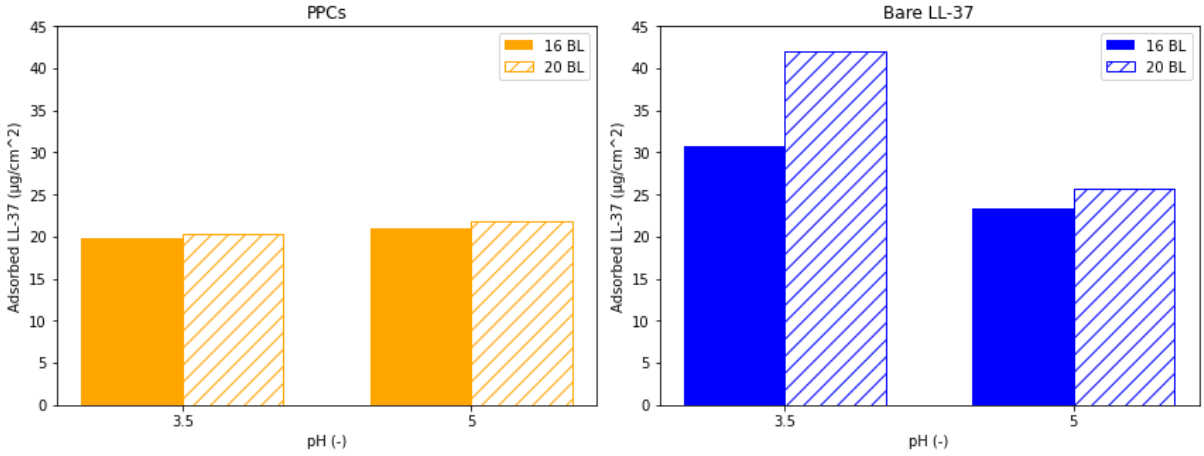

Figure 37: Adsorbed LL-37 per square centimeter as a function of pH for different number of BLs ($\mu g/cm^2$) (left = PPCs, right = bare LL-37)

This observation that the adsorbed LL-37 quantity increases with the number of BLs has been confirmed by Coralie Nerincx and Noémie de Suraÿ in former experiments. *Figures 38* and *39* depict the amount of LL-37 adsorbed in $\mu g/cm^2$, in the case of PPCs and bare LL-37 for different numbers of BLs, at pH 3.5 and 5.

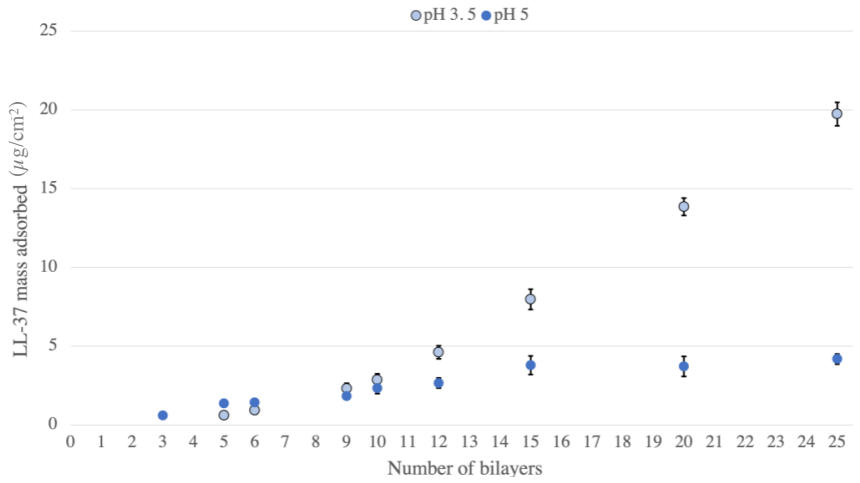

Figure 38: Average mass of LL-37 per square centimeter in different bare LL-37 film constructions at pH 3.5 (light blue dots) and pH 5 (dark blue dots) by Coralie Nerincx and Noémie de Suraÿ

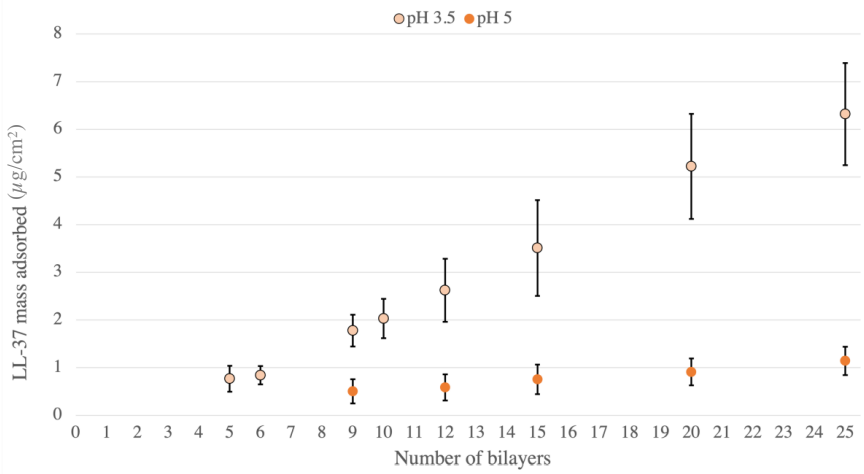

Figure 39: Average mass of LL-37 adsorbed per square centimeter in different PPCs film constructions at pH 3.5 (light orange dots) and pH 5 (dark orange dots) by Coralie Nerincx and Noémie de Suraÿ

Overall, for every condition, it is clear that the amount of LL-37 adsorbed in the coating increases as the number of BLs increases.

The pH variable can also be discussed as both *Figures 38* and *39* highlight the importance of pH in the adsorption of bare LL-37, a tendency that our results also display (*Figure 38*) in the case of bare LL-37.

For PPCs-based coatings (*Figure 39*), adsorption shows linear evolution with the number of BLs, the slopes varying according to pH values. This graph shows favored adsorption of LL-37 as PPCs at pH 3.5, an observation that our data does not display as clearly. In fact, results from *Figure 33* shows a difference of adsorbed LL-37 between pH 3.5 and 5 of ~ 4 μg/cm^2 for 20 BLs, while our data from *Table 11* shows a difference of ~ 1 μg/cm^2. Either way, the adsorption of PPCs compared to bare LL-37 is not favored and will be discussed further on.

As for bare LL-37-based coatings (*Figure 38*), we note an exponential increase in adsorption at pH 3.5 and a linear increase at pH 5. Indeed, above a certain BLs number, we observed a trend towards a better adsorption of bare LL-37 at pH 3.5, a tendency we had also observed and explained by the fact that the peptide's charge density was greater at this pH value. A higher charge density could confer the LL-37 the ability to diffuse into the film, as shown by the exponential nature of its adsorption.

Let us now discuss the intrinsic adsorption ability of both used forms of LL-37: bare and complexed. Our observation that PPCs do not adsorb in a coating as well as bare LL-37 can explain why this type of coating has a low release capacity, which led to no signal detection of the PPCs in CD.

This observation that bare LL-37 adsorbs better than complexed LL-37 does not follow the conclusion of the similar experiment performed by Aurélien vander Straeten showing a better adsorption of lysozyme when complexed with PSS. [9]

Factor that can explain this difference is the LL-37 structure (*Figure 4*), way different from the lysozyme's. Thanks to the specific arrangement of its aa, two parts are distinguishable in LL-37 structure: polar and non-polar. A hypothesis would be that this polar part interacts effectively with oppositely-charged layers through electrostatic interactions and dynamic rearrangement within the coating. Although PPCs have a net negative crown, the rearrangement within PPCs could distribute the charges heterogeneously. The adsorption capacity of LL-37 is therefore higher when bare, as it has more interaction sites and can arrange itself to interact more intensely through electrostatic forces.

3.3 Conclusion and perspectives

This experiment allowed us to confirm some hypothesis and answer to several questions raised from the release experiment. First, the results showed that the higher values of complexed LL-37 remaining in the PPCs-based coating, after the release experiment, compared to the bare LL-37-based coating is well due to a lower PPCs release potential, and not to a higher adsorption of PPCs inside the coating during coating construction.

Results showed that the release potential of the coatings is not fully exploited, as a high quantity of LL-37 remained in the wells. The data also allowed to confirm the hypothesis stated in the release experiment, which was that a coating containing a higher number of BLs contains a higher quantity of LL-37, and allows to reach a higher released concentration of LL-37. This observation answered the second goal of this experiment.

The third goal stated for this experiment was that quantifying the adsorption capacity was interesting to assess the optimal conditions for LL-37 immobilization, and therefore, for coating's potential contact-activity on bacteria. To this end, three factors have been discussed: the number of BLs, the pH values, and the intrinsic adsorption ability of both forms of LL-37 used: bare and PPCs.

Results showed that the adsorption efficiency of LL-37 can be improved by using bare LL-37 rather than PPCs. Adjusting pH to 3.5 and increasing the number of BLs also have a significant impact on the adsorption capacity of LL-37, as shown by our results and those obtained by Coralie Nerincx and Noémie de Suraÿ.

If further experiments demonstrate the contact-killing activity of LL-37, it could be interesting to build the AMC following the variables, highlighted by this experiment, that optimize the AMC's LL-37 stock, if it shown that LL-37 contained in the lower layers of the coating can also enter in contact with bacteria through coating's dynamic behavior.

However, even if it would be interesting to build AMCs from bare LL-37, as it offers increased adsorption capacity, constituting a better stock, there is a first need for a prove that its activity on bacteria is comparable to (or better than) the one offered by LL-37 contained in PPCs coating. Indeed, if bare LL-37 offers a lower activity compared to the complexed LL-37, the use of PPCs-based coating may be more interesting in the fight against bacteria, even if the adsorption of the constituting components is less straightforward.

4. Antibiotics synergy with LL-37-based antimicrobial coating

To follow the second objective of this Master's thesis, the activity of the coating has been tested on pre-formed biofilms of *S. epidermidis,* through the assessment of whether a synergistic effect of the coating is obtained when put together with antibiotics treatment, or not.

Figures 40 and *41* present the results for, respectively, biomass and metabolism reduction of 24h pre-formed biofilms of *S. epidermidis ATCC 35984* that have undergone the antibiotic treatment as described in the *Materials and Methods* section. Red data on the figures present results for biofilms treated with antibiotics alone while green data show the obtained results when antibiotics are put together with the (bare) LL-37-based AMC.

On the graphs, X axis represents the different concentrations for each antibiotic, as described in the *Materials and Methods* section. C^+ are positive control values that correspond to biofilms non-treated with antibiotics. In the case of the green data, C^+ values are then associated with the effect of the LL-37 coating acting alone on biofilms formation.

Y axis shows the reduction of whether biomass (*Figure 40*) or metabolism (*Figure 41*) in percentage values by comparison with biomass and metabolism of biofilms that have been grown on non-coated plates, and on which no antibiotics treatment was applied at all, corresponding to the C^+ value of the red results (0%).

All conditions were performed in triplicates (n = 3) (see *Materials and Methods* section) and the whole experiment has been performed three times (N = 3). The means of the results for three replicates and three repetitions are represented on the graph ± SEM[31]. Student's *t*-tests were performed for statistical analysis of the two values (coating and no coating), for each condition of MIC of each antibiotic, and represent if there is a significant effect of the antibiotic along with the coating compared to the same conditions without the coating. Whether *t*-tests are significant or not is assessed by the p-values as explained in *Figures 40* and *41*'s legends.

[31] SEM stands for Standard Error of the Mean and is a measure that quantifies the amount of sampling variability or uncertainty in the estimation of the population mean.

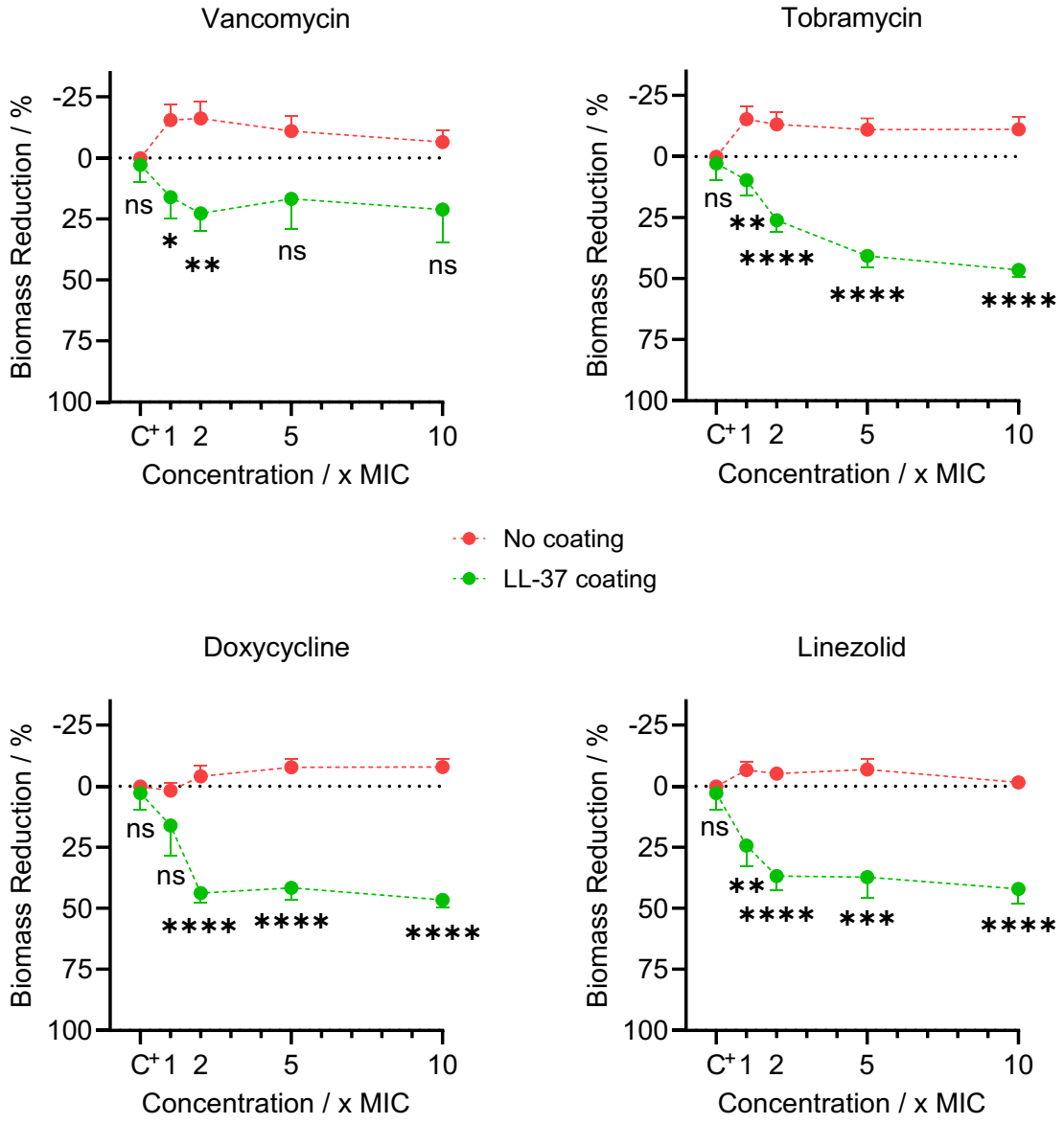

Figure 40: Percentage **biomass** reductions for 24h pre-formed *S. epidermidis ATCC 35984* biofilms when combining a LL-37-based coating with different multiples of the MIC of either vancomycin, tobramycin, doxycycline, or linezolid. C^+ = untreated biofilm (positive control). Values are mean ± SEM. Statistical analyses were performed by Student's t-tests (N=3, with n=3 per replicate). The significantly different values between LL-37 coated and non-coated surfaces, for a given MIC value of the antibiotic, are shown by the p-values as follows: ns = non-significant, * = $p<0.05$, ** = $p<0.01$, *** = $p<0.001$, **** = $p<0.0001$.

Figure 40 shows that when bacteria are exposed only to the LL-37 coating and no antibiotics treatment is applied (C^+ results for green data), a very slight effect on the biofilm's biomass is observable. The diminution being so small, the effect of the coating alone compared to untreated *S. epidermidis ATCC 35984* biofilm (C^+ results for red data), is considered non-significant (ns) by Student *t*-test.

Results show that for antibiotic treatment alone (red data on *Figure 40*) no significant efficacy of the antibiotics is observed on biomass, for any antibiotic concentration. In other words,

results for antibiotic treatment without coating show no net decrease of biomass, even when the biofilm is exposed to doses of the antibiotic way above its MIC. As a matter of fact, this treatment even results in a slight increase (negative reduction) in biomass in most conditions.

However, biomass reduction is superior for antibiotic treatment put together with LL-37 from the coating (green data) compared to when it is not coupled with AMC (red data). In addition, antibiotic treatment with LL-37 coating do present a tendency of offering a better reduction in biomass when the biofilm is exposed to a higher multiple of the MIC, at least before reaching a certain observable concentration threshold after 2x the MIC for vancomycin, doxycycline, and linezolid.

Results for vancomycin do not all show a significant effect when antibiotics are coupled with the LL-37 coating compared to the treatment without LL-37 (ns for 5x and 10x MIC). For all other three antibiotics, there is a significant effect of the treatment when put in coated wells conditions ($p<0.01$ to $p<0.0001$) in exception for 1x the MIC of doxycycline (ns).

4.2 Results for metabolic activity reduction

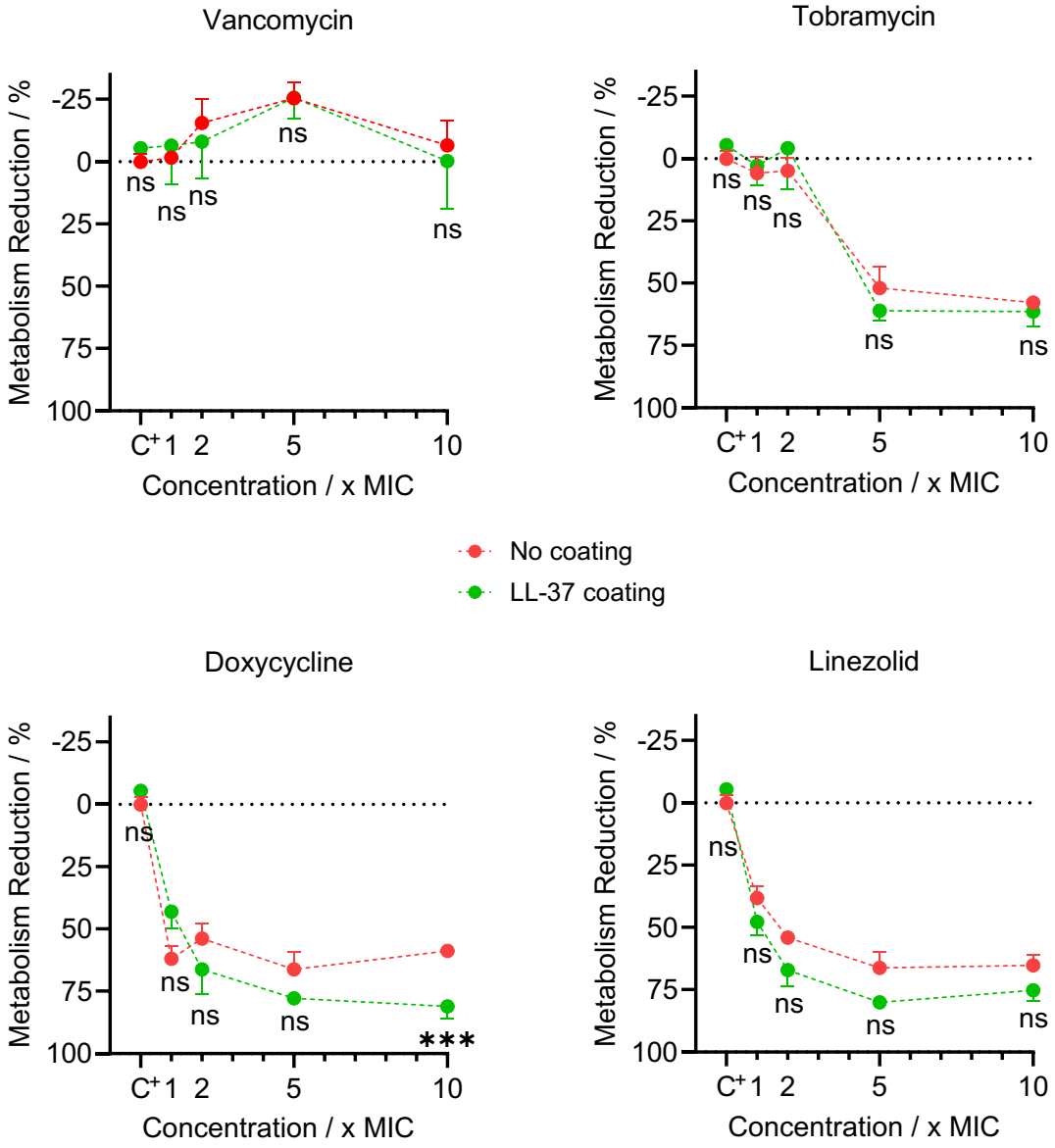

Figure 41: Percentage **metabolism** reductions for 24h pre-formed *S. epidermidis ATCC 35984* biofilms when combining a LL-37-based coating with different multiples of the MIC of either vancomycin, tobramycin, doxycycline, or linezolid. C^+ = untreated biofilm (positive control). Values are mean ± SEM. Statistical analyses were performed by Student's t-tests (N=3, with n=3 per replicate). The significantly different values between LL-37 coated and non-coated surfaces, for a given MIC value of the antibiotic, are shown by the p-values as follows: ns = non-significant, * = p<0.05, ** = p<0.01, *** = p<0.001, **** = p<0.0001.

Results for metabolism reduction of 24h pre-formed biofilms of *S. epidermidis* that have undergone the antibiotics treatment explained in the *Materials and Methods* section are shown on *Figure 41*. As for biomass reduction results, *Figure 41* shows no significant effect of the coating alone, when green C^+ data is compared with red C^+ data, non-treated biofilms.

Figure 41 displays metabolic activity reduction results as being quite different from the biomass' results. Indeed, for tobramycin, doxycycline, and linezolid, all treatment conditions, whether LL-37 and antibiotics-based or antibiotics acting alone, allow the global metabolic activity of the biofilm to decrease.

The only condition showing significant ($p<0.001$) effect of the coating and antibiotics on metabolic activity, compared to the antibiotic treatment alone, is 10x MIC for doxycycline. All other conditions do not allow to see any significant (ns) effect on metabolism for antibiotic treatment coupled with AMC in comparison with the same antibiotics' treatment alone.

For vancomycin-based treatment, no significant decrease in metabolic activity for antibiotic treatment in the presence of coating, compared to the antibiotic treatment alone is observed (ns). As a matter of fact, in opposition to the other three antibiotics treatment, coated and non-coated vancomycin-based treatment do not allow to observe a decrease in metabolism in the biofilm and, subsequently a significant effect of the LL-37-based treatment compared to a treatment without the coating.

4.3 Discussion on treatment's effect on biomass and metabolic activity

The (red) results for antibiotics treatment alone on the biofilm do not show effect on biomass for any condition. This observation could lead to think that the treatment had no activity on the biofilm, maybe not being able to penetrate the extracellular matrix and reach bacteria cells. However, attention must be paid to the fact that the quantification of biomass through crystal violet staining cannot tell the difference between dead and alive biomass. The bacteria inside the biofilm, as well as the extracellular matrix, can have been altered by the antibiotics in a way that is detectable with the resazurin and not the crystal violet dye. Indeed, such results are obtained for tobramycin, doxycycline, and linezolid, the three treatments showing significant effect on metabolism while no effect on biomass is detected, leading to think that the chosen antibiotics do have an important activity on metabolism reduction, at least before reaching an apparent plateau around 5x CMI. It is then totally plausible than the antibiotics treatment alone do have a bactericidal or bacteriostatic effect on bacteria that was not detected by the biomass quantification method used.

However, the fact that biomass reduction is non observable while metabolic activity is present can also lead to another hypothesis, if we consider that the quantified biomass still contains viable cells. The hypothesis is based on recalcitrance mechanism of a whole population of bacteria being the slow metabolic rate, as described in the *State of the art*. As a matter of fact, the biofilm could, as a response to an environmental stress caused by biofilm conditions, be influenced by antibiotics presence, adopt a slow metabolic rate while keeping the same biomass. However, this second hypothesis has not been retained as a similar behavior would have been

expected from bacteria in contact with vancomycin, although no reduction of metabolism is observed.

Considering the vancomycin treatment alone, as for the other three treatments, no effect is detected on biomass. But, nor for metabolism of the biofilm. As a reminder, vancomycin is the only of the four antibiotics acting extracellularly, on cell wall synthesis, while the other three drugs have intracellular activity, targeting essentially protein synthesis. Vancomycin could then have less activity on bacteria metabolism compared to tobramycin, doxycycline, and linezolid, for whose it is the first target.

As for results for antibiotics treatment when coupled with the LL-37-based AMC, the tested synergistic effect was not observed for metabolism activity. Indeed, tobramycin, doxycycline, and linezolid treatments allowed obvious decrease of metabolic activity, with and without LL-37 coating (except for 10x the MIC of doxycycline). No synergistic effect was neither observed for vancomycin, as *Figure 41* shows no decrease of metabolic activity for vancomycin with the coating compared to the treatment based on vancomycin alone.

The results of *Figure 40*, between antibiotics and the LL-37-based AMC, for all four antibiotics, showed that the biomass decreases significatively compared to the antibiotics treatment alone, leading us to think of a potential synergy[32] between the coating and the chosen antibiotics. However, not all concentration conditions of vancomycin treatment showed significant decrease compared to the antibiotics treatment alone (ns). Presence of LL-37 does not seem to increase in any way the MOA of vancomycin on metabolism, maybe due to the fact that the drug does not directly target cellular metabolism, as do the MOAs of the three other antibiotics.

For vancomycin, doxycycline, and linezolid, we can visually assess that concentration of antibiotics higher than 2x the MIC do not lead to better reduction of biomass. On the other hand, tobramycin graph suggests that an increase in the concentration could increase the biomass reduction even more, in opposition to all three other treatments that have reached an observable threshold after 2x the MIC. This could be due to the fact that the *ATCC 35984* strain is already resistant to tobramycin, as shows its high MIC of 256 μg/mL and, subsequently, a higher concentration of tobramycin could be necessary to achieve the same results as for antibiotics to which the strain is not resistant yet.

From results shown on *Figure 40*, synergy of antibiotics and LL-37 acting on biofilm's biomass seems quite obvious. However, the whole challenge lies in the identification of the mechanism that would allow such coupled and enhanced effect.

First hypothesis is that this activity is attributed to the only presence of LL-37. This hypothesis is plausible since the coating could have prevented the growth of the biofilm on the coated well. Indeed, as already mentioned in the State of the art, a study performed by J. Overhage et al in 2008 has demonstrated that LL-37 had also prevention role on biofilms of *Pseudomonas*

[32] As a reminder, synergy could be seen as a 1 + 1 = 3 effect, being distinct from an additive effect (1 + 1 = 2).

aeruginosa. Indeed, they have shown that concentration below the MIC of LL-37 could already have a significant inhibitory effect on biofilm formation. They estimated the effect of 1/128 MIC to reduce 40% of biofilms biomass compared to biofilms formed in absence of LL-37 treatment. [59] Unfortunately, C^+ results for green data, displaying the results for LL-37-based coating working alone, shows ns activity of the LL-37 on the biofilm's biomass. Moreover, an effect of the antibiotics' concentration is observable, since for each antibiotic, the diminution of the biomass for 2x the MIC is more important than the 1x MIC condition.

We secondly considered the possibility that the diminution of the metabolism could be the cause for biomass decrease. In fact, the EPS constituting the extracellular matrix are made of proteins, extracellular DNA, and mainly polysaccharides depending on enzyme activity for their biosynthesis, regulation, or even transport. Altering the cell metabolism could be the reason for a less developed extracellular matrix, contributing to the biomass of the biofilm. However, this hypothesis is not consistent as a diminution of metabolism under the antibiotics' treatment of tobramycin, doxycycline, and linezolid acting alone did not lead to subsequent biomass decrease.

The other way around, we assessed the question of whether it was this decrease of biomass, when the antibiotics and LL-37 work together, that led to a diminution of the global biofilm metabolism. As the antibiotics and the LL-37 together may have altered the biofilm's biomass through the inhibition of cell growth, this could lead to less total metabolic activity of the biofilm. However, again, this hypothesis has been refuted as no significant decrease in metabolism was observed when LL-37 and antibiotics act together compared to the previous treatment of antibiotics acting alone, showing that this metabolic activity decline was not due to biomass reduction. Indeed, 10x the MIC of doxycycline do offer a significant effect on the biofilm's metabolism of doxycycline and LL-37 compared to doxycycline alone. Moreover, the tendency of having greater metabolism reduction for green data is observable for other conditions of doxycycline, and for linezolid. However, all these conditions are considered ns by Student *t*-test, and no such effect is observed for vancomycin, nor tobramycin. The hypothesis that the reduction of metabolism is due to an upstream diminution of biomass caused by the LL-37 working together with antibiotics can then not be confirmed.

Lastly, a plausible hypothesis would be that antibiotics along with LL-37 target the EPS, the extracellular matrix. This would explain a decrease of the biofilm's biomass, not directly coupled with the decline in metabolic activity of the cells, kept alive even if not encased in a powerful extracellular matrix. CFU analysis could help determine whether the viable cells amount decreases in a similar way as does the total biomass, or not, the latter potentially confirming this hypothesis. Unfortunately, the CFU experiment conducted in this Master's thesis is not presented as the experimental error was too high to consider the obtained results reliable (see *Appendices* section *3.2 CFU counting*).

In conclusion, it is quite undeniable that LL-37 displays a significant synergistic activity on biofilms' biomass when coupled with antibiotics. First hypothesis is that the LL-37 released from the coating can have an effect on bacteria, even under its MIC[33]. But LL-37 could also have an activity on bacteria while still inside the coating. Indeed, contact-killing AMCs do exist, and, furthermore, even if it was shown by CD in the past that bare LL-37 was not in α-helical conformation in the solutions used to build the coating; firstly, nothing showed that it did not readopt this structure somehow inside the coating and, secondly, this α-helical conformation could be readopted when the AMP binds to bacteria cell membrane since it has been showed that the helicity of LL-37 increased while in contact with bacteria, as explained in the *State of the art*.

Indeed, said pores could be a way exploited by tobramycin, doxycycline, and linezolid to enter the bacteria more easily and allow increased activity on biomass, either through inhibition of EPS synthesis, transport, etc., or through cell lysis. Vancomycin's activity on biomass would be less enhanced by pore formation as it has no intracellular effect and this membrane disruption caused by LL-37 will have lower effect on cell wall synthesis inhibition.

However, the mechanism allowing this synergistic activity of LL-37 and antibiotics on biomass has not been highlighted by our research and there is a need for further experimentation, such as CFU counting. More experimentation is also needed to assess why an obvious decline of biomass has no effect on the biofilms' global metabolic activity. This experiment has also highlighted the difference in MOAs of vancomycin compared to the other three antibiotics'

[33] It is assessed that the peptide is acting under its MIC as a 14.5 BLs coating could not have released a concentration of >512 μg/mL, considering that former experiments have shown that a 50 BLs coating did not even allow a release of 30 μg/mL.

PART VI – Conclusion

This Master's thesis studied the activity of an AMC whose antimicrobial's properties are imparted by to the LL-37 AMP. The said AMC have been constructed by LbL methods, in two different ways. A first coating was based on bare LL-37 and a second one was built with LL-37 complexed with HEP under the form of PPCs.

Experiments have been performed on PPCs to determine their optimal PE-to-protein, or HEP-to-LL-37 (-/+) charge ratio to use for PPCs formation. Results showed that (-/+) charge ratio of 1.5 optimized PPCs formation, which matched former results obtained by Cédric Vranckx.

Activity of LL-37-based AMC has been assessed following two objectives and subsequent strategies. First objective was based on the hypothesis that the studied AMC displays an antimicrobial activity by release of the antimicrobial agent. Following this idea, CD analysis was performed to determine whether the LL-37 was released under its active conformation (α-helix) or not. This experiment was nourished by the fact that bare LL-37, when not-complexed in PPCs, do not display this secondary structure in the aqueous solutions used to form the coating. Note that no experiment was done to determine the conformation of LL-37 inside the coating. This means that the α-helix form could have been re-adopted by bare LL-37 before being released from the coating. Additionally, PPCs could decomplex and consequently free LL-37, which could also lose its α-helical conformation, yet maintained in aqueous solution.

Unfortunately, despite experiments performed to determine which conditions would optimize the release of LL-37 from the coating, no sufficient concentration (30 μg/mL) could have been reached to detect a signal in CD for either bare or complexed LL-37. No conclusion can be made on the structure of the released peptide.

Nevertheless, this experiment allowed to confirm that 30 μg/mL of LL-37 is around the minimal acceptable concentration for CD signal detection and subsequent acquisition of interpretable results. This conclusion showed that LL-37 released from 50 BLs did not reach such concentration and that LL-37 quantity released from the coating is not directly linked to its adsorbed quantity. A hypothesis was evoked that the main reason for this insufficient concentration was that only the layers in contact with the PBS used to release the LL-37 do release the peptide. Increasing the numbers of BLs for coating construction for a higher quantity of LL-37 adsorbed would not indefinitely allow better release of the coating. In other words, a higher stock of LL-37 in the coating would not directly lead to a higher concentration of released LL-37.

The second strategy to test the AMC activity was to study its coupled activity with routinely-used antibiotics, in order to highlight a potential synergistic effect of the LL-37 with either vancomycin, tobramycin, doxycycline, or linezolid, on 24h pre-formed biofilms of *S. epidermidis*. Results showed significant synergistic effect of the antibiotics coupled with LL-37 for biomass reduction. In the case of metabolic activity, no significant effect of the antibiotics with

the coating whether with or without the coating was observed. Indeed, in the case of vancomycin, no effect on metabolism was observed with and without the coating, while tobramycin, doxycycline and linezolid showed significant, but similar, effect on metabolism either way. The reason why vancomycin showed no effect on biofilm's metabolism can be due to its MOA, not directly targeting cell metabolism, in contrast with the other three antibiotics.

The fact that the biomass of the biofilm was reduced in the case of the presence of the coating for all four antibiotics but that the same trend was not observed for biofilm's metabolism has led to several hypothesis. The hypothesis that LL-37 alone could prevent biofilm formation upstream and therefore reduce the total biomass was not retained as the effect of the AMC alone on the pre-formed biofilm showed no significant effect, highlighting the importance of the coupled effect of antibiotics.

Therefore, the most plausible hypothesis to date would be that antibiotics together with LL-37 have effect on EPS, reducing the extracellular matrix formation, which accounts for the biomass of the biofilm but has no direct effect on the cell's metabolism. This hypothesis is to be considered with caution and further experimentation, such as CFU counting, needs to be performed to further study the mechanism of this obvious synergistic effect between LL-37 and antibiotics.

However, the experiment showed that the AMC could display an antibacterial activity when coupled with antibiotics, even when releasing concentration of LL-37 under its MIC (>512 μg/mL). Indeed, AMC used for second objective experiment was made of 14.5 BLs of bare LL-37 and must have released a small concentration of LL-37 considering the concentration below 30 μg/mL of LL-37 released from a 50 BLs.

Bare LL-37 displaying antimicrobial activity under its MIC led us to think of two hypotheses concerning LL-37 structure when released. First, bare LL-37 may re-adopt its α-helical conformation at some point after the construction of the coating, either when immobilized inside the latter, or when it is released. In this case, this re-adoption of the structure could be thanks to physiological conditions of PBS which offer soft conditions under which bare LL-37 could re-adopt this secondary structure, even after losing it in aqueous solution. This also shows that aqueous solution at pH 3.5 and 5 did not cause the peptide to completely denature. Secondly, LL-37 could also re-adopt its α-helical conformation when entering in contact with bacteria, as it has been shown that the helicity of LL-37 increases when it encounters cell membrane.

Yet, another reason for the coating's activity could be that the AMC, firstly thought to display antimicrobial activity through release of antimicrobial agent, could actually also have a contact-killing activity. Subsequently, maximize the release of LL-37 could maybe not be the best strategy to increase activity of the AMC. Conserving a certain amount of the AMP inside the coating, and find a compromise between LL-37 being released and remaining immobilized, could be an interesting proposition.

PART VII – Future prospects

This part will focus on interesting prospects to further study the coating's structure, behavior, and activity. Different experiments that could help confirm or pursue the goals of our research are described below. Additionally, perspectives for the application of the coating on hip joint prostheses are presented.

Firstly, PPCs should be further studied as it has been showed by Cédric Vranckx that they allowed LL-37's secondary structure to be conserved in aqueous solution, which was not the case when the latter was bare, non-complexed as PPCs. In this interest, their structure and behavior should be studied in more details, since their formation and dynamism in the coating are still poorly understood. DLS analysis could be performed to determine whether the optimal charge ratio for their formation favors a higher quantity or a higher size of the formed complexes, which could lead to a different interaction with CHI to form the multilayered coating. Inside the said layers, the behavior of PPCs could also be studied. In fact, if the complexed form of the PPCs is not maintained inside the BLs, the positively-charged LL-37, not standardized by the negative charges of HEP anymore, could find itself repulsed by the positively-charged the CHI, causing the PPCs-based coating to adsorb less LL-37, more easily washed out. A following interesting prospect would be to test whether, if the α-helical structure of LL-37 is more conserved in PPCs than when bare LL-37 is immobilized in the coating, PPCs-based offer a better activity on *S. epidermidis biofilm*.

Secondly, we would find interesting to study the mode of action of the coating. In fact, whether the AMC is release-active or contact-acting, or both, may have an influence on the conditions followed for coating construction. However, an experiment that would confirm if the activity of the LL-37 is either due to released LL-37 immobilized or released is not straightforward. Additionally, attention must be paid that that α-helical conformation does increase when the peptide encounters bacteria's membrane, meaning that the activity of the LL-37 can be recovered and that upstream secondary structure might not be a condition sine qua non for LL-37 activity. In this idea, experimentation to prove whether α-helical structure of the LL-37 is conserved in the coating, or rather when released from the coating, is not a sufficient condition to confirm one MOA of the coating rather than the other.

In this context, we would preconize to study a coating whose specific area would be increased, for example, through nanotexturing, micro texturing, or using a porous support. [101] Indeed, both MOAs could take advantage of this increased specific area. If the release-active coating proves itself to release LL-37 only from the external parts in contact with the physiological environment, this would explain why the released quantity of LL-37 was insufficient to allow a detectable signal in CD. Consequently, increasing the amount of adsorbed LL-37 by adding more BLs would be of limited interest. Instead, increasing the specific surface area of the

coating to enhance its contact with the physiological environment is a promising approach. This would take advantage of the potential of the external BLs to release peptides from the coating.

On the contrary, or complementarily, if the LL-37 is active when still immobilized in the coating, such MOA also could take advantage of a higher specific area, which not only increases the interaction surface but also the adsorption potential of the peptide. Additionally, for contact-active coating, increased number of BLs may be of interest, only if it is shown that the lower layers have an antimicrobial activity, through BLs rearrangement in the dynamic rearrangement of the coating.

As for the prospects regarding AMC application on protheses, current experiments conducted on polystyrene could be replicated on Ti, which is the preferred material for implant manufacture due to its unique properties that enhance the longevity and effectiveness of prostheses. Ti allows excellent biocompatibility, enhanced osseointegration, corrosion resistance, and reduced the risk of allergic reactions or local toxicity. [20] Along with its interesting characteristics as material for medical implant, the charges of Ti have a different behavior than polystyrene's. In fact, while polystyrene is a polymer that can acquire negative charges when interacting with certain substances, a mechanism essential for the LbL technique used in this Master's thesis, Ti alloys can develop different set of surfaces properties, such as surface charges since they don't carry an inherent charge such as polymers. Surface properties of Ti can be influenced by several factors, a property that can be exploited to make Ti surface more reactive than polystyrene. In fact, after treatment like anodization, plasma spraying or chemical etching, the first layer of the LbL coating can see its affinity enhanced for Ti material. More stable and uniform coatings can therefore be achieved thanks to Ti use.

These perspectives, in our vison, may provide a promising path for the continuation of this project, focusing on technical innovation and clinical application to enhance the prevention and treatment of bacterial infections on hip joint prosthesis.

References

[1] D. Apostu, O. Lucaciu, C. Berce, D. Lucaciu, and D. Cosma, "Current methods of preventing aseptic loosening and improving osseointegration of titanium implants in cementless total hip arthroplasty: a review," *J Int Med Res*, vol. 46, no. 6, pp. 2104–2119, Jun. 2018, doi: 10.1177/0300060517732697.

[2] A. J. Tande and R. Patel, "Prosthetic Joint Infection," *Clin Microbiol Rev*, vol. 27, no. 2, pp. 302–345, Apr. 2014, doi: 10.1128/CMR.00111-13.

[3] "Joint Replacement Infection - OrthoInfo - AAOS." Accessed: Mar. 28, 2024. [Online]. Available: https://www.orthoinfo.org/en/diseases--conditions/joint-replacement-infection/

[4] C. Ghosh, P. Sarkar, R. Issa, and J. Haldar, "Alternatives to Conventional Antibiotics in the Era of Antimicrobial Resistance," *Trends in Microbiology*, vol. 27, no. 4, pp. 323–338, Apr. 2019, doi: 10.1016/j.tim.2018.12.010.

[5] C. W. Hall and T.-F. Mah, "Molecular mechanisms of biofilm-based antibiotic resistance and tolerance in pathogenic bacteria," *FEMS Microbiology Reviews*, vol. 41, no. 3, pp. 276–301, May 2017, doi: 10.1093/femsre/fux010.

[6] N. Venkatesan, G. Perumal, and M. Doble, "Bacterial resistance in biofilm-associated bacteria," *Future Microbiology*, vol. 10, no. 11, pp. 1743–1750, Nov. 2015, doi: 10.2217/fmb.15.69.

[7] A. H. Benfield and S. T. Henriques, "Mode-of-Action of Antimicrobial Peptides: Membrane Disruption vs. Intracellular Mechanisms," *Front. Med. Technol.*, vol. 2, p. 610997, Dec. 2020, doi: 10.3389/fmedt.2020.610997.

[8] J. Xuan *et al.*, "Antimicrobial peptides for combating drug-resistant bacterial infections," *Drug Resistance Updates*, vol. 68, p. 100954, May 2023, doi: 10.1016/j.drup.2023.100954.

[9] A. Vander Straeten, A. Bratek-Skicki, A. M. Jonas, C.-A. Fustin, and C. Dupont-Gillain, "Integrating Proteins in Layer-by-Layer Assemblies Independently of their Electrical Charge," *ACS Nano*, vol. 12, no. 8, pp. 8372–8381, Aug. 2018, doi: 10.1021/acsnano.8b03710.

[10] K. Schilcher and A. R. Horswill, "Staphylococcal Biofilm Development: Structure, Regulation, and Treatment Strategies," *Microbiol Mol Biol Rev*, vol. 84, no. 3, pp. e00026-19, Aug. 2020, doi: 10.1128/MMBR.00026-19.

[11] I. J. Banke *et al.*, "Antimicrobial peptides in human synovial membrane as (low-grade) periprosthetic joint infection biomarkers," *European Journal of Medical Research*, vol. 25, no. 1, p. 33, Aug. 2020, doi: 10.1186/s40001-020-00434-1.

[12] A. Premkumar *et al.*, "Projected Economic Burden of Periprosthetic Joint Infection of the Hip and Knee in the United States," *J Arthroplasty*, vol. 36, no. 5, pp. 1484-1489.e3, May 2021, doi: 10.1016/j.arth.2020.12.005.

[13] C. Pabinger, H. Lothaller, N. Portner, and A. Geissler, "Projections of hip arthroplasty in OECD countries up to 2050," *HIP International*, vol. 28, no. 5, pp. 498–506, Sep. 2018, doi: 10.1177/1120700018757940.

[14] H. Australia, "Hip replacement." Accessed: Feb. 11, 2024. [Online]. Available: https://www.healthdirect.gov.au/hip-replacement

[15] R. Pivec, A. J. Johnson, S. C. Mears, and M. A. Mont, "Hip arthroplasty," *Lancet*, vol. 380, no. 9855, pp. 1768–1777, Nov. 2012, doi: 10.1016/S0140-6736(12)60607-2.

[16] C. Lombard *et al.*, "Imaging in Hip Arthroplasty Management Part 2: Postoperative Diagnostic Imaging Strategy," *JCM*, vol. 11, no. 15, p. 4416, Jul. 2022, doi: 10.3390/jcm11154416.

[17] J. W. McCutchen, J. P. Collier, and M. B. Mayor, "Osseointegration of titanium implants in total hip arthroplasty," *Clin Orthop Relat Res*, no. 261, pp. 114–125, Dec. 1990.

[18] B. R. Johnstone, M. Fitzgerald, K. R. Smith, and L. J. Currie, "Cemented Versus Uncemented Surface Replacement Arthroplasty of the Proximal Interphalangeal Joint With a Mean 5-Year Follow-Up," *The Journal of Hand Surgery*, vol. 33, no. 5, pp. 726–732, May 2008, doi: 10.1016/j.jhsa.2008.01.030.

[19] J. Matthias, M. P. Bostrom, and J. M. Lane, "A Comparison of Risks and Benefits Regarding Hip Arthroplasty Fixation," *J Am Acad Orthop Surg Glob Res Rev*, vol. 5, no. 11, p. e21.00014, Nov. 2021, doi: 10.5435/JAAOSGlobal-D-21-00014.

[20] W. C. Head, D. J. Bauk, and R. H. J. Emerson, "Titanium As the Material of Choice for Cementless Femoral Components in Total Hip Arthroplasty," *Clinical Orthopaedics and Related Research®*, vol. 311, p. 85, Feb. 1995.

[21] A. Khemka, C. I. FarajAllah, S. J. Lord, B. Bosley, and M. Al Muderis, "Osseointegrated total hip replacement connected to a lower limb prosthesis: a proof-of-concept study with three cases," *J Orthop Surg Res*, vol. 11, no. 1, p. 13, Dec. 2016, doi: 10.1186/s13018-016-0348-3.

[22] A. J. Tande and R. Patel, "Prosthetic Joint Infection," *Clin Microbiol Rev*, vol. 27, no. 2, pp. 302–345, Apr. 2014, doi: 10.1128/CMR.00111-13.

[23] S. Klouche, E. Sariali, and P. Mamoudy, "Total hip arthroplasty revision due to infection: a cost analysis approach," *Orthop Traumatol Surg Res*, vol. 96, no. 2, pp. 124–132, Apr. 2010, doi: 10.1016/j.rcot.2010.02.005.

[24] Z. Song, L. Borgwardt, N. Høiby, H. Wu, T. S. Sørensen, and A. Borgwardt, "Prosthesis Infections after Orthopedic Joint Replacement: The Possible Role of Bacterial Biofilms," *Orthop Rev (Pavia)*, vol. 5, no. 2, p. e14, Jun. 2013, doi: 10.4081/or.2013.e14.

[25] A. Brauner, O. Fridman, O. Gefen, and N. Q. Balaban, "Distinguishing between resistance, tolerance and persistence to antibiotic treatment," *Nat Rev Microbiol*, vol. 14, no. 5, pp. 320–330, May 2016, doi: 10.1038/nrmicro.2016.34.

[26] W. C Reygaert and Department of Biomedical Sciences, Oakland University William Beaumont School of Medicine, Rochester, MI, USA, "An overview of the antimicrobial resistance mechanisms of bacteria," *AIMS Microbiology*, vol. 4, no. 3, pp. 482–501, 2018, doi: 10.3934/microbiol.2018.3.482.

[27] N. Q. Balaban *et al.*, "Definitions and guidelines for research on antibiotic persistence," *Nat Rev Microbiol*, vol. 17, no. 7, pp. 441–448, Jul. 2019, doi: 10.1038/s41579-019-0196-3.

[28] Z. Li *et al.*, "Identifying Common Pathogens in Periprosthetic Joint Infection and Testing Drug-resistance Rate for Different Antibiotics: A Prospective, Single Center Study in Beijing," *Orthop Surg*, vol. 10, no. 3, pp. 235–240, Aug. 2018, doi: 10.1111/os.12394.

[29] H. M. Mian, J. G. Lyons, J. Perrin, A. W. Froehle, and A. B. Krishnamurthy, "A review of current practices in periprosthetic joint infection debridement and revision arthroplasty," *Arthroplasty*, vol. 4, p. 31, Sep. 2022, doi: 10.1186/s42836-022-00136-5.

[30] M. Otto, "Staphylococcus epidermidis – the 'accidental' pathogen," *Nat Rev Microbiol*, vol. 7, no. 8, pp. 555–567, Aug. 2009, doi: 10.1038/nrmicro2182.

[31] H. Büttner, D. Mack, and H. Rohde, "Structural basis of Staphylococcus epidermidis biofilm formation: mechanisms and molecular interactions," *Front Cell Infect Microbiol*, vol. 5, p. 14, Feb. 2015, doi: 10.3389/fcimb.2015.00014.

[32] S. Sharma, J. Mohler, S. D. Mahajan, S. A. Schwartz, L. Bruggemann, and R. Aalinkeel, "Microbial Biofilm: A Review on Formation, Infection, Antibiotic Resistance, Control Measures, and Innovative Treatment," *Microorganisms*, vol. 11, no. 6, Art. no. 6, Jun. 2023, doi: 10.3390/microorganisms11061614.

[33] D. H. Limoli, C. J. Jones, and D. J. Wozniak, "Bacterial Extracellular Polysaccharides in Biofilm Formation and Function," *Microbiol Spectr*, vol. 3, no. 3, p. 10.1128/microbiolspec.MB-0011–2014, Jun. 2015, doi: 10.1128/microbiolspec.MB-0011-2014.

[34] K. Sauer *et al*., "The biofilm life cycle: expanding the conceptual model of biofilm formation," *Nat Rev Microbiol*, vol. 20, no. 10, pp. 608–620, Oct. 2022, doi: 10.1038/s41579-022-00767-0.

[35] P. S. Stewart and J. William Costerton, "Antibiotic resistance of bacteria in biofilms," *The Lancet*, vol. 358, no. 9276, pp. 135–138, Jul. 2001, doi: 10.1016/S0140-6736(01)05321-1.

[36] T.-F. C. Mah and G. A. O'Toole, "Mechanisms of biofilm resistance to antimicrobial agents," *Trends in Microbiology*, vol. 9, no. 1, pp. 34–39, Jan. 2001, doi: 10.1016/S0966-842X(00)01913-2.

[37] V. Siciliano, R. A. Passerotto, M. Chiuchiarelli, G. M. Leanza, and V. Ojetti, "Difficult-to-Treat Pathogens: A Review on the Management of Multidrug-Resistant Staphylococcus epidermidis," *Life*, vol. 13, no. 5, p. 1126, May 2023, doi: 10.3390/life13051126.

[38] C. Uruén, G. Chopo-Escuin, J. Tommassen, R. C. Mainar-Jaime, and J. Arenas, "Biofilms as Promoters of Bacterial Antibiotic Resistance and Tolerance," *Antibiotics*, vol. 10, no. 1, p. 3, Dec. 2020, doi: 10.3390/antibiotics10010003.

[39] S. A. Rudhart, F. Günther, L. I. Dapper, F. Gehrt, B. A. Stuck, and S. Hoch, "Analysis of bacterial contamination and the effectiveness of UV light-based reprocessing of everyday medical devices," *PLoS ONE*, vol. 17, no. 11, p. e0268863, Nov. 2022, doi: 10.1371/journal.pone.0268863.

[40] M. Lualdi *et al*., "Ultraviolet C lamps for disinfection of surfaces potentially contaminated with SARS-CoV-2 in critical hospital settings: examples of their use and some practical advice," *BMC Infect Dis*, vol. 21, no. 1, p. 594, Dec. 2021, doi: 10.1186/s12879-021-06310-5.

[41] M. A. Kohanski, D. J. Dwyer, and J. J. Collins, "How antibiotics kill bacteria: from targets to networks," *Nat Rev Microbiol*, vol. 8, no. 6, pp. 423–435, Jun. 2010, doi: 10.1038/nrmicro2333.

[42] "PubMed Central Full Text PDF." Accessed: Mar. 07, 2024. [Online]. Available: https://www.ncbi.nlm.nih.gov/pmc/articles/PMC10340576/pdf/healthcare-11-01946.pdf

[43] J. Talapko *et al*., "Antimicrobial Peptides—Mechanisms of Action, Antimicrobial Effects and Clinical Applications," *Antibiotics*, vol. 11, no. 10, Art. no. 10, Oct. 2022, doi: 10.3390/antibiotics11101417.

[44] J. T. Mhlongo, A. Y. Waddad, F. Albericio, and B. G. De La Torre, "Antimicrobial Peptide Synergies for Fighting Infectious Diseases," *Advanced Science*, vol. 10, no. 26, p. 2300472, Sep. 2023, doi: 10.1002/advs.202300472.

[45] K. E. Ridyard and J. Overhage, "The Potential of Human Peptide LL-37 as an Antimicrobial and Anti-Biofilm Agent," *Antibiotics (Basel)*, vol. 10, no. 6, p. 650, May 2021, doi: 10.3390/antibiotics10060650.

[46] J. Steinmann, "Induction and regulation of CAMP gene expression".

[47] H. X. Luong, T. T. Thanh, and T. H. Tran, "Antimicrobial peptides – Advances in development of therapeutic applications," *Life Sciences*, vol. 260, p. 118407, Nov. 2020, doi: 10.1016/j.lfs.2020.118407.

[48] Q.-Y. Zhang *et al*., "Antimicrobial peptides: mechanism of action, activity and clinical potential," *Military Medical Research*, vol. 8, no. 1, p. 48, Sep. 2021, doi: 10.1186/s40779-021-00343-2.

[49] L. Martin, A. Van Meegern, S. Doemming, and T. Schuerholz, "Antimicrobial Peptides in Human Sepsis," *Front. Immunol*., vol. 6, Aug. 2015, doi: 10.3389/fimmu.2015.00404.

[50] A. A. Bahar and D. Ren, "Antimicrobial Peptides," *Pharmaceuticals (Basel)*, vol. 6, no. 12, pp. 1543–1575, Nov. 2013, doi: 10.3390/ph6121543.

[51] A. Bin Hafeez, X. Jiang, P. J. Bergen, and Y. Zhu, "Antimicrobial Peptides: An Update on Classifications and Databases," *International Journal of Molecular Sciences*, vol. 22, no. 21, Art. no. 21, Jan. 2021, doi: 10.3390/ijms222111691.

[52] C. Vranckx, L. Lambricht, V. Préat, O. Cornu, C. Dupont-Gillain, and A. Vander Straeten, "Layer-by-Layer Nanoarchitectonics Using Protein–Polyelectrolyte Complexes toward a Generalizable Tool for Protein Surface Immobilization," *Langmuir*, vol. 38, no. 18, pp. 5579–5589, May 2022, doi: 10.1021/acs.langmuir.2c00191.

[53] U. H. N. Dürr, U. S. Sudheendra, and A. Ramamoorthy, "LL-37, the only human member of the cathelicidin family of antimicrobial peptides," *Biochimica et Biophysica Acta (BBA) - Biomembranes*, vol. 1758, no. 9, pp. 1408–1425, Sep. 2006, doi: 10.1016/j.bbamem.2006.03.030.

[54] A. Neshani *et al.*, "LL-37: Review of antimicrobial profile against sensitive and antibiotic-resistant human bacterial pathogens," *Gene Reports*, vol. 17, p. 100519, Dec. 2019, doi: 10.1016/j.genrep.2019.100519.

[55] K. E. Ridyard and J. Overhage, "The Potential of Human Peptide LL-37 as an Antimicrobial and Anti-Biofilm Agent," *Antibiotics (Basel)*, vol. 10, no. 6, p. 650, May 2021, doi: 10.3390/antibiotics10060650.

[56] C. N. LaRock and V. Nizet, "Cationic Antimicrobial Peptide Resistance Mechanisms of Streptococcal Pathogens," *Biochimica et biophysica acta*, vol. 1848, no. 11 0 0, p. 3047, Nov. 2015, doi: 10.1016/j.bbamem.2015.02.010.

[57] S. Al-Adwani *et al.*, "Studies on citrullinated LL-37: detection in human airways, antibacterial effects and biophysical properties," *Sci Rep*, vol. 10, no. 1, p. 2376, Feb. 2020, doi: 10.1038/s41598-020-59071-7.

[58] A. Mutschler *et al.*, "Unexpected Bactericidal Activity of Poly(arginine)/Hyaluronan Nanolayered Coatings," *Chem. Mater.*, vol. 28, no. 23, pp. 8700–8709, Dec. 2016, doi: 10.1021/acs.chemmater.6b03872.

[59] J. Overhage, A. Campisano, M. Bains, E. C. W. Torfs, B. H. A. Rehm, and R. E. W. Hancock, "Human Host Defense Peptide LL-37 Prevents Bacterial Biofilm Formation," *Infect Immun*, vol. 76, no. 9, pp. 4176–4182, Sep. 2008, doi: 10.1128/IAI.00318-08.

[60] W. Bäumler, D. Eckl, T. Holzmann, and W. Schneider-Brachert, "Antimicrobial coatings for environmental surfaces in hospitals: a potential new pillar for prevention strategies in hygiene," *Critical Reviews in Microbiology*, vol. 48, no. 5, pp. 531–564, Sep. 2022, doi: 10.1080/1040841X.2021.1991271.

[61] "Layer-by-layer method: initially a base electrode is modified with a... | Download Scientific Diagram." Accessed: Mar. 22, 2024. [Online]. Available: https://www.researchgate.net/figure/Layer-by-layer-method-initially-a-base-electrode-is-modified-with-a-charged-layer-This_fig8_258528216

[62] M. McShane and Y. Lvov, "Electrostatic Self-Assembly: Layer-by-Layer," 2014, pp. 1342–1358. doi: 10.1081/E-ENN3-120013616.

[63] J. Borges and J. F. Mano, "Molecular Interactions Driving the Layer-by-Layer Assembly of Multilayers," *Chem. Rev.*, vol. 114, no. 18, pp. 8883–8942, Sep. 2014, doi: 10.1021/cr400531v.

[64] Y. Ghimire and A. Bhattarai, "A Review on Polyelectrolytes (PES) and Polyelectrolyte Complexes (PECs)," *International Journal of Engineering and Technical Research*, vol. 9, Jul. 2021, doi: 10.17577/IJERTV9IS080112.

[65] P. Wang, L. Chi, Z. Zhang, H. Zhao, F. Zhang, and R. J. Linhardt, "Heparin: An old drug for new clinical applications," *Carbohydrate Polymers*, vol. 295, p. 119818, Nov. 2022, doi: 10.1016/j.carbpol.2022.119818.

[66] L. Litov *et al*., "Molecular Mechanism of the Anti-Inflammatory Action of Heparin," *IJMS*, vol. 22, no. 19, p. 10730, Oct. 2021, doi: 10.3390/ijms221910730.
[67] M. Lundin, F. Solaqa, E. Thormann, L. Macakova, and E. Blomberg, "Layer-by-Layer Assemblies of Chitosan and Heparin: Effect of Solution Ionic Strength and pH," *Langmuir*, vol. 27, no. 12, pp. 7537–7548, Jun. 2011, doi: 10.1021/la200441u.
[68] B. Hu, Y. Guo, H. Li, X. Liu, Y. Fu, and F. Ding, "Recent advances in chitosan-based layer-by-layer biomaterials and their biomedical applications," *Carbohydrate Polymers*, vol. 271, p. 118427, Nov. 2021, doi: 10.1016/j.carbpol.2021.118427.
[69] X. W. Ng, R. C. Mundargi, and S. S. Venkatraman, "Nanomedicine: Size-Related Drug Delivery Applications, Including Periodontics and Endodontics," in *Nanotechnology in Endodontics*, A. Kishen, Ed., Cham: Springer International Publishing, 2015, pp. 71–95. doi: 10.1007/978-3-319-13575-5_5.
[70] I. Aranaz *et al*., "Chitosan: An Overview of Its Properties and Applications," *Polymers (Basel)*, vol. 13, no. 19, p. 3256, Sep. 2021, doi: 10.3390/polym13193256.
[71] A. J. Doig and M. J. E. Sternberg, "Side-chain conformational entropy in protein folding," *Protein Science*, vol. 4, no. 11, pp. 2247–2251, Nov. 1995, doi: 10.1002/pro.5560041101.
[72] "ZetaPotential-Introduction-in-30min-Malvern.pdf."
[73] A. vander Straeten, D. Lefèvre, S. Demoustier-Champagne, and C. Dupont-Gillain, "Protein-based polyelectrolyte multilayers," *Advances in Colloid and Interface Science*, vol. 280, p. 102161, Jun. 2020, doi: 10.1016/j.cis.2020.102161.
[74] C. Staii, "Conformational Changes in Surface-Immobilized Proteins Measured Using Combined Atomic Force and Fluorescence Microscopy," *Molecules*, vol. 28, no. 12, p. 4632, Jun. 2023, doi: 10.3390/molecules28124632.
[75] F. R. Bruniera *et al*., "The use of vancomycin with its therapeutic and adverse effects: a review".
[76] S. Patel, C. V. Preuss, and F. Bernice, "Vancomycin," in *StatPearls*, Treasure Island (FL): StatPearls Publishing, 2024. Accessed: Mar. 09, 2024. [Online]. Available: http://www.ncbi.nlm.nih.gov/books/NBK459263/
[77] Q. Hu, H. Peng, and X. Rao, "Molecular Events for Promotion of Vancomycin Resistance in Vancomycin Intermediate Staphylococcus aureus," *Front. Microbiol.*, vol. 7, Oct. 2016, doi: 10.3389/fmicb.2016.01601.
[78] C. Schwarz, G. Taccetti, P.-R. Burgel, and S. Mulrennan, "Tobramycin safety and efficacy review article," *Respiratory Medicine*, vol. 195, p. 106778, Apr. 2022, doi: 10.1016/j.rmed.2022.106778.
[79] "mode-of-action-of-aminoglycosides." Accessed: Mar. 16, 2024. [Online]. Available: https://microscopiaiwm.wordpress.com/tag/mode-of-action-of-aminoglycosides/
[80] M. Rosalia *et al*., "Tobramycin Nanoantibiotics and Their Advantages: A Minireview," *Int J Mol Sci*, vol. 23, no. 22, p. 14080, Nov. 2022, doi: 10.3390/ijms232214080.
[81] E. National Academies of Sciences, H. and M. Division, C. to R. L.-T. H. E. of A. Drugs, B. on P. H. and P. H. Practice, A. N. Styka, and D. A. Savitz, "Doxycycline," in *Assessment of Long-Term Health Effects of Antimalarial Drugs When Used for Prophylaxis*, National Academies Press (US), 2020. Accessed: Mar. 09, 2024. [Online]. Available: https://www.ncbi.nlm.nih.gov/books/NBK556599/
[82] E. M. Graber, "Treating acne with the tetracycline class of antibiotics: A review," *Dermatological Reviews*, vol. 2, no. 6, pp. 321–330, Dec. 2021, doi: 10.1002/der2.49.
[83] C. Foti, A. Piperno, A. Scala, and O. Giuffrè, "Oxazolidinone Antibiotics: Chemical, Biological and Analytical Aspects," *Molecules*, vol. 26, no. 14, p. 4280, Jul. 2021, doi: 10.3390/molecules26144280.

[84] "Linezolid: a review of its properties, function, and use in critical care - PMC." Accessed: Mar. 10, 2024. [Online]. Available: https://www.ncbi.nlm.nih.gov/pmc/articles/PMC6014438/
[85] "LinezolidMoleculeoftheMonthAugust2005.pdf."
[86] "Circular Dichroism by LibreTexts".
[87] T. J. Dolinsky, J. E. Nielsen, J. A. McCammon, and N. A. Baker, "PDB2PQR: an automated pipeline for the setup of Poisson-Boltzmann electrostatics calculations," *Nucleic Acids Research*, vol. 32, no. Web Server, pp. W665–W667, Jul. 2004, doi: 10.1093/nar/gkh381.
[88] "Isothiocyanate de fluorescéine," *Wikipédia*. May 19, 2022. Accessed: Jun. 12, 2024. [Online]. Available: https://fr.wikipedia.org/w/index.php?title=Isothiocyanate_de_fluoresc%C3%A9ine&oldid=193814571
[89] "Fluorescence spectroscopy and its applications: A Review," *Int J of And Pharm Anal*.
[90] "Bicinchoninic Acid (BCA) Protein Assay Kit," GenDEPOT. Accessed: Apr. 26, 2024. [Online]. Available: https://gendepot.com/products/bicinchoninic-acid-bca-protein-assay-kit
[91] Y. Liu, H. Yu, Y. Cheng, Y. Guo, W. Yao, and Y. Xie, "Non-destructive Monitoring of Staphylococcus aureus Biofilm by Surface-Enhanced Raman Scattering Spectroscopy," *Food Anal. Methods*, vol. 13, no. 9, pp. 1710–1716, Sep. 2020, doi: 10.1007/s12161-020-01792-6.
[92] "Figure 57. Principe de fonctionnement du test résazurine basé sur une...," ResearchGate. Accessed: Mar. 25, 2024. [Online]. Available: https://www.researchgate.net/figure/Principe-de-fonctionnement-du-test-resazurine-base-sur-une-reaction-doxydo-reduction_fig31_282734958
[93] "Figure 2.24.2 Reduction of resazurin and formation of resorufin...," ResearchGate. Accessed: May 07, 2024. [Online]. Available: https://www.researchgate.net/figure/2-Reduction-of-resazurin-and-formation-of-resorufin-product-Resazurin-a_fig2_316232176
[94] T. L. Riss, R. A. Moravec, A. L. Niles, H. A. Benink, T. J. Worzella, and L. Minor, "Cell Viability Assays".
[95] "Tous les conseils pour choisir correctement sa hotte à flux laminaire." Accessed: Mar. 25, 2024. [Online]. Available: https://www.initio-shop.fr/19-comment-choisir-sa-hotte-a-flux-laminaire.html
[96] "Dictionnaire médical de l'Académie de Médecine." Accessed: Mar. 27, 2024. [Online]. Available: https://www.academie-medecine.fr/le-dictionnaire/index.php?q=Concentration%20Minimale%20Inhibitrice%20%28d%27un%20antibiotique%29
[97] S. Zoll, B. Pätzold, M. Schlag, F. Götz, H. Kalbacher, and T. Stehle, "Structural Basis of Cell Wall Cleavage by a Staphylococcal Autolysin," *PLoS Pathog*, vol. 6, no. 3, p. e1000807, Mar. 2010, doi: 10.1371/journal.ppat.1000807.
[98] "Normes McFarland," *Wikipédia*. Jul. 04, 2023. Accessed: May 15, 2024. [Online]. Available: https://fr.wikipedia.org/w/index.php?title=Normes_McFarland&oldid=205710020
[99] "Surface spécifique," *Wikipédia*. Nov. 25, 2022. Accessed: Jun. 09, 2024. [Online]. Available: https://fr.wikipedia.org/w/index.php?title=Surface_sp%C3%A9cifique&oldid=198973554
[100] Y. Zhang, E. Yildirim, H. S. Antila, L. D. Valenzuela, M. Sammalkorpi, and J. L. Lutkenhaus, "The influence of ionic strength and mixing ratio on the colloidal stability of PDAC/PSS polyelectrolyte complexes," *Soft Matter*, vol. 11, no. 37, pp. 7392–7401, 2015, doi: 10.1039/C5SM01184A.

[101] K. Harawaza, B. Cousins, P. Roach, and A. Fernandez, “Modification of the surface nanotopography of implant devices: A translational perspective,” *Materials Today Bio*, vol. 12, p. 100152, Sep. 2021, doi: 10.1016/j.mtbio.2021.100152.

Appendices

1. PPCs charge ratio determination

Table I : Volumes of HEP, LL-37 and ultrapure water used to build PPCs for PPCs charge ratio determination experiment.

Charge ratio (-/+)	LL-37 (μL)	HEP (μL)	Ultrapure water (μL)
0	172.90	0	627.10
0.25	172.90	16.63	610.47
0.5	172.90	33.26	593.84
0.75	172.90	49.89	577.21
1	172.90	66.52	560.58
1.25	172.90	83.15	543.95
1.5	172.90	99.78	527.32
1.75	172.90	116.41	510.69
2	172.90	133.04	494.06
2.25	172.90	149.67	477.43
2.5	172.90	166.30	460.80
2.75	172.90	182.93	444.17
3	172.90	199.56	427.54

Table II: Untreated absorbance values obtained by PPCs charge ratio determination experiment (3 plates) with means and their associated standard deviation.

Charge ratio r (-/+)	Plate 1	Plate 2	Plate 3	$\overline{x}$	$\overline{x}$- Blank	s
Blank	0.039	0.042	0.042	0.041	0	0.0013
0	0.049	0.051	0.051	0.050	0.0096	0.0013
0.25	0.068	0.081	0.065	0.071	0.030	0.0086
0.5	0.076	0.090	0.089	0.084	0.043	0.0073
0.75	0.12	0.11	0.093	0.11	0.066	0.013
1	0.13	0.12	0.10	0.12	0.080	0.015
1.25	0.14	0.13	0.12	0.13	0.088	0.0069
1.5	0.13	0.16	0.16	0.15	0.10	0.016
1.75	0.095	0.22	0.16	0.13	0.088	0.061
2	0.082	0.12	0.10	0.10	0.060	0.017
2.25	0.074	0.096	0.11	0.094	0.053	0.018
2.5	0.097	0.12	0.10	0.11	0.065	0.010
2.75	0.087	0.11	0.10	0.10	0.060	0.013
3	0.081	0.11	0.16	0.12	0.079	0.040

2. Study of LL-37 release from the coating

Table III: Quantity of released complexed LL-37 (PPCs) from a coated polystyrene microwell for 13 sampling depending on the condition at different times. (μg) Each condition has been performed in duplicate.

PBS	300		300		200		300		300		200	
BL	20		16		16		20		16		16	
pH	3.5						5					
30'	0.32	0.33	0.26	0.27	0.19	0.19	0.39	0.40	0.35	0.35	0.25	0.29
1h	0.25	0.25	0.23	0.23	0.23	0.16	0.52	0.43	0.42	0.34	0.27	0.30
1h30	0.24	0.25	0.23	0.24	0.21	0.16	0.41	0.42	0.37	0.33	0.28	0.32
2h	0.25	0.24	0.23	0.23	0.17	0.16	0.36	0.40	0.36	0.32	0.27	0.31
2h30	0.24	0.24	0.23	0.23	0.16	0.16	0.38	0.38	0.33	0.35	0.28	0.30
3h	0.24	0.23	0.23	0.23	0.16	0.16	0.35	0.37	0.32	0.32	0.25	0.28
3h30	0.23	0.23	0.23	0.23	0.21	0.16	0.33	0.33	0.31	0.31	0.27	0.24
4h	0.24	0.23	0.23	0.23	0.17	0.15	0.33	0.33	0.31	0.30	0.24	0.26
4h30	0.24	0.25	0.23	0.23	0.21	0.16	0.32	0.32	0.30	0.29	0.22	0.24
5h	0.27	0.24	0.24	0.24	0.17	0.15	0.37	0.37	0.30	0.29	0.22	0.23
5h30	0.24	0.23	0.22	0.22	0.18	0.15	0.37	0.35	0.31	0.33	0.24	0.26
6h	0.23	0.24	0.22	0.23	0.18	0.15	0.34	0.42	0.33	0.32	0.23	0.24
24h	0.38	0.36	0.30	0.32	0.30	0.23	2.52	2.31	1.56	1.73	1.79	2.36
CUMUL (μg)	3.38	3.31	3.08	3.14	2.54	2.14	7.00	6.83	5.57	5.59	4.80	5.63
MOY (μg)	3.35		3.11		2.34		6.92		5.58		5.22	
Cf (μg/mL)	0.86		0.80		0.90		1.77		1.43		2.01	

Table IV: Quantity of released bare LL-37 from a coated polystyrene microwell for 13 sampling depending on the condition at different times. (μg) Each condition has been performed in duplicate.

PBS	300		300		200		300		300		200	
BL	20		16		16		20		16		16	
pH	3.5						5					
30'	20.77	24.51	8.06	7.39	7.56	7.13	1.81	1.64	0.87	0.86	0.61	0.62
1h	2.27	2.15	1.50	1.57	1.11	1.55	0.91	0.71	0.68	0.65	0.56	0.56
1h30	1.19	1.22	1.02	1.01	0.82	0.90	0.73	0.67	0.66	0.61	0.41	0.42
2h	1.04	1.16	0.92	0.85	0.77	0.79	0.67	0.61	0.50	0.52	0.38	0.38
2h30	1.03	1.27	0.97	0.89	0.72	0.76	0.64	0.60	0.52	0.52	0.36	0.40
3h	1.02	0.93	0.89	0.93	0.80	0.74	0.61	0.62	0.65	0.49	0.35	0.36
3h30	0.99	1.02	0.85	0.86	1.00	0.73	0.64	0.63	0.47	0.46	0.34	0.35
4h	1.08	1.16	0.90	0.86	0.71	0.72	0.66	0.60	0.49	0.54	0.39	0.39
4h30	1.93	2.04	1.29	1.42	0.75	0.77	1.01	0.62	0.89	0.86	0.37	0.39
5h	1.27	1.19	1.17	1.13	0.61	0.16	1.03	0.56	0.46	0.48	0.32	0.31
5h30	2.00	1.57	1.27	1.25	0.71	0.84	1.20	0.80	0.58	0.58	0.39	0.42
6h	1.68	1.25	1.12	1.27	1.00	1.05	0.68	0.54	0.48	0.53	0.42	0.49
24h	14.86	13.58	10.46	8.94	18.35	17.43	7.33	5.46	4.49	3.75	3.54	3.89
CUMUL (μg)	51.14	53.03	30.42	28.37	34.91	33.58	17.91	14.04	11.74	10.87	8.43	8.98
MOY (μg)	52.09		29.39		34.24		15.98		11.30		8.70	
Cf (μg/mL)	13.36		7.54		13.17		4.10		2.90		3.35	

Table V: Calculations for the predicted released concentration of bare LL-37 obtained by using gold nanoparticles. (μg/mL)

48 microwells plate	
Bottom area (mm^2)	100
Wall area (mm^2)	70.95
Total area (wall + bottom) (mm^2)	170.95
Nanoparticles	
Wanted specific area with np (mm^2)	4273.63
Specific area for 1 np (mm^2/np)	1.26E-09
np/mL in the suspension (np/mL)	6.54E+11
Specific area for 1 mL of suspension (mm^2/mL)	821.82
Volume of suspension for specific area (mL)	5.20
Quantity released ($\mu g/cm^2$)	6
Expected quantity (μg)	256.42
Volume for the release (mL)	4
Expected released concentration of LL-37 (μg/mL)	64.10

Table VI: Quantity of LL-37 released according to the BLs number based on data from *Figure 33*. (μg/cm^2)

BLs	Released LL-37 (μg/ cm^2)	μg/(cm^2*BL)
9	4	/
12	4.6	0.2
20	5.8	0.15
25	6.8	0.2

Table VI shows the amount of LL-37 released for each number of BLs per unit area. When we calculate the difference in quantity per unit area between a higher and a lower number of BLs, then divide this difference by the difference in the number of BLs, we obtain the amount of LL-37 gained for each additional BL. On average, we have 0.183 μg more LL-37 released per BL added. Following this linear trend, for a coating of 50 BLs, this gives a total of 11.4 μg/cm^2 of LL-37 released.

Given that release takes place with a volume of 100 μL of PBS after 6 and 24 hours in 10 microwells of a 96-well plate, the total volume is 2 mL and the contact surface between PBS and microwell is 9.5 cm^2. The predicted concentration of LL-37 released is 54.15 μg/mL.

Table VII: Calculations for the predicted released concentration in LL-37 for 96 microwells plate based on data of *Figure 33* (μg/mL)

Area of a 96-well plate (cm^2)	0.95
Predicted released quantity of LL-37 per surface unit for 50 BL (μg/cm^2)	11.4
Microwells number	10
Released quantity of LL-37 (μg)	108.3
Volume total PBS (mL)	2
Expected concentration in LL-37 (μg/mL)	54.15

3. Antibiotics synergy with LL-37-based antimicrobial coating

3.1 Antibiotics solutions preparation

Table VIII: Volumes used of vancomycin solution (50 μg/mL) and RPG to prepare the different MIC (1x, 2x, 5x, 10x) solutions.

MIC	Dilution of the stock solution (1 mg/mL)	50 μg/mL solution (μL)	RPG (μL)
1x	50x	100	4900
2x	25x	200	4800
5x	10x	500	4500
10x	5x	1000	4000

Table IX: Volumes used of tobramycin solution (12800 μg/mL) and RPG to prepare the different MIC (1x, 2x, 5x, 10x) solutions.

MIC	Dilution of the stock solution (12.8 mg/mL)	12 800 μg/mL solution (μL)	RPG (μL)
1x	50x	100	4900
2x	25x	200	4800
5x	10x	500	4500
10x	5x	1000	4000

Table X: Volumes used of doxycycline solution (50 μg/mL) and RPG to prepare the different MIC (1x, 2x, 5x, 10x) solutions.

MIC	Dilution of the stock solution (1 mg/mL)	50 μg/mL solution (μL)	RPG (μL)
1x	200x	25	4975
2x	100x	50	4950
5x	40x	125	4875
10x	20x	250	4750

Table XI: Volumes used of linezolid solution (50 μg/mL) and RPG to prepare the different MIC (1x, 2x, 5x, 10x) solutions.

MIC	Dilution of the stock solution (1 mg/mL)	50 μg/mL solution (μL)	RPG (μL)
1x	50x	100	4900
2x	25x	200	4800
5x	10x	500	4500
10x	5x	1000	4000

3.2 CFU counting

3.2.1 Protocol

For CFU counting testing, the protocol for coating, biofilm formation, antibiotics solutions preparation, etc. was done as described in *Materials and Methods* section. Again, this experiment was performed with and without coating to study the activity of antibiotics alone and with the AMP on viable cells.

Coating of the plate for CFU counting was done as follows:

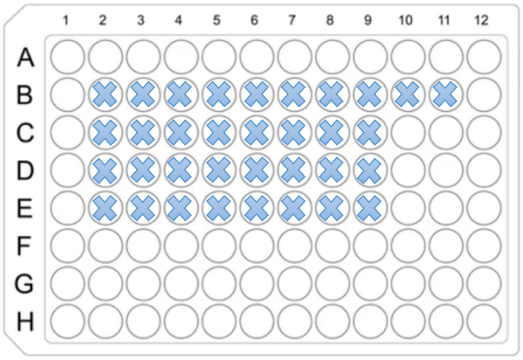

Figure I: Coated 96 microwells plate for CFU counting experiment. Wells on which biofilms of *S. epidermidis ATCC 35984* are grown are shown with blue crosses. Said wells were all coated upstream with a $(LL\text{-}37 - HEP)_{14.5}$ coating.

Antibiotics solution prepared as described in the Materials and Methods section were introduced on the coated plate as shown on the following figure. C^+ stands for positive control and no antibiotic treatment was introduced in these two wells.

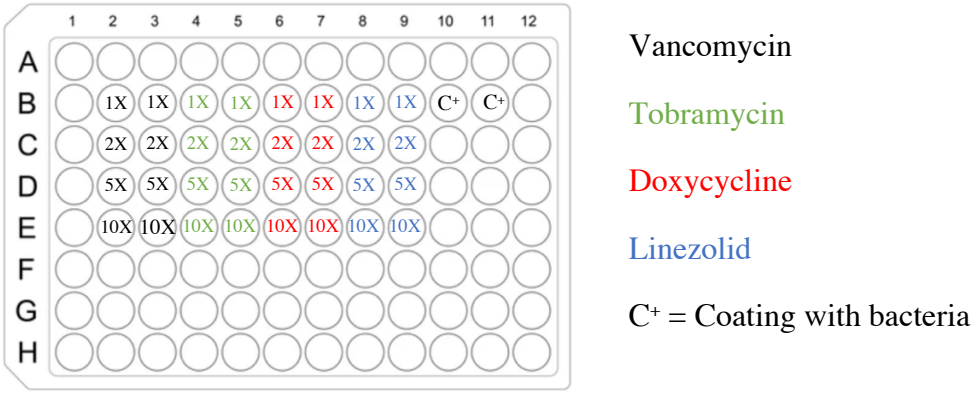

Figure II: Introduction of antibiotics at different concentrations, corresponding to a multiple of their MIC (1x, 2x, 5x, or 10x) on 24h-preformed biofilms of *S. epidermidis ATCC 35984* on coated wells for CFU counting experiment.

In order to carry out this part of the experiment, the bottom of each microwell containing the bacteria must be scraped for about one minute in order to detach and destroy the biofilm. Next, 200 μL of PBS are added to each biofilm-containing microwell, and the plate is introduced into the sonicator for 30 seconds at an amplitude of 60. This sonication step is crucial as it loosens

and disperses the biofilm elements throughout the PBS, ensuring greater homogeneity. Unfortunately, misuse of sonicator during this experiment made the wells to inter-mix and led us to be not confident about the obtained results.

On a new 96-well plate, 100 μL of each duplicate for each condition is introduced into the first microwell of the new plate at dilution 100.

As shown on the *Figure III and IV*, 200 μL of each condition for each antibiotic are placed on the first row of the new microwells plates. Next, 10x dilutions up to dilution 10^5 are made for each antibiotic. These will go up to 10^6 for the positive control. To do this, 180 μL of PBS are added to the microwells from 10^1 to $10^5/10^6$. Then, 20 μL of solution 10^0 is mixed with 180 μL of dilution 10^1, and so on, until the desired dilutions of $10^5/10^6$are reached.

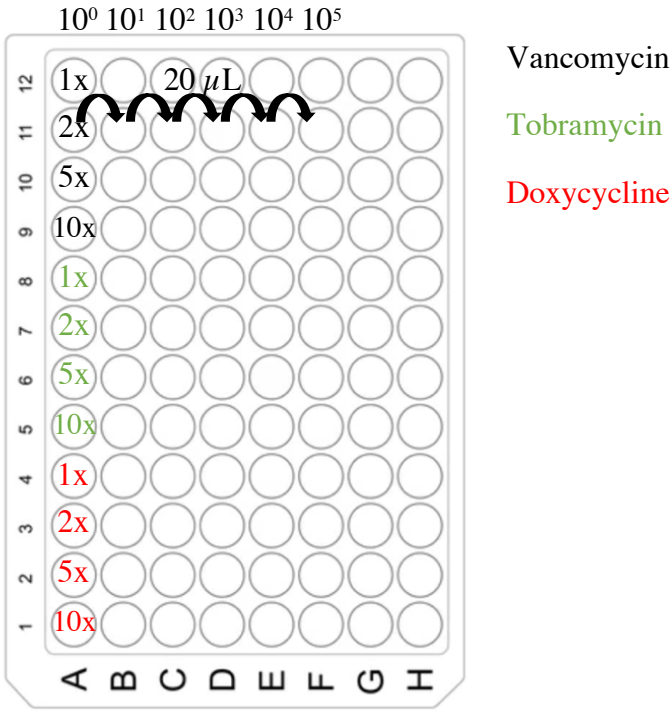

Figure III: Serial dilution protocol for CFU counting experiment (plate 1)

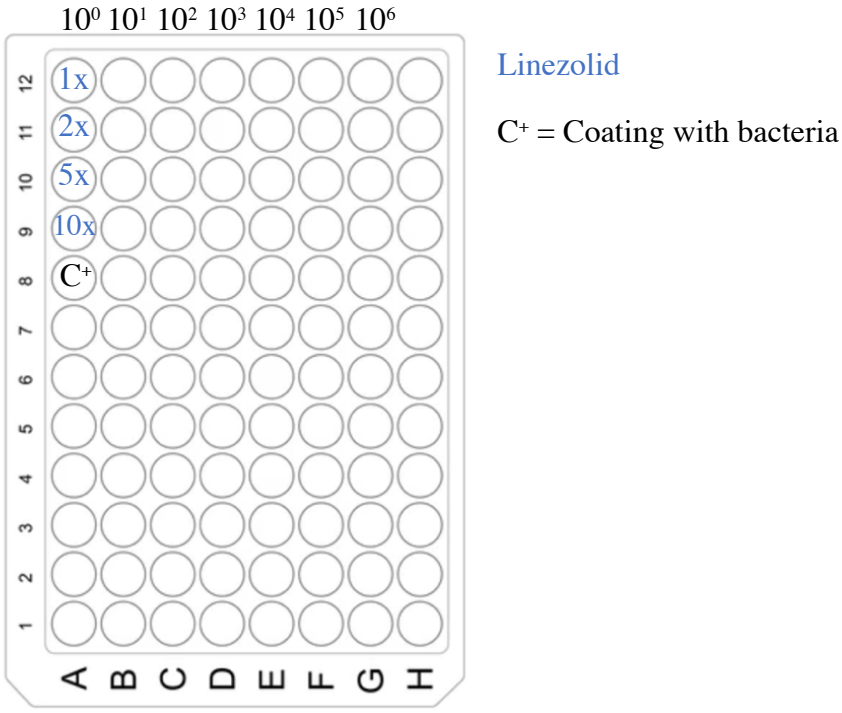

Figure IV: Dilution protocol for CFU counting experiment (plate 2)

Once the dilutions have been made, the rest of the experiment takes place on TSA plates. Once these have been prepared, 50 μL of dilutions 10^3, 10^4 and 10^5 for each condition of each antibiotic are laid on TSA plates. For the positive control, 50 μL of dilutions 10^3, 10^4 and 10^5 and 10^6 are disposed on TSA plates. Meticulous spread of the solutions on the plates are done thanks to sterilized beads. This step is crucial for good colony dispersion on the plates and subsequent easier counting.

Plates should remain in the incubator for at 37°C overnight. Counting can be done from the day after. The colonies formed on the Petri dishes are counted to determine the quantity of bacteria for each condition.

3.2.2 Results for antibiotics activity with coating

Hereunder are presented the results for "Antibiotics synergy with LL-37-based antimicrobial coating" experiment obtained for CFU counting after experimental error that let the wells inter-mixing. Indeed, the misuse of the sonicator led the wells to mix with each other and being conscient this issue, following results have to be considered with caution.

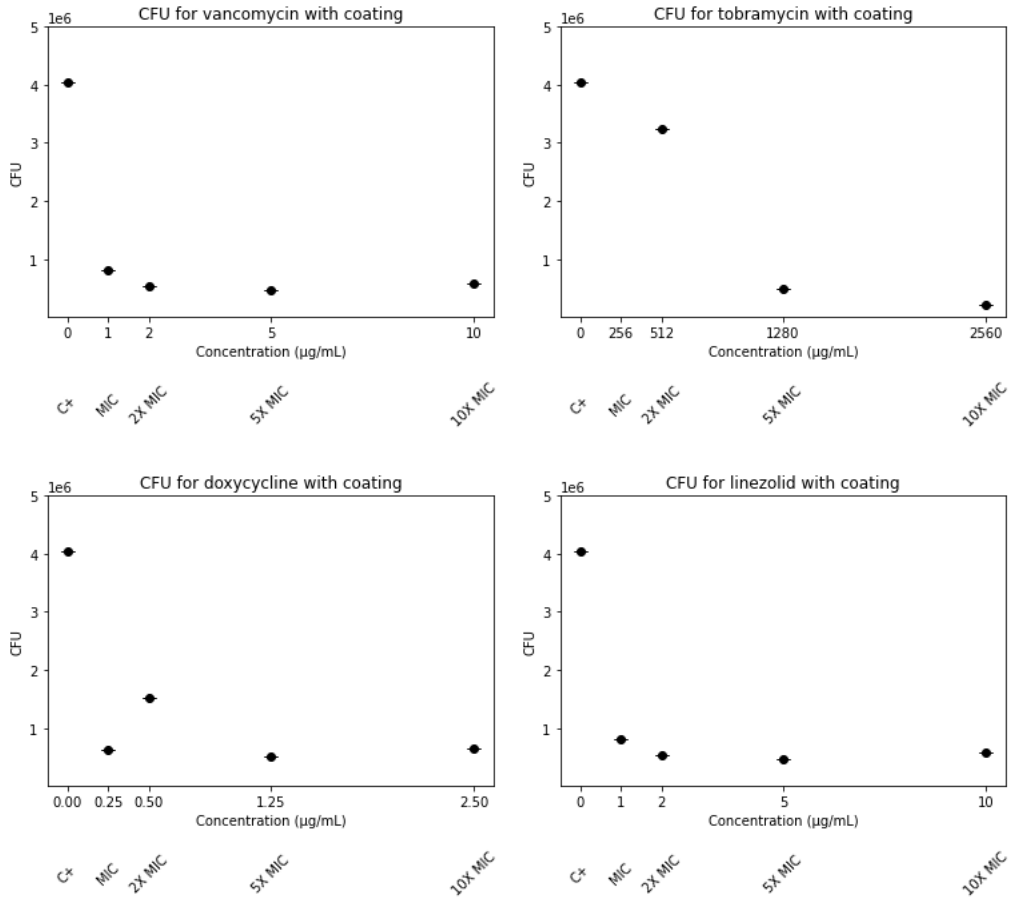

Figure V: **CFU** number for 24h pre-formed *S. epidermidis ATCC 35984* biofilms when combining a LL-37-based coating with different multiples of the MIC of either vancomycin, tobramycin, doxycycline, or linezolid. C^+ = untreated biofilm (positive control).

3.2.3 Results for antibiotics activity without coating (Cédric Vranckx)

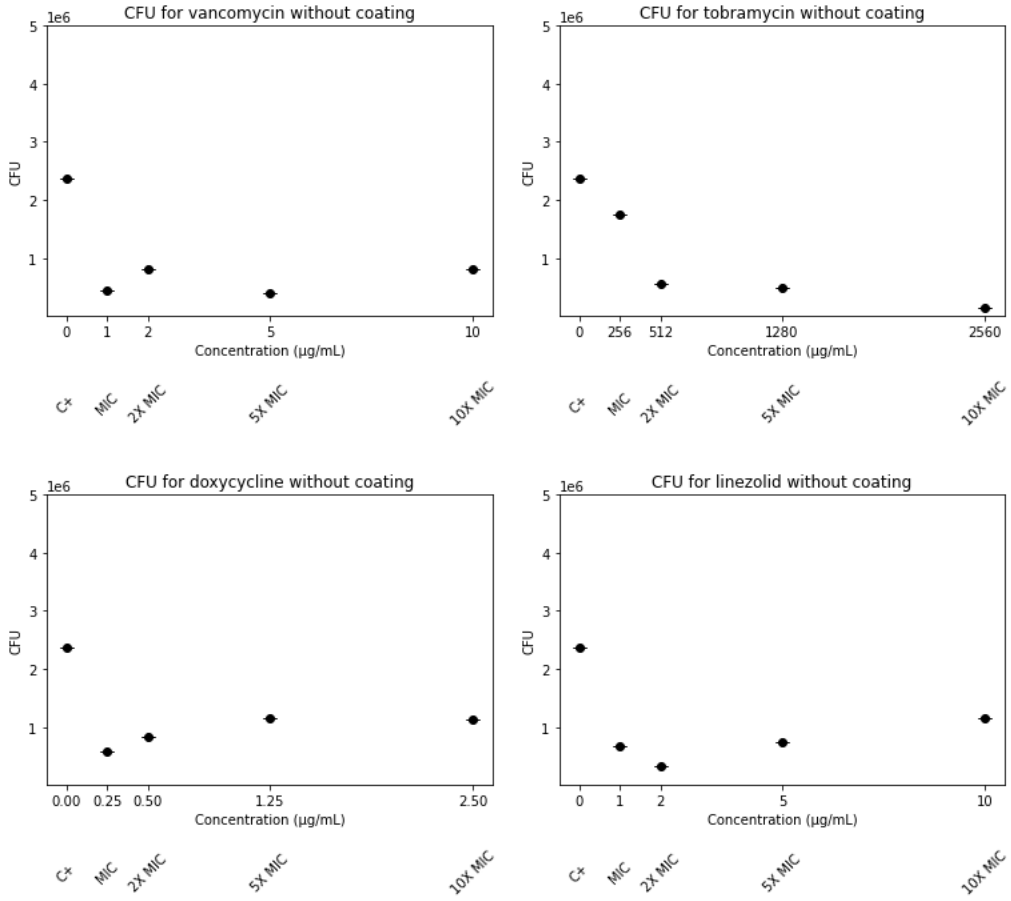

Figure VI: **CFU** number for 24h pre-formed *S. epidermidis ATCC 35984* biofilms without a LL-37-based coating with different multiples of the MIC of either vancomycin, tobramycin, doxycycline, or linezolid. C^+ = untreated biofilm (positive control) obtained by Cédric Vranckx.

3.3 Results after potential autolysin AtlE activity on *S. epidermidis ATCC 35984* strain

Hereunder are presented the results for antibiotics activity being tested with the LL-37-based AMC. The *S. epidermidis* colonies being let for incubation for close to 72h, hypothesis has been raised that the bacteria have undergone the activity of autolysin AltE after resulting in uneven biofilm formation as the obtained results for the three following tests were not reproductible with prior and later same experiments' results. Protocols were the same as the one explained in *Materials and Methods* section for biomass and metabolism tests, and the same as the one explained in the previous section for CFU counting.

3.3.1 Biomass reduction test through crystal violet staining

Results are represented in means of two repetitions (N = 2) in triplicates (n = 3). Error bars are the SEM.

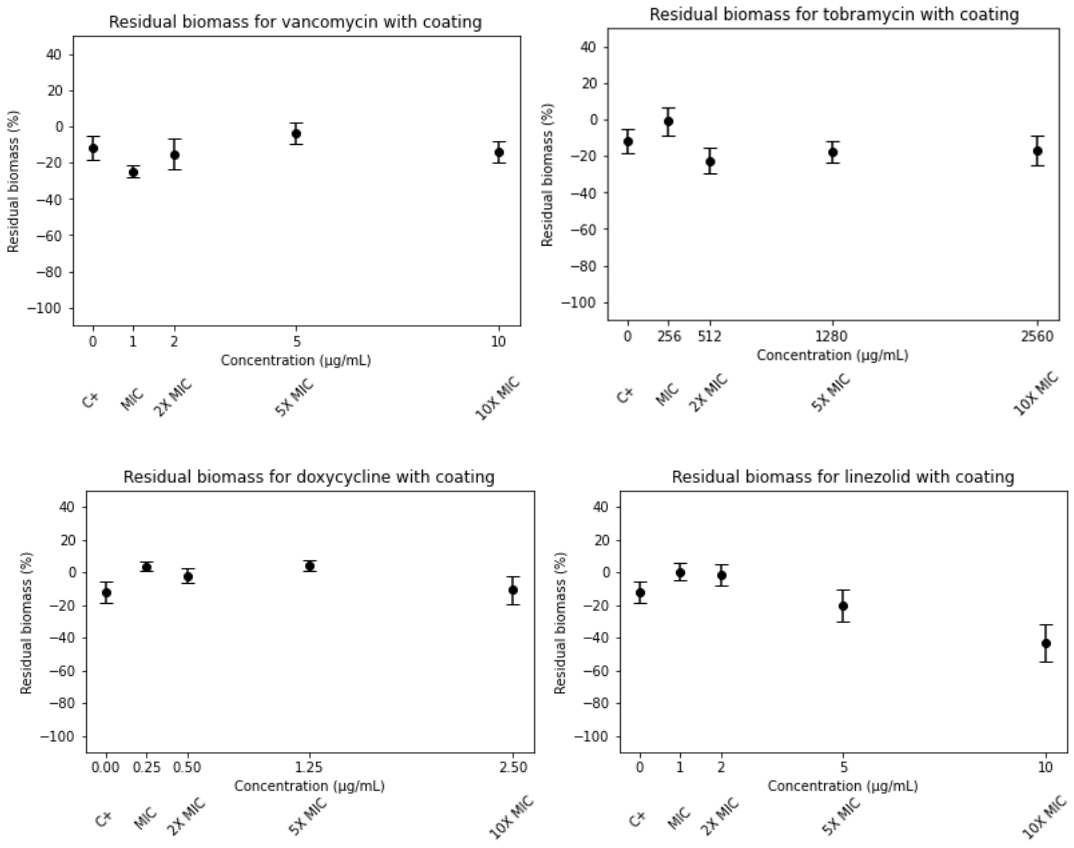

Figure VII: Percentage **biomass** reductions for 24h pre-formed *S. epidermidis ATCC 35984* biofilms when combining a LL-37-based coating with different multiples of the MIC of either vancomycin, tobramycin, doxycycline, or linezolid. C^+ = untreated biofilm (positive control) after potential autolysin AtlE activity.

3.3.2 Metabolic activity reduction test through resazurin method

Results are represented in means of two repetitions (N = 2) in triplicates (n = 3). Error bars are the SEM.

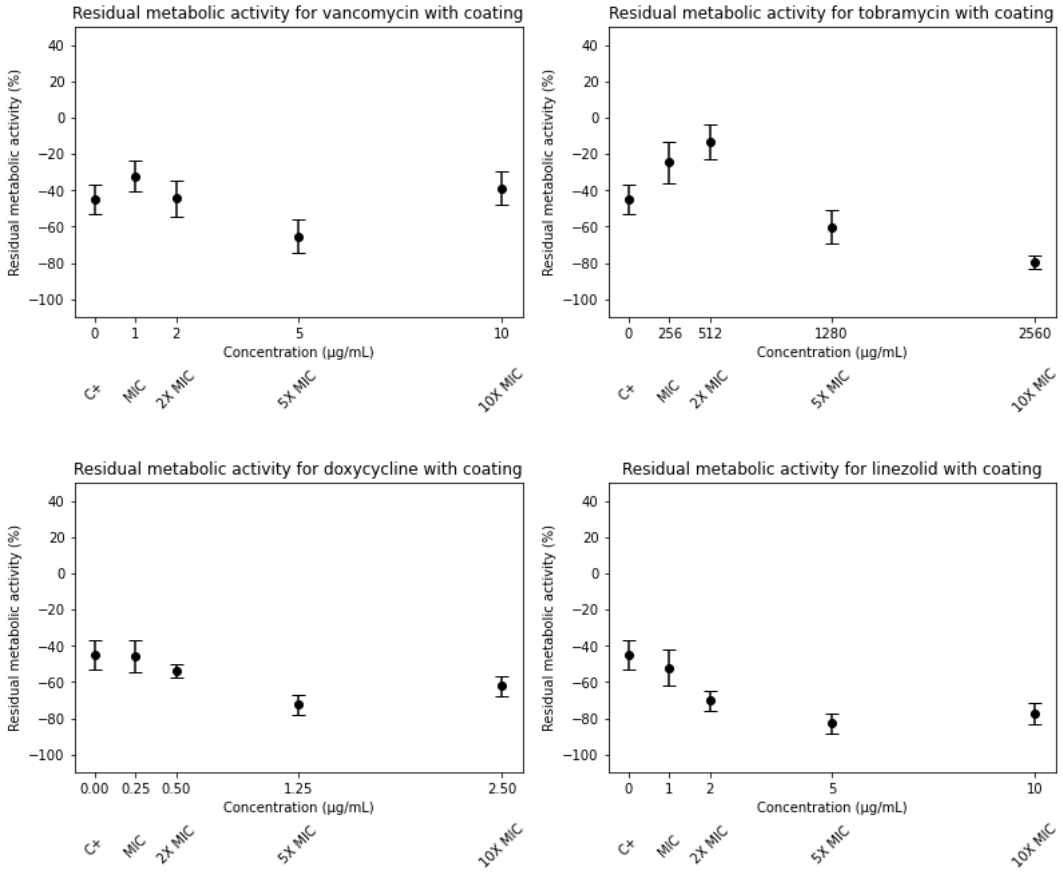

Figure VIII: Percentage **metabolism** reductions for 24h pre-formed *S. epidermidis ATCC 35984* biofilms when combining a LL-37-based coating with different multiples of the MIC of either vancomycin, tobramycin, doxycycline, or linezolid. C^+ = untreated biofilm (positive control) after potential autolysin AtlE activity.

3.3.3 CFU counting

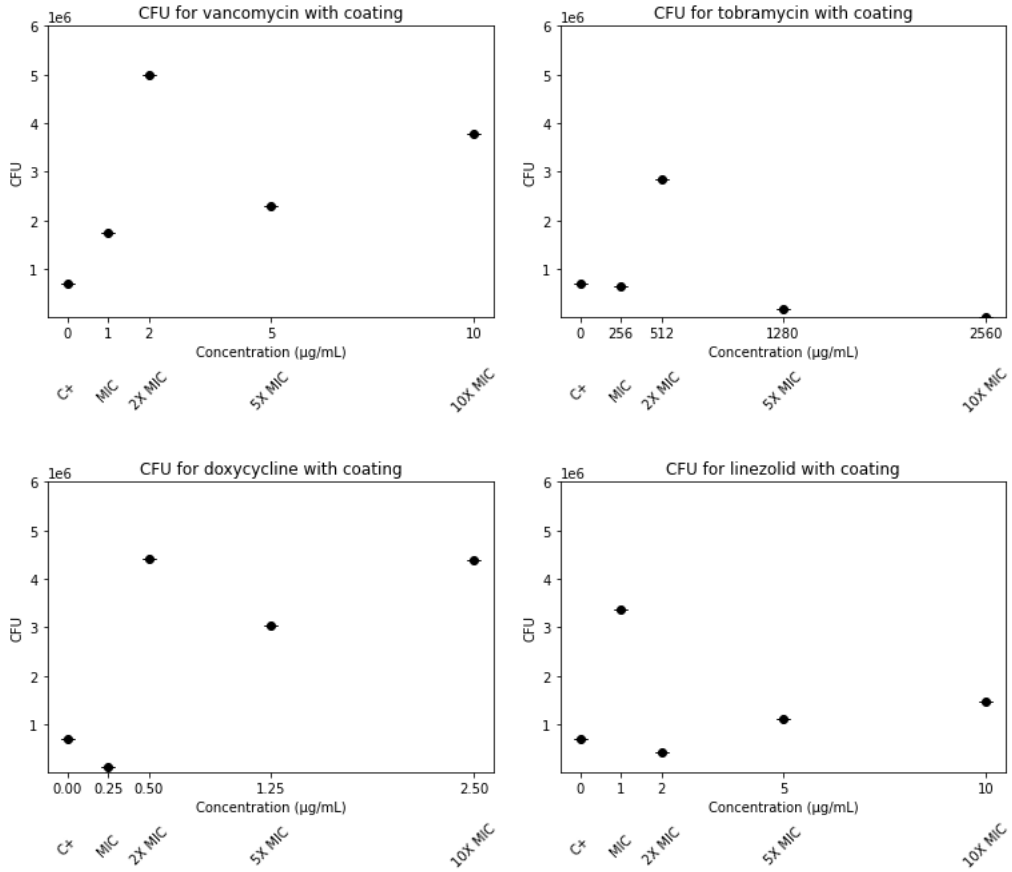

Figure IX: **CFU** number for 24h pre-formed *S. epidermidis ATCC 35984* biofilms when combining a LL-37-based coating with different multiples of the MIC of either vancomycin, tobramycin, doxycycline, or linezolid. C^+ = untreated biofilm (positive control) after potential autolysin AtlE activity.

Preventing infections of hip joint prostheses: activity of an antimicrobial coating based on the LL-37 peptide

Bastien Croës and Juliette Dewez

This Master's thesis studies the activity of an antimicrobial coating designed for the battle against *S. epidermidis* biofilms, which are the leading cause for nosocomial infections related to implants and medical devices, including prosthetic joint infection, an important worldwide consideration nowadays. New strategies based on the design of antimicrobial coatings are under current research to prevent and treat such infections.

The antimicrobial property of the investigated coating is conferred by LL-37, an antimicrobial peptide. The coating is constructed using the Layer-by-Layer self-assembly technique, allowing easy immobilization of proteins and other charged compounds on a surface. These multilayered films constitute a powerful tool for nanoscale surface functionalization. Here, LL-37 was immobilized together with chitosan and heparin, two bioactive PEs.

Two different LL-37-based coatings were constructed. A first coating was made of bare, positively-charged, LL-37, alternately adsorbed with negatively-charged heparin ((bare LL-37-HEP)$_n$). The second coating was made of LL-37 whose charges had been standardized by complexation with heparin to form Protein-Polyelectrolyte Complexes or PPCs, displaying a negatively-charged corona, and alternately adsorbed with positively-charged chitosan ((PPCs-CHI)$_n$).

Coatings activity was assessed through two approaches. The first objective was to study the secondary structure of LL-37 released from the coatings. The bactericidal activity of the peptide is conferred by its α-helical conformation, which could be revealed by circular dichroism (CD). To enable such analysis, the release protocol had to be optimized to maximize the concentration of the released peptide. Despite the use of different strategies to maximize this concentration, results showed that the concentration of LL-37 released by the coatings was not high enough for CD analysis.

Secondly, activity of the coating with bare LL-37 was assessed by studying its potential synergistic effect with four routinely-used antibiotics. Results showed a potential synergistic activity with all four antibiotics regarding the reduction of the biofilm biomass. In contrast, no significant effect of the coating compared to antibiotics alone was revealed for the reduction of metabolic activity of the biofilm.

This work brings a contribution to the understanding of the activity of LL-37-based antimicrobial coatings, that offer new ways to prevent prosthetic joint infections.

UNIVERSITÉ CATHOLIQUE DE LOUVAIN
Faculté des bioingénieurs
Croix du Sud, 2 bte L7.05.01, 1348 Louvain-la-Neuve, Belgique | **www.uclouvain.be/agro**